Assessment of Carbaryl Exposure Following Turf Application Using a Physiologically Based Pharmacokinetic Model

Prepared by

Miles S. Okino
Frederick W. Power
Rogelio Tornero-Velez
Jerry N. Blancato
Curtis C. Dary

U.S. Environmental Protection Agency
Office of Research and Development
Human Exposure and Atmospheric Sciences Division
Exposure and Dose Research Branch
P.O. Box 93478
Las Vegas, NV 89193-3478

Disclaimer: The information in this document has been funded in part by the United States Environmental Protection Agency under interagency agreement number DW47939443 to the General Services Administration for a work assignment to Anteon Corporation. It has been subjected to the Agency's peer and administrative review and has been approved for publication as an EPA document.

Preface

The document entitled "Assessment of carbaryl exposure following turf application using a physiologically based pharmacokinetic model" was developed by EPA's National Exposure Research Laboratory in collaboration with the Office of Pesticide Programs (OPP). This effort represents one part of EPA's on-going efforts to improve risk assessment methodologies and approaches. This document and the relevant attachments and models reflect research efforts only. All results contained in this draft are considered preliminary in nature and therefore, OPP does not anticipate using them as part of the either the risk assessment for carbaryl or the cumulative risk assessment for *N*-methyl carbamates. EPA issued the Interim Reregistration Eligibility Decision for carbaryl on June 30, 2003. That assessment contains EPA's most recent aggregate risk assessment for carbaryl. The IRED is available to the public at http://www.epa.gov/oppsrrd1/REDs/carbaryl_ired.pdf. Moreover, given the preliminary nature of the methodology, it is important to note that they do not reflect current OPP risk assessment policies regarding evaluation of inter- and intra-species extrapolation. Specific considerations mandated by the Food Quality Protection Act (FQPA) of 1996 such as aggregation of multiple pathways of exposure and specific consideration of potential sensitivity of infants and children are not considered here. As this methodology matures, OPP will need to examine how it can be incorporated into the overall approach to the assessment of risks to human health.

Abstract

Carbaryl (1-naphthol *N*-methylcarbamate, CAS# 63252) is a widely used neurotoxic insecticide in agriculture, residential applications, and professional turf management. A member of the *N*-methylcarbamate class of pesticides, carbaryl is a reversible inhibitor of acetylcholinesterase (AChE).

A physiologically based pharmacokinetic (PBPK) model was used to evaluate the available pharmacokinetic data and perform necessary species-to-species and route-to-route extrapolations to evaluate the dose metrics relevant to risk. The National Exposure Research Laboratory (NERL) has developed a PBPK modeling system that includes a comprehensive description of chemical absorption, distribution, metabolism and excretion (ADME), as well as the flexibility to evaluate diverse chemical inputs corresponding to different exposure scenarios. This model, the Exposure Related Dose Estimating Model (ERDEM) has been used in the current assessment as a tool for aiding in risk characterization of carbaryl following turf exposure. The approach illustrated by this assessment is representative of the investigations possible with PBPK models.

The PBPK model was first developed to be consistent with rat data from the literature and registrant, Bayer CropScience. The human scenarios were then implemented by substituting human physiologic parameters in the PBPK model. Oral hand-to-mouth and dermal exposure scenarios were implemented for children, and the degree of acetylcholinesterase inhibition and tissue concentrations were evaluated. The magnitude of exposure was constrained by a biomonitoring study conducted by Bayer CropScience that measured carbaryl metabolite mass in urine. The urine metabolite levels corresponded to absorbed doses of approximately 0.08 mg/kg, relative to the no observed adverse effect level (NOAEL) of 1 mg/kg.

Acetylcholinesterase activity based on the assumptions in this analysis was predicted to remain >99% of the baseline levels for the children's exposure scenarios. The simulated scenarios were intentionally designed to be conservative. All the excreted metabolite was associated with a single activity period, which results in high peak tissue concentrations. The expected variability in model parameters associated with brain concentration levels and acetylcholinesterase inhibition were investigated. Minimal changes were observed for the predicted acetylcholinesterase inhibition, but peak brain concentrations were found to be dependent on values used for the blood:brain partition coefficient and the metabolism rates. Additional data on these pathways would reduce the uncertainties in the assessment of carbaryl. (Note: The results contained in this report are preliminary in nature and do not reflect current OPP and EPA policies regarding evaluation of inter- and intra-species extrapolation, aggregate risk, and application of the FQPA safety factor for potential sensitivity of infants and children).

Table of Contents

1.0 INTRODUCTION

1.1 Overview

Carbaryl (1-naphthol *N*-methylcarbamate, CAS# 63252) is a widely used neurotoxic insecticide in agriculture, residential applications, and professional turf management. A member of the *N*-methylcarbamate class of pesticides, carbaryl is a reversible inhibitor of acetylcholinesterase (AChE). In response to the widespread use of this carbamate pesticide, the U. S. EPA evaluated the risks of carbaryl and, in June 2003, reached an Interim Reregistration Eligibility Decision (IRED). The IRED identifies additional pharmacokinetic data as a means to refine post-application risks from broadcast applications to turf lawns with liquid formulations.

At the present time, appropriate pharmacokinetic studies with blood or urine levels of carbaryl or its metabolites in humans exposed to carbaryl following turf application are not available. Biomonitoring studies, such as Bayer 2004b, provide information on the amount of chemical absorbed over the observation period, but it is not feasible to record or control all exposure activities. The relevant health effect, acetylcholinesterase inhibition, occurs over a much shorter time-scale (hours) than can be estimated from daily urine collection. However, physiologically based pharmacokinetic (PBPK) models may be used to evaluate the available pharmacokinetic data and perform necessary species-to-species and route-to-route extrapolations to evaluate the dose metrics relevant to risk. PBPK models describe the time course disposition of chemicals and their metabolites. PBPK models are well suited to help assess risk from carbaryl following turf application. They provide a representation of the absorption, distribution, metabolism, and excretion (ADME) of xenobiotics that are believed to contribute to the potential of inducing adverse human health responses.

The National Exposure Research Laboratory (NERL) has developed a PBPK modeling system that includes a comprehensive description of chemical ADME, as well as the flexibility to evaluate diverse chemical inputs corresponding to different exposure scenarios. This model, ERDEM (Exposure Related Dose Estimating Model) has been used in the current assessment as a tool for aiding in risk characterization of carbaryl following exposure to treated turf. The approach illustrated by this assessment is representative of the investigations possible for the cumulative assessment for the *N*-methyl carbamate pesticides.

1.2 Carbaryl ADME Characteristics

Pharmacokinetic models provide a framework in which to organize the available pharmacokinetic and pharmacodynamic (PD) data. The laboratory studies in rats are suitable for characterizing various ADME and PD behaviors of carbaryl, dependent on the type of study and measurements collected. The studies used

to characterize the behavior of carbaryl, and ultimately for development of the PBPK/PD model are listed in Table 1.

Table 1. Pharmacokinetic studies in rats for estimation of kinetic parameters

Source	Scenario	Measurements
Bayer 2004a	Oral 1 mg/kg	Brain ^{14}C, blood ^{14}C
Bayer 2004a	Oral 10 mg/kg	Brain ^{14}C, blood ^{14}C, brain carbaryl, brain naphthol, fat ^{14}C, liver ^{14}C, plasma naphthyl sulfate, plasma naphthol, plasma carbaryl (n.d.)
Bayer 2004a	IV 1 mg/kg	Brain ^{14}C, blood ^{14}C
Bayer 2004a	IV 10 mg/kg	Brain ^{14}C, blood ^{14}C, brain carbaryl, brain naphthol, fat ^{14}C, liver ^{14}C, plasma naphthyl sulfate, plasma naphthol, plasma carbaryl, fat carbaryl, fat naphthol, liver carbaryl, liver naphthol
Bayer 2004a	Oral 0.075 mg/kg x2 with dermal 0.75 mg/kg	Brain ^{14}C, blood ^{14}C, brain carbaryl, brain naphthol
Brooks and Broxup 1995a	Oral 10, 50, 125 mg/kg	Blood, brain cholinesterase inhibition
Brooks and Broxup 1995b	Oral 10, 30, 90 mg/kg	Blood, brain cholinesterase inhibition
Cheng 1994	Dermal 0.793 mg	Urine ^{14}C, total carcass ^{14}C, blood ^{14}C, skin carbaryl, skin surface carbaryl
Knaak *et al.* 1984	Dermal 1.74 mg	Urine ^{14}C, fat ^{14}C, liver ^{14}C, rapidly perfused tissue ^{14}C, slowly perfused tissue ^{14}C, kidney ^{14}C, blood ^{14}C, skin carbaryl, skin surface carbaryl, evaporated carbaryl
Knaak *et al.*, 1965	Oral and IP doses of 20 mg/kg	Major urine metabolites: urine Naphthyl sulfate, urine naphthyl glucuronide, urine 4-OH carbaryl sulfate, urine 4-OH carbaryl glucuronide, urine 5,6 DIOH carbaryl glucuronide
Marshall and Dorough 1979	Oral dose 0.01 mg/kg to bile cannulated animals	Urine ^{14}C, bile ^{14}C

1.2.1 Absorption

Important absorption pathways following turf application are dermal for direct contact with treated surfaces and oral resulting from hand-to-mouth activities. Several types of studies are considered to characterize absorption. The comparison of intravenous (IV) studies to oral or dermal studies illustrates the kinetics of absorption. The completeness of the absorption is characterized by comparison to IV studies, and by total mass balance studies that account for the excretion pathways.

Oral absorption of carbaryl into the blood is rapid, where peak blood concentrations of ^{14}C (ring label) occur within 15 minutes in rats after dosing with 1 mg/kg (Figure 1). The fast kinetics from Bayer 2004a of oral absorption are consistent with other oral studies (Casper *et al.* 1973, Ahdaya and Guthrie 1982).

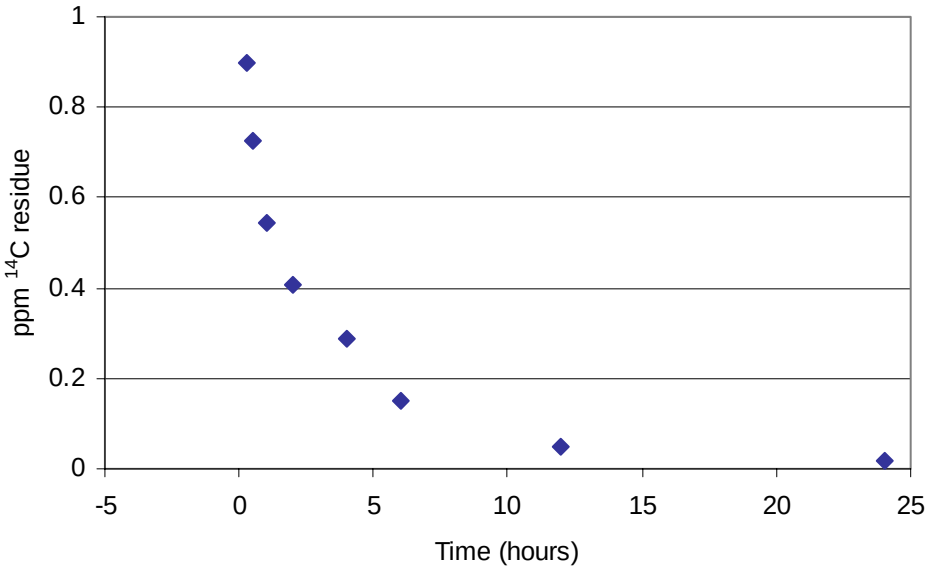

Figure 1. Blood ^{14}C concentrations (ring label) after 1 mg/kg carbaryl oral dosing in rats. Data from Bayer 2004a, average of 4 animals at each sample time.

Oral absorption is essentially complete, where the peak concentration observed after an oral dose of 1 mg/kg (Figure 1) is similar to the peak observed after 1 mg/kg IV dose (Bayer 2004a). This observation is consistent with the high percent recovery of radiolabeled carbaryl in urine (>85%) relative to feces (< 10%, Bayer 2004b, Struble 1994).

As expected, dermal absorption is slower, where peak concentrations in blood are observed 10-12 hours after initial application (Figure 2). The slower kinetics of dermal absorption are consistent with other dermal absorption studies (Cheng 1994, Shah *et al.* 1981).

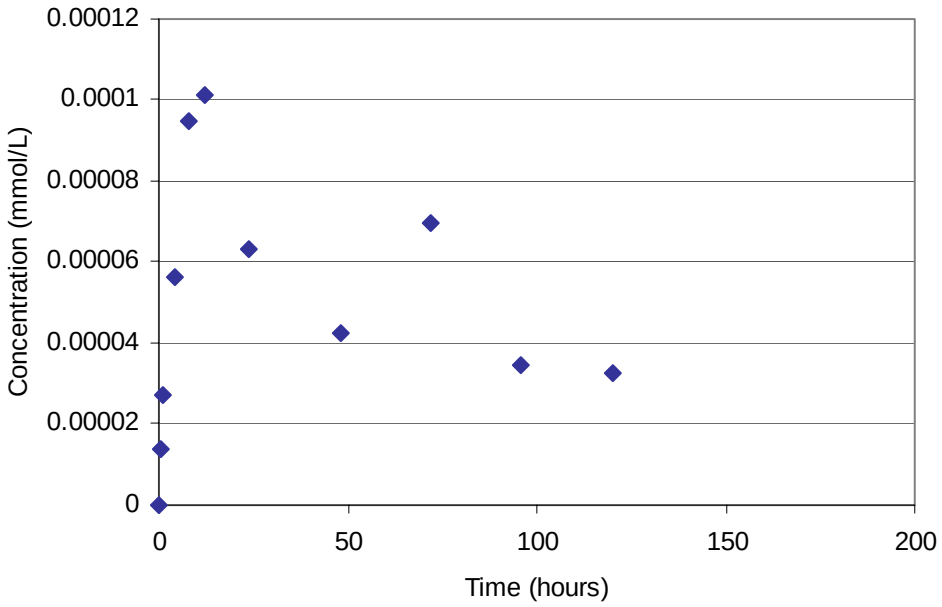

Figure 2. Blood ^{14}C concentrations (ring label) after 1.74 mg (20 cm^2) carbaryl dermal application on rats. Data from Knaak *et al.* 1984, average of 3 animals at each sample time.

1.2.2 Distribution

Once a chemical enters the blood stream, its disposition in blood, other fluids (e.g. bile), organs and tissues determines its access to the site or sites of action. Chemical disposition involves distribution from blood and fluids to tissues and organs, metabolism in liver and other organs of metabolism, and elimination in exhaled breath, fluids, e.g. milk, and excreta.

Measurements of each specific chemical, the parent compound and metabolites, in the tissues of interest are ideal to assess distribution. Most of the available data are for ^{14}C (Table 1), which are not sufficient for characterization since each chemical distributes to the tissues differently based on its physical and chemical properties.

Due to its high octanol:water partition coefficient, carbaryl is expected to favor sequestration in tissues, while its more water soluble metabolites will favor the blood. The distribution of carbaryl to tissues is limited by its rapid metabolism, although its metabolites are available for distribution in the body for longer time periods. At a high intravenous (IV) dose in rats, carbaryl was detected in blood, brain, liver and fat (Bayer 2004a), and the sharp peak in brain (Figure 3) provides

evidence for the fast metabolism. Similar profiles were observed in the other compartments.

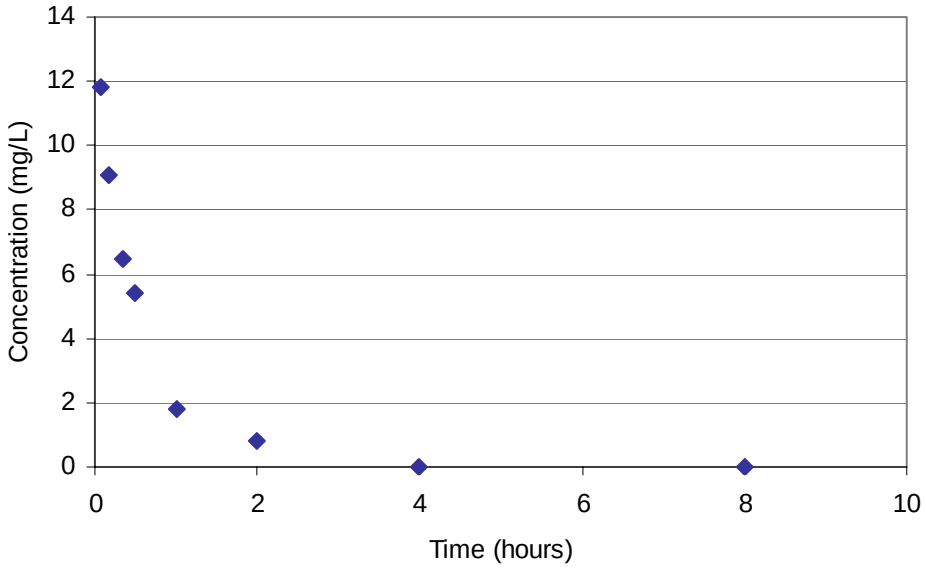

Figure 3. Brain carbaryl concentration after 10 mg/kg carbaryl IV dose in rats. Data from Bayer 2004a, average of 4 animals at each sample time.

Measurements of ^{14}C for a variety of doses and exposures illustrates the distribution of the metabolites. In addition to transport by the blood, the glucuronidated species are recirculated through the bile. ^{14}C residues were found in blood (Figures 1 and 2), fat, brain, liver, bile, and rapidly and slowly perfused tissues (Bayer 2004a, Knaak *et al.* 1984, Marshall and Dorough 1979). Few measurements have been taken for specific chemicals in the tissues, but their identity can be inferred from metabolism studies.

1.2.3 Metabolism and Excretion

The metabolism of carbamate pesticides has been the subject of several reviews (Roberts and Hutson 1999, Cool and Jankowski 1985, Kuhr and Dorough 1976). The pathways are shown in Figure 4.

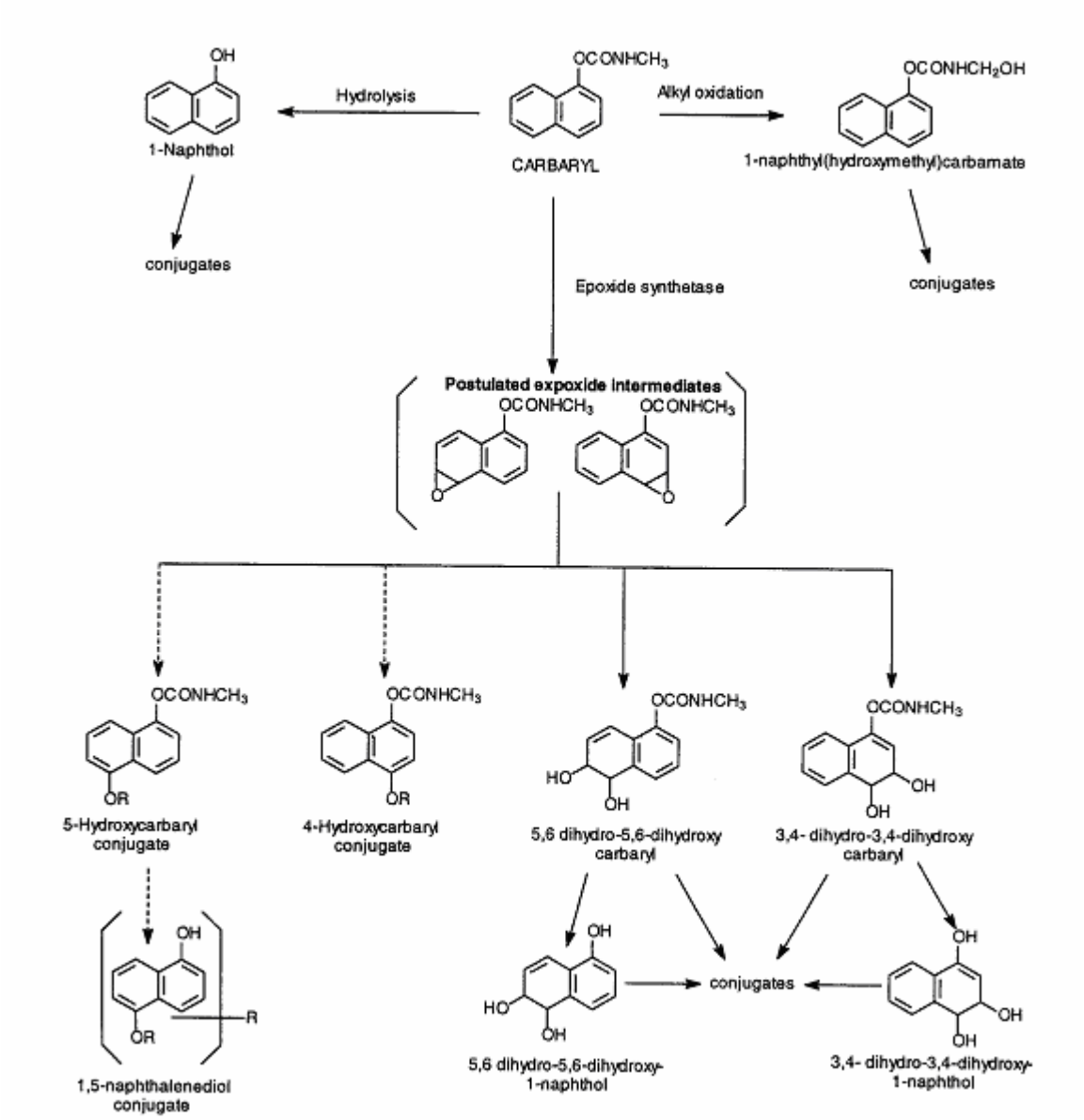

Figure 4. Metabolism pathways for carbaryl. Adapted from Ross and Driver 2002.

The metabolism of carbaryl in rats has been studied by Knaak *et al.* (1965), Hassan *et al.* (1966), Bend *et al.* (1971), and Sullivan *et al.* (1972). A comparison of the metabolite profiles in urine showed that the rat metabolism pathways were conserved in humans (Knaak *et al.* 1965; Knaak *et al.* 1968).

The primary metabolites of carbaryl are 4-hydroxy carbaryl, 3,4-dihydroxy carbaryl, 5,6-dihydroxycarbaryl, and 1-naphthol. Based on the chemistry, 5-hydroxycarbaryl and hydroxymethylcarbaryl are possible products, but these have not been detected in *in vivo* studies in rats or humans. The carbaryl products can be further metabolized to the corresponding naphthol species, and

all the metabolites are subject to conjugation with sulfate or glucuronide. Conjugation increases the aqueous solubility to facilitate urinary excretion. Minimal excretion occurs via the feces (Struble 1994, Krishna and Casida 1966). Hydroxylation reactions are catalyzed by liver microsomal P450 enzymes (Tang *et al.* 2002), while hydrolases, including carboxylesterase (Sogorb *et al.* 2002), catalyze the hydrolysis reactions.

Following an intraperitoneal dose of 20 mg/kg ^{14}C carbaryl (ring label) in rats, the major urinary metabolites identified after 24 hours were naphthyl sulfate, naphthyl glucuronide, 4-hydroxycarbaryl glucuronide, 4-hydroxycarbaryl sulfate, and 5,6-dihydroxycarbaryl glucuronide (Knaak *et al.* 1965, Sullivan *et al.* 1972).

Measurements of total ^{14}C in rat urine indicate that excretion of carbaryl and its metabolites after an oral dose occurs within 1-3 days (Knaak *et al.* 1965, Benson and Dorough 1984). Excretion occurs over a longer time-scale following dermal exposure due to the slower absorption rate that results in continuous absorption over a longer period and susceptibility of the carbaryl on the skin surface to other removal mechanisms, i.e., evaporation (Knaak *et al.* 1984, Cheng 1994).

1.2.4 Carbaryl Pharmacodynamics

Acetylcholinesterase (AChE) inhibition in the blood and brain is a health effect of interest for the *N*-methyl carbamates, including carbaryl. The inhibition occurs through carbamylation of the serine hydroxyl group located in the active site of the enzyme, and results in accumulation of acetylcholine at a nerve synapse or neuromuscular junction. Continued accumulation of the neurotransmitter acetylcholine may result in the overstimulation of cholinergic pathways in the central and peripheral nervous systems and possibly to the expression of cholinergic signs and symptoms such as nausea, gastrointestinal distress, vomiting, tremors, paralysis and depression of respiratory function.

Generally, cholinesterase (ChE)-inhibiting chemicals compete with the acetylcholine for binding to the enzyme (AChE). As more ChE-inhibiting chemical binds with the enzyme, the acetycholine is subject to slower or less hydrolysis and its activity is prolonged. In rat studies, carbaryl was given orally at doses from 10 to 125 mg/kg, and the blood and brain ChE activity was measured over time. The time-scale of ChE recovery to baseline activity levels was observed to be less than a day (Brooks and Broxup 1995a,b).

2.0 METHODS

The objective of this study is to develop a structure to organize and evaluate the existing data on carbaryl. Physiologically based pharmacokinetic models (PBPK), with integrated PK components, are suitable for this purpose since the known physiologic and biochemical processes that affect chemical ADME are explicitly represented. The deterministic framework of the model enables the

extension of the model to other exposure scenarios (route-to-route extrapolation), and provides the basis for systematic scaling among species and age-groups.

An established PBPK modeling system was utilized, the Exposure Related Dose Estimating Model (ERDEM). The system is adapted for the carbaryl scenarios by implementing parameters specific to the subjects and chemicals. The suitability of these parameter values is then evaluated by comparing the model results to the available data.

2.1 PBPK Models

2.1.1 Exposure Related Dose Estimating Model (ERDEM)

ERDEM is an exposure and dose-modeling system developed by ORD scientists. The heart of ERDEM is a physiologically based pharmacokinetic (PBPK) model that simulates the absorption, distribution, metabolism, and elimination of chemicals in mammals. Simulated chemicals are introduced into the physiological system by any of several routes including injection, ingestion, inhalation, and/or dermal absorption. The ERDEM system is complex and flexible, with over 30 physiological compartments such as arterial and venous blood, brain, derma, fat, intestine, kidney, liver, rapidly and slowly perfused tissue, and stomach (Figure 5). Any subset of compartments can be included for the PBPK model of a specific chemical.

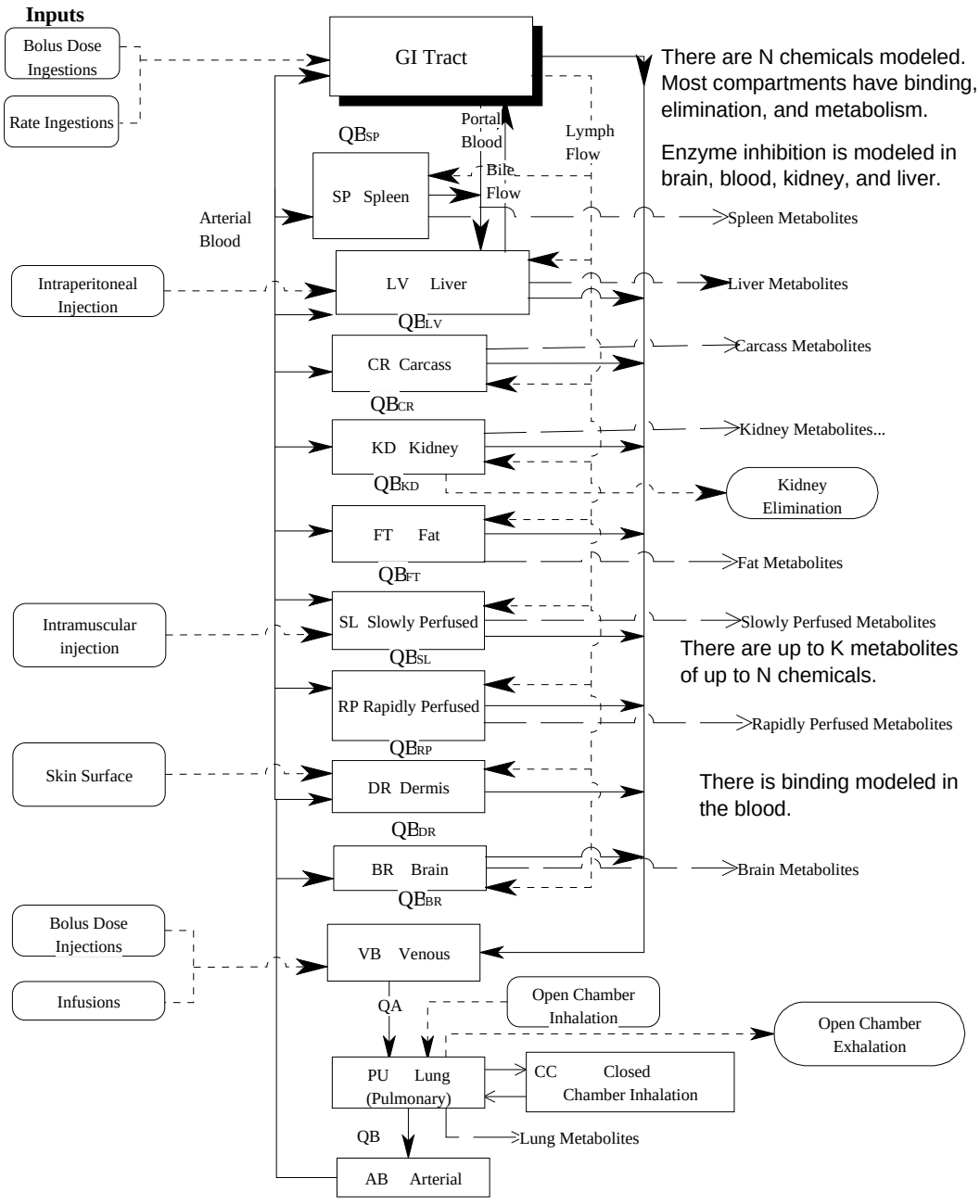

Figure 5. ERDEM System Flow with Static Lung and Full GI

Metabolism can occur in many of these compartments and multiple metabolites are tracked as they and the parent compound(s) circulate through the system. It is important to note that adjustments are made for differences in metabolism and physiology between children and adults. ERDEM is programmed in the Advanced Continuous Simulation Language (ACSL). To execute ERDEM, the

user enters physiological, biological, and pharmacodynamic modeling data specific to their chemical and/or scenario of interest (U.S. EPA, 2002).

Any PBPK model, including ERDEM, is made up of a series of the differential equations which describe the rates of inflow, distribution, metabolism, or outflow of a chemical and various metabolites in each separate biological compartment. Appendix A describes in detail the equations for each of the biological compartments contained in ERDEM.

2.1.2 Carbaryl Model Structure in ERDEM

The structure of the carbaryl model is defined by the scenarios and metrics of interest, and available data for evaluation. Exposure following turf application is expected to occur through the dermal and oral routes. The relevant dose and effect metrics for carbaryl are the concentrations in blood and brain, and level of acetylcholinesterase inhibition in those compartments.

Based on the model requirements and available measurements, the model for carbaryl includes the following compartments: blood (venous, arterial, portal), brain, liver, fat, rapidly and slowly perfused tissues, and bile. The liver is required as the primary site of metabolism, the brain as the target tissue, and kidney as the site of urinary elimination. Also, the skin, stomach and other GI tract components are modeled to account for the absorption routes of interest.

2.1.2.1 Absorption Model in ERDEM

Mathematical representations of oral and dermal absorption are included in ERDEM to simulate exposure following turf application. Dermal absorption occurs due to direct contact with treated surfaces, while oral absorption would occur through hand-to-mouth activities of young children.

Oral absorption is modeled as a first order kinetic process as transfer from the luminal volume to the walls of the GI tract. Chemical can be input as either a bolus dose or as a rate process into the stomach lumen. The stomach and other GI components (duodenum, small and large intestine, colon) are modeled, with absorption in each compartment, and transfer from the stomach to the remainder of the GI tract. The equation for flow through the stomach lumen is below:

$$\frac{dA_{STL_i}}{dt} = \frac{dA_{RIG_i}}{dt} + \frac{dA_{BIG_i}}{dt} - Q_{F,STL} C_{STL_i} - K_{NL,SW_i} A_{STL_i}$$

where

A_{STL_i} = amount of *i*th chemical in stomach lumen

C_{STL_i} = concentration of *i*th chemical in stomach lumen

$\frac{dA_{STL_i}}{dt}$ = the rate of change of the *i*th chemical in the stomach lumen

$Q_{F,STL}$ = the volume rate of food flowing through the stomach lumen to the duodenum

K_{NL,SW_i} = the rate constant for the amount of the *i*th chemical from the stomach lumen to the stomach wall

$\frac{dA_{RIG_i}}{dt}$ =the rate of change of the amount of the *i*th chemical as a rate ingestion

$\frac{dA_{BIG_i}}{dt}$ =the rate of change of the amount of the *i*th chemical as a bolus ingestion

Complete equations for GI absorption are in Appendix A.

Two compartments are used for GI absorption (stomach; and lumped duodenum, small and large intestines, colon) to account for the known biological processes that affect the ADME of carbaryl. The glucuronidated metabolites of carbaryl are known to circulate from the liver to the duodenum through the bile, so the lumped compartment is necessary.

In the dermal model, movement of carbaryl from the vehicle into the skin is determined by the concentration (mg/L) of carbaryl on the skin surface, the area of exposed skin (cm^2), and permeation coefficient (cm/hr) as follows:

$$\frac{dA_{sks,dr_i}}{dt} = K_{sks,dr,prm_i} A_{sk} C_{sks_i}$$

where

$C_{sks_i} = \frac{A_{sks_i}}{V_{sk}}$

and

A_{sk} = area of skin exposed

V_{sk} = volume of skin exposed

A_{sks_i} = amount of the *i*th chemical on the skin

K_{sks,dr,prm_i} = the permeation coefficient for the *i*th chemical from the skin surface to dermis

$\frac{dA_{sks,dr_i}}{dt}$ = the rate that the *i*th chemical moves from the skin surface into the dermis

The mass of carbaryl absorbed into the skin over the exposure period slowly enters the vascular compartment (Figure 2). Mass on the skin surface may also be removed by evaporation or washing. Only the mass absorbed into the skin contributed to the internal dose. The complete equations for dermal exposure are in Appendix A.

2.1.2.2 Distribution Model in ERDEM

Distribution of chemicals from the blood to tissues is modeled as perfusion limited, where it is dependent on the blood flow rate and equilibrium partition coefficient between the blood and tissue. The transport of the *i*th chemical to the brain (BN) through the circulation is described below:

$$V_{BN}\frac{dC_{BN_i}}{dt} = Q_{B,BN}C_{AB_i} - Q_{B,BN}\frac{C_{BN_i}}{R_{BN,VB_i}}$$

where

V_{BN} = volume of the brain

$Q_{B,BN}$ = blood flow to the brain

C_{BN_i} = concentration of *i*th chemical in the brain

C_{AB_i} = concentration of *i*th chemical in the arterial blood

R_{BN,VB_i} = partition coefficient for the *i*th chemical between the brain and blood

The chemical in tissues is also subject to changes due to metabolism and excretion. The complete equations are described in Appendix A.

2.1.2.3 Metabolism Model in ERDEM

For this assessment, metabolism is modeled to occur in the liver. Based on the metabolism studies (Knaak *et al.* 1965), the pathways to the following metabolites are included in the model: naphthyl sulfate, naphthyl glucuronide, 4-hydroxycarbaryl glucuronide, 4-hydroxycarbaryl sulfate, and 5,6-dihydroxycarbaryl glucuronide. Other metabolites consistent with the carbaryl scheme account for the unidentified species in the studies. The modeled pathways are summarized in Table 2.

Table 2. Metabolism Structure for Carbaryl in Rats and Humans

Metabolic Reaction	Enzyme	Compartment
Carbaryl to 4-OH carbaryl	Cytochrome P450 isozymes	liver
Carbaryl to 3,4-diOH carbaryl	Cytochrome P450 isozymes	liver
Carbaryl to 5,6-diOH carbaryl	Cytochrome P450 isozymes	liver
Carbaryl to 1-naphthol	hydrolases	liver
4-OH carbaryl to 4-OH carbaryl glucuronide	UDPGA transferase	liver
4-OH carbaryl to 4-OH carbaryl sulfate	sulfotransferase	liver
3,4-diOH carbaryl to 3,4-diOH 1-naphthol	hydrolases	liver
3,4-diOH carbaryl to 3,4-diOH carbaryl glucuronide	UDPGA transferase	liver
3,4-diOH carbaryl to 3,4-diOH carbaryl sulfate	sulfotransferase	liver
5,6-diOH carbaryl to 5,6-diOH carbaryl glucuronide	UDPGA transferase	liver
1-Naphthol to 3,4-diOH 1-naphthol	Cytochrome P450 isozymes	liver
1-Naphthol to 1-naphthyl glucuronide	UDPGA transferase	liver
1-Naphthol to 1-naphthyl sulfate	sulfotransferase	liver
3,4-diOH 1-naphthol to 3,4-diOH 1-naphthyl glucuronide	UDPGA transferase	liver
3,4-diOH 1-naphthol to 3,4-diOH 1-naphthyl sulfate	sulfotransferase	liver

A saturable Michaelis-Menten form of metabolism was assumed:

$$\frac{dA_{LV,M,i,j}}{dt} = \frac{V_{\max,LV,i,j} C_{LV,i}}{K_{m,LV,i,j} + C_{LV,i}}$$

where the formation rate of the *j*th metabolite from the *i*th chemical in the liver is determined from the maximum velocity of metabolism (V_{max}), the Michaelis-Menten constant (K_m) and the concentration of the *i*th chemical in the liver.

The parameters V_{max} and K_m, were determined using ERDEM by adjusting these values to fit to the available data (see Results). The V_{max} was scaled as to body weight at the 0.7 power for the different rat body weights. V_{max} was further scaled from the rat to the human according to age (3 and 9 years of age).

$$V_{\max,LV,i,j} = V_{\max,LV,US,i,j}\left(\frac{V_{BW}}{V_{BW,\mathrm{Re}\,f}}\right)^{0.7}$$

where the subscript *US* represents the unscaled quantity. The V_{max} and K_m values, obtained after a number of iterations of comparing model runs with multiple sets of experimental data for the rat, were then used in the modeling of the human. This is an important quality assurance step (see Appendix B) for establishing model parameters based on experimental data.

The total metabolism rate for carbaryl is expected to scale from rat to human, but the ratio of products based on the relative rates of each specific pathway may not be representative of actual human metabolism. The few human studies show evidence of different ratios of enzyme activity, resulting in a different metabolite profile between the rat and man (Knaak *et al.* 1965). The model would benefit from additional metabolism data in humans from which to determine appropriate values for rate constant ratios in man.

2.1.2.4 Excretion Model in ERDEM

The urine elimination rate for the *i*th chemical was modeled as saturable, determined from the concentration of the *i*th chemical in the kidney and the urine elimination rate constants (V_m and K_{mM}) for the *i*th chemical.

$$\frac{dA_{Urine,i}}{dt} = V_{m,Urine,i}\frac{C_{KD,i}}{K_{mM,Urine,i} + C_{KD,i}}$$

Elimination rate constants were determined for the rat by fitting the available data (see Results) to the model. The scaling for the rat V_{max} was set by body weight to the 0.7 power.

$$V_{m,Urine,i} = V_{m,Urine,US,i}\left(\frac{V_{BW}}{V_{BW,\mathrm{Re}\,f}}\right)^{0.7}$$

where the subscript *US* represents the unscaled quantity. The human values for the urine elimination rate constant specific to each age group were scaled from the rat to the human based on body weight.

2.1.2.5 Acetylcholinesterase Inhibition Model in ERDEM

The following outlines the basic process of ChE-inhibition for a single *N*-methyl carbamate pesticide.

1. There is a certain amount of ChE in each tissue and a certain amount is synthesized to keep this level at a near physiological steady-state (K_s). This is a basic physiological process independent of any foreign chemicals entering the system.

2. A certain amount of enzyme is degraded (K_d). This also reduces the amount of free enzyme available to perform its normal physiological function. When no inhibitor is present this degradation process is balanced by the synthesis described above. However in the presence of inhibitor, the formation of the complex can be thought of as another stress that reduces the amount of enzyme available for normal physiological function. This reduces the activity of the enzyme on its normal physiological substrate, acetylcholine at the neurological site.

3. Inhibitors, such as the *N*-methyl carbamates, enter the system and reduce the amount of free enzyme by forming a complex with the enzyme. The enzyme that is complexed with the ChE-inhibiting chemical is no longer available to perform its normal physiological activity leading to the build up of acetylcholine. (Each *N*-methyl carbamate pesticide has a unique rate constant for the formation of the complex with the enzyme, K_i).

4. The enzyme-inhibitor complex in turn reacts to result in a break down of the ChE-inhibiting chemical and a return or regeneration of free enzyme. This process is also governed by a chemical specific rate constant, K_r. The period of inhibition varies for different compounds and is generally dependent upon the rate of regeneration. Because the period of inhibition is often brief (due to rapid regeneration), the whole process has been dubbed as ‘reversible’.

Figure 6 summarizes this process. The “released metabolite” represents the *N*-methyl carbamate that is broken down. Each carbamate has its own specific rate constants for the process. Any number of *N*-methyl carbamates can interact at same time or at any time with the free AChE.

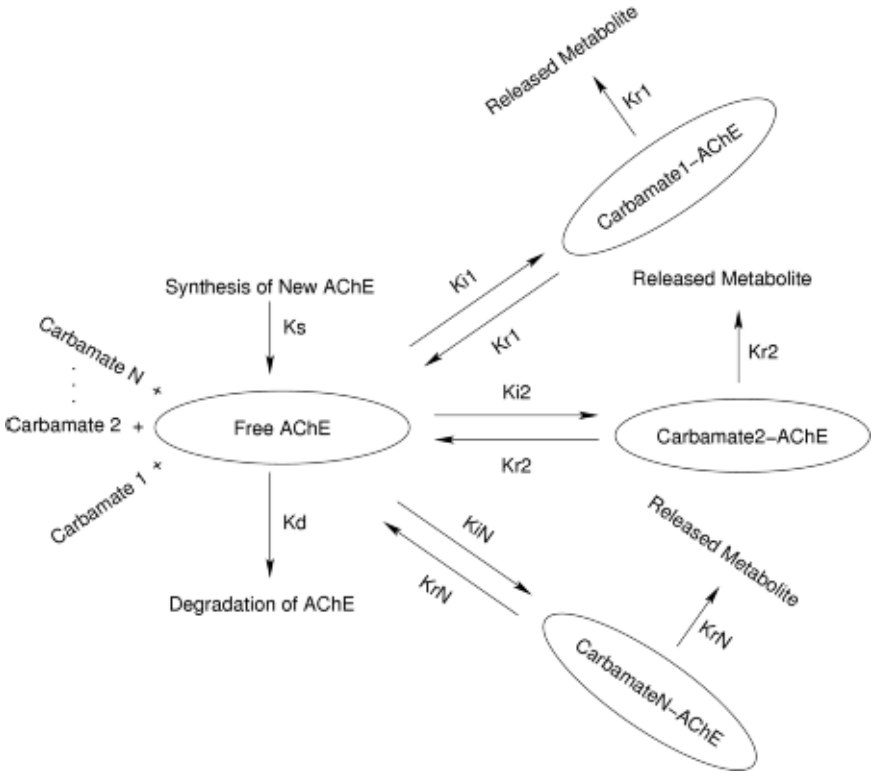

Figure 6. Schematic diagram of *N*-methyl carbamates binding to AChE.

The following differential equations represent the mass balance for the Figure 6:

$$\frac{dAce_x}{dt} = K_s - Ace_x \times \left(K_d + \sum_j K_{ij} \times C_{jx} \right) + \sum_j K_{rj} \times INce_j$$

$$\frac{dINce_{xj}}{dt} = Ace_x \times K_{ij} \times C_{jx} - K_{rj} \times INce_j$$

where
Ace_x is the amount of AChE (µmol) in compartment x,
$INce_{xj}$ is the amount (µmol) complex of AChE and inhibitor j in compartment x,
K_s is zero-order rate of enzyme synthesis,
K_d is the first-order rate of enzyme degradation (hr^{-1}),
K_{ij} is the bimolecular rate of inhibition for *j*th inhibitor,
K_{rj} is the first-order rate of regeneration for *j*th complex,
subscript x indicates tissue compartment, and
subscript j indicates the identity of the inhibiting chemical.

Thus, the total amount of active enzyme is equal to the amount present in the system minus the amount degraded minus the amount forming a complex with the inhibitor plus the amount regenerated after the enzyme breaks down or metabolizes the inhibitor.

This assessment considers only a single carbamate, carbaryl. The PD model integrated with the PBPK model in the compartments where acetylcholinesterase inhibition occurs enables the evaluation of the relevant health effects. The carbaryl model provides a basis for the consideration of multiple compounds acting in combination at any of the steps outlined above. The simplest interaction would be simply adding the inhibition caused by each compound. In such cases, depending upon the specific rate constants, different chemical molecules would each contribute to enzyme inhibition. It might be possible however that interaction would involve competition between the various chemicals for binding with the enzyme. If data suggest that interactions between the *N*-methyl carbamates other than dose-additive ones are observed, these will be included in future modeling efforts.

2.2 PBPK/PD Model Parameters

Parameters for PBPK models include three distinct types of data: physiological, physiochemical, and biochemical. The physiological data are independent of the chemical being modeled and refer to such things as organ volumes and blood flows. Distribution within, between and among organs, tissues, and fluid is modeled according to compartmental volumes, blood flow rates, and blood tissue partitioning. Compartments are modeled in ERDEM based on the information available for the exposure to a particular chemical or chemicals and the metabolites. The compartments used for a metabolite may be a subset of those used for the parent chemical.

2.2.1 Physiological Parameters

The body volume is determined for each species, where the rat values were measured in the experimental studies, and human values are based on age. The compartment volumes are expressed as a percentage of the body volume (Table 3). These compartments are the components that are active in the carbaryl model in ERDEM (Figure 5).

Table 3. Volumes of Compartments for Humans by Percentage for PBPK Modeling with ERDEM

	rat	human	
Ages	adult	3	9
Volume of the Body (kg)[a]	as measured	15	20.4
Compartments (% of Volume of the Body)			
Arterial Blood	1.75	1.75	1.75
Brain [f]	1.21	2.1	2.1
Dermis [b]	5.1	5.1	5.1
Fat [c,g]	6	11.5	11.5
GI Tract Walls [h] (not including stomach)	1.7	1.7	1.7
Kidney [b,h]	0.9	0.4	0.4
Liver [d,h]	3.55	2.6	2.6
Portal Blood	0.5	0.5	0.5
Rapidly Perfused Tissue [d]	1.24	3	3
Slowly Perfused Tissue [e]	73.9	67.2	67.2
Stomach Wall [h]	0.4	0.4	0.4
Venous Blood	3.75	3.75	3.75

a. Assume density of 1 L/kg
b. Value from Corley *et al.* (1990)
c. Boot *et al.*, 1997, the age range is 4-21 years in both males and females
d. Fisher *et al.* (1998) Adjusted based on fat volume percentage.
e. Value estimated from the Fat content using Fisher *et al.* (1998)
f. Estimated from many sources, Milner (1990)
g. Fisher *et al.* 1991
h. ILSI 1994

Cardiac output is determined for each species and human demographic group. The compartment blood flows are specified as a percentage of the cardiac output. The compartments requiring blood flow input are the brain, liver, kidney, fat, dermis, slowly perfused tissue (muscle), rapidly perfused tissue, and the walls of the GI tract. The same blood flow percentages are used for each age group (Table 4).

Table 4. Blood Flows (Percentage of Cardiac Output)

	rat	**human**	
Age	adult	3 Years	9 Years
Cardiac Output (L/hr)[a,c]	5.66	303	337
Compartment	**Blood Flow by Compartment- Percentage of Cardiac Output**		
Brain [b,d]	3	10	10
Dermis [b]	7.4	7.4	7.4
Fat [b,c]	9	5	5
GI Tract Wall [e] **(not including stomach)**	9.4	9.4	9.4
Kidney [b,d]	17.4	13.5	13.5
Liver [b,c]	20	20.8	20.8
Rapidly Perfused Tissue [b,c]	17.7	17.8	17.8
Slowly Perfused Tissue [b,c]	15	15	15
Stomach Wall [e]	1.1	1.1	1.1

a. Agata et al (1994), Schmitz et al, (1998), See Appendix C
b. Fisher *et al.* (1998). No age adjustment was made for human blood flow percentages.
c. Fisher *et al.* 1991
d. Keys *et al.* 2003
e. ICRP 2002

2.2.2 Physiochemical Parameters

The distribution of carbamate pesticides and their metabolites between body tissues and sub-cellular organelles is largely dependent upon the manner in which they partition between water and lipids (Poulin and Theil 2000). The partitioning behavior has been associated with the chemical structure, enabling parameter estimates from quantitative structure-activity relationships (QSAR). The derivation of carbaryl specific tissues to blood partition coefficients is

examined in Appendix D. A summary of partition coefficients for each physiological compartment in relation to the blood flow are presented in Table 5.

Table 5. Partition Coefficients for Carbaryl and Metabolites

	Chemical					
Compartment to Venous Blood	**Carbaryl**	**4-OH carbaryl**	**3,4 DIOH carbaryl**	**5,6 DIOH carbaryl**	**Naphthol**	**3,4 DIOH Naphthol**
Brain/Blood [b]	1	1	1	0.1	1	0.3
Dermis/Blood	5.45[a]	n/a	n/a	n/a	n/a	n/a
Fat/Blood	5.5[b]	4.81[a]	5.07[a]	0.17[a]	10[b]	0.31[a]
GI/Blood [c]	4.11	2.12	2.18	0.84	1	0.9
Kidney/Blood	4.11[a]	2.12[a]	2.18[a]	0.84[a]	1[b]	0.9[a]
Liver/Blood	4.41[a]	2.2[a]	2.27[a]	0.78[a]	1[b]	0.84[a]
Rapidly Perfused Tissue/Blood	1.5[b]	2.12[c]	2.18[c]	0.84[c]	1[b]	0.9[c]
Slowly Perfused Tissue/Blood	1[b]	1.55[a]	1.59[a]	0.81[a]	1[b]	0.84[a]

a. Calculated using QSAR techniques of Poulin and Theil (2000), see Appendix 4.
b. Based on consistency with pharmacokinetic data (Table 5) and QSAR considerations
c. Same as kidney (other rapidly perfused tissue)
n/a. The Dermal compartment is not active for this chemical.

The tissue:blood partition coefficients for the other metabolites and tissues were assumed to be 1, except that the brain:blood value was set to a low value (0.1) for the glucuronides. The partition coefficients for the downstream metabolites have a minor impact on the simulation results relative to the ^{14}C measurements.

The QSAR predictions based on tissue composition are typically within a factor of 3 of the *in vitro* measured value (Poulin and Theil 2000, Payne and Kenny 2002). The values in Table 5 that are based on the pharmacokinetic data are within a factor of 3 of the QSAR predicted value, except for the brain:blood partition coefficients that are significantly less than the QSAR predicted values. Large disagreements between the actual and QSAR values have been attributed to active transport mechanisms at the blood:barrier (Liu *et al.* 2004), but this phenomenon has not been studied for carbaryl or its metabolites.

2.2.3 Biochemical Parameters

The biochemical parameters include the rate constants that describe the rate at which chemical ADME occurs. These parameters have been fit to available pharmacokinetic studies in rats, and scaled to humans as described previously (Section 2.1.2). The studies are listed in Table 1.

Chemical absorption parameters were estimated based on the rate of appearance of ^{14}C or carbaryl in blood. The fast appearance after oral dosing (Figure 1) indicates that a significant amount of the carbaryl dose is absorbed in the stomach. The data from bile cannulated rats (Marshall and Dorough 1979) indicate that reabsorption of the glucuronides occurs more slowly than the parent compound. Dermal absorption occurs on a slower time-scale (Figure 2), and for modeling purposes, is assumed to occur through a depth of 1 cm of skin. The parameters associated with absorption are shown in Table 6.

Table 6. Carbaryl absorption parameters

Parameter	Value	Units
Carbaryl absorption rate (stomach)	27.3	$1/(h\text{-}kg^{0.25})$
Food flow, stomach to remaining GI	0.0436	$L/(h\text{-}kg^{0.74})$
Carbaryl absorption rate (GI)	10	$1/(h\text{-}kg^{0.25})$
Glucuronide recirculation rate, liver to GI through bile	1.5	$1/(h\text{-}kg^{0.25})$
Glucuronide absorption rate (GI)	1	$1/(h\text{-}kg^{0.25})$
Carbaryl dermal permeation coefficient	0.012	cm/h
Effective skin depth	1	cm

The metabolism processes are defined by saturable Michaelis-Menten kinetics. The parameters are the maximum velocity of metabolism (V_{max}) and the Michaelis-Menten constant, K_m.

The total metabolism rate of the parent compound was found to be constrained by the plasma ^{14}C data, and carbaryl-specific data where available. The metabolism to specific chemicals was constrained by the species specific data in tissues, blood, and urine. The reported values in Table 7 reasonably simulate the study results in Table 1. An emphasis was placed on the low-dose studies since those are expected to be closer to the exposures resulting from the turf application.

Table 7. Metabolism Rates for carbaryl in Rats and Humans

Metabolic Reaction	Enzyme	Compartment	V_{max} mM/(hr-kg$^{0.7}$)	K_m (mM)
Carbaryl to 4-OH carbaryl	Cytochrome P450 isozymes	liver	0.021	0.05
Carbaryl to 3,4-diOH carbaryl	Cytochrome P450 isozymes	liver	0.034	0.04
Carbaryl to 5,6-diOH carbaryl	Cytochrome P450 isozymes	liver	0.016	0.04
Carbaryl to 1-naphthol	hydrolases	liver	0.071	0.048
4-OH carbaryl to 4-OH carbaryl glucuronide	UDPGA transferase	liver	0.012	0.01
4-OH carbaryl to 4-OH carbaryl sulfate	sulfotransferase	liver	0.002	0.01
3,4-diOH carbaryl to 3,4-diOH 1-naphthol	hydrolases	liver	0.009	0.01
3,4-diOH carbaryl to 3,4-diOH carbaryl glucuronide	UDPGA transferase	liver	0.009	0.01
3,4-diOH carbaryl to 3,4-diOH carbaryl sulfate	sulfotransferase	liver	0.007	0.01
5,6-diOH carbaryl to 5,6-diOH carbaryl glucuronide	UDPGA transferase	liver	0.02	0.01
1-Naphthol to 3,4-diOH 1-naphthol	Cytochrome P450 isozymes	liver	0.073	0.013
1-Naphthol to 1-naphthyl glucuronide	UDPGA transferase	liver	0.09	0.01
1-Naphthol to 1-naphthyl sulfate	sulfotransferase	liver	0.05	0.01
3,4-diOH 1-naphthol to 3,4-diOH 1-naphthyl glucuronide	UDPGA transferase	liver	0.01	0.01
3,4-diOH 1-naphthol to 3,4-diOH 1-naphthyl sulfate	sulfotransferase	liver	0.005	0.01

In vitro assays exist to estimate the metabolism rates (Tang *et al.* 2002, Lipscomb *et al.* 1998), but the appropriate methods and models by which to scale up to the *in vivo* system require further research (Lipscomb *et al.* 1998).

Urinary elimination is also modeled as a saturable process. The rate constants were initially set relative to the metabolism rates, so that the glucuronidated and sulfated conjugates would be rapidly eliminated after formation. The specific values were constrained by the ^{14}C profiles in urine, as well as by the specific metabolite data in urine. Also, the elimination constant values are weakly constrained by the tissue and blood profiles. The elimination parameters for metabolites modeled by ERDEM are presented in Table 8.

Table 8. Parameters for Urine Elimination

Metabolite	V_{max} mM/(hr-kg$^{0.7}$)	K_m **(mM)**
4-OH carbaryl	0.0001	0.005
3,4 DIOH carbaryl	0.0001	0.005
5,6 DIOH carbaryl	0.0001	0.005
Naphthol	0.0002	0.005
3,4 DIOH naphthol	0.001	0.005
Naphthyl sulfate	0.004	0.005
Naphthyl glucuronide	0.004	0.005
3,4 DIOH naphthyl sulfate	0.002	0.005
3,4 DIOH naphthyl glucuronide	0.002	0.005
4-OH carbaryl sulfate	0.002	0.005
4-OH carbaryl glucuronide	0.002	0.005
3,4 DIOH carbaryl sulfate	0.002	0.005
3,4 DIOH carbaryl glucuronide	0.002	0.005
5,6 DIOH carbaryl glucuronide	0.002	0.005

2.2.4 Pharmacodynamic Parameters

The pharmacodynamic parameters for acetylcholinesterase inhibition are based on the kinetic profile of inhibition and recovery. Initial values were based on *in vitro* experiments (Hetnarski and O'Brien 1975), and then refined based on the rat experiments (Table 1). The parameter values must also be consistent with the concentration profiles in the compartments where inhibition occurs. The values for the acetylcholinesterase inhibition parameters (Section 2.1.2.5) are shown in Table 9.

Table 9. Parameters for Acetylcholinesterase Inhibition

Parameter	Value	Units
Brain		
Baseline concentration	3.74×10^{-5}	mM
Inhibition Rate	250	1/(h-mM)
Regeneration Rate	1	1/h
Synthesis Rate	0.01	mM/h
Degradation Rate	0.001	1/h
Blood		
Baseline concentration	1.1×10^{-6}	mM
Inhibition Rate	200	1/(h-mM)
Regeneration Rate	1	1/h
Synthesis Rate	0.01	mM/h
Degradation Rate	0.001	1/h

2.3 Exposure Pathways Following Turf Application

Oral exposure through hand-to-mouth activities and dermal exposure were simulated as representative activities following turf application. Hand-to-mouth activities are characteristic of toddlers, and a 3-year-old subject was implemented. An exposure frequency of 20 events/hour over two hours was simulated, based on the Phase 5 ORE Risk Assessment (U.S. EPA 2003). Hand-to-mouth activities are not expected to be significant for older children, where exposure is expected to occur through the dermal pathway. A 9-year-old subject was implemented to be representative of older children. A skin area of 1000 cm^2 was assumed to be exposed over 3.55 hours of contact time following turf application. The contact time is based on reported values from a biomonitoring study (Bayer 2004c).

In the Bayer 2004 biomonitoring study, the potential absorbed doses of carbaryl to homeowners and residents were evaluated during and following the residential application of carbaryl by measuring urinary pesticide metabolite levels in the applicator, spouse, and children of representative families that use pesticides. Non-professional adult and child volunteers were used to measure carbaryl absorbed doses in homeowners and their families during and after application of Sevin® GardenTech Ready-To-Spray, a formulation of carbaryl. Sites were selected in Missouri and California. Ten families were monitored in Missouri and 13 families were monitored in California. The focus for this assessment was the exposure of the children.

The simulated absorbed doses in this assessment were based on the Bayer 2004 biomonitoring study. Based on the reported values of urinary 1-naphthol in the various children's age groups, distributions were created to establish likely ranges of metabolite excretion that would correspond to ranges of carbaryl absorbed dose (Appendix C). The data analysis is based on the Missouri cohort

since their application behavior was consistent with the label instructions of 4 lbs a.i./acre. The Missouri group applied 2.3-6.5 lbs a.i./acre, compared to 2.0 to 163 lbs a.i./acre in California.

After 4 days, the excreted mass for the 99.9%ile of the 4-5 year old group is 1.8 mg carbaryl equivalents, and 2.5 mg carbaryl equivalents for the 9-12 year old group. The 4-5 year old group is assumed to be representative of toddler exposure, including age 3. For the simulations, carbaryl doses that resulted in similar excretion levels were applied.

The proposed simulations are intentionally conservative for the dose metric of brain cholinesterase inhibition. By assuming continuous turf exposure over the estimated duration, as opposed to distributing the exposure duration over several periods during the day, higher peak carbaryl concentrations are possible. The excretion data actually imply that the exposure is spread over the observation period since a plateau in metabolite levels is not clearly reached after 4 days (Appendix C); the excretion of carbaryl from a single event is expected to occur within 1-3 days (Knaak *et al.* 1965, Benson and Dorough 1984). Also, the source of all metabolites is assumed to be from exposure events associated with activities on the carbaryl-treated turf, but non-zero metabolite levels on day 0 (pre-treatment) indicate that other exposures, including to non-carbaryl sources of 1-naphthol, may be occurring (Appendix C). These other exposures would contribute to the total amount of carbaryl absorbed, but the peak carbaryl values in brain, and thus the maximum acetylcholinesterase inhibition, would be reduced.

3.0 RESULTS

3.1 Overview

A robust PBPK model enables the estimation of relevant dose metrics for a variety of exposure scenarios in different populations. For carbaryl, the brain and blood concentrations, and degree of acetylcholinesterase inhibition in those compartments are the metrics of interest. The PBPK model was designed to predict those values for scenarios associated with turf post-application activities for children.

The PBPK model was first developed to be consistent with the rat data (Table 1). The physiologic parameters were implemented for the rat, and the kinetic parameters were estimated based on the experimental data.

The human scenarios were then implemented by substituting human physiologic parameters in the PBPK model. The kinetic parameters were appropriately scaled as described in Section 2.1.2. The oral hand-to-mouth and dermal exposure scenarios were implemented for children, and the degree of acetylcholinesterase inhibition and tissue concentrations were evaluated.

3.2 Rat Model

The PBPK model simulates results consistent with the available data. These data include studies published in the literature and those delivered to the U.S. EPA by registrants (Table 1). Priority was given to the studies at lower doses, since exposures following turf application will likely be low relative to the laboratory setting.

Intravenous (IV) dosing experiments enable the evaluation of the model distribution, metabolism, and excretion behaviors independent of the absorption characteristics. IV doses of approximately 1 and 10 mg/kg of ^{14}C carbaryl (ring label) were administered to rats, and radioactive residues were measured in a variety of tissues (Bayer 2004a).

Representative comparisons of the PBPK model to the experimental data are shown in Figures 7 and 8. The complete set of simulation charts is in Appendix E.

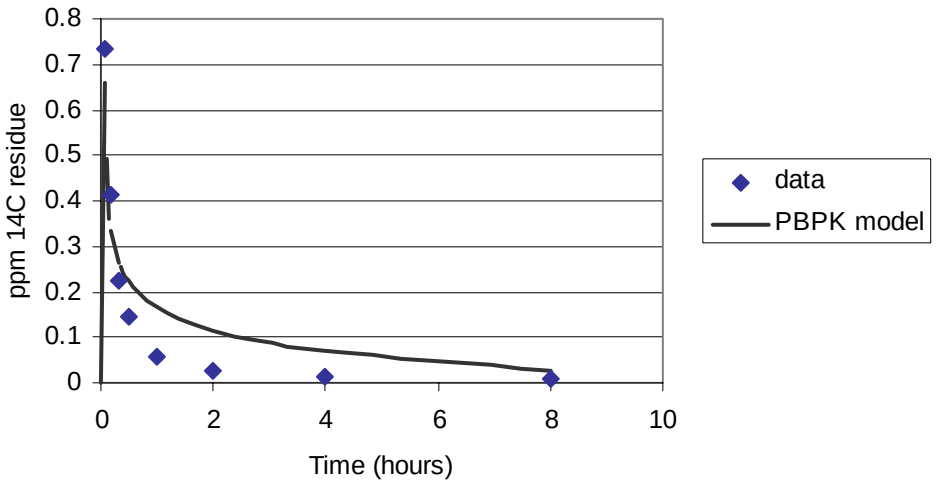

Figure 7. ^{14}C concentration in brain after IV dose of 0.8 mg/kg carbaryl in rats. Data from Bayer 2004a, average of 4 animals at each sample time.

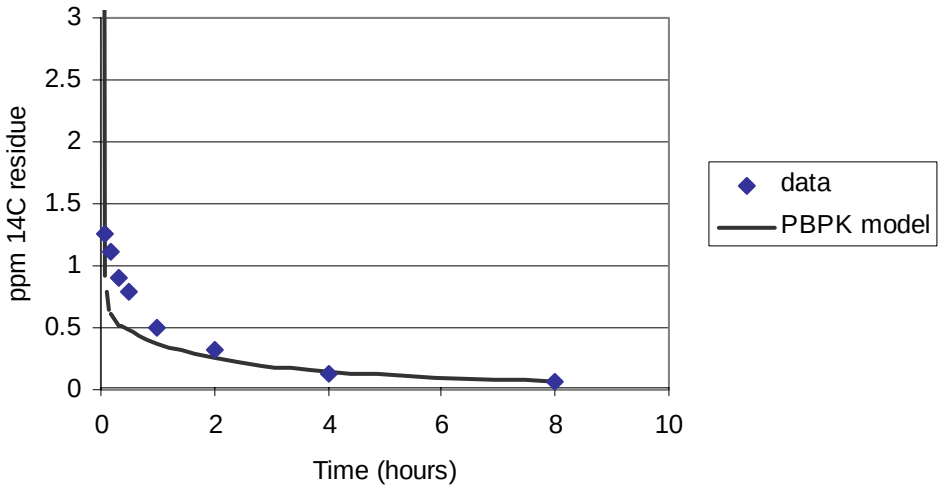

Figure 8. ^{14}C concentration in blood after IV dose of 0.8 mg/kg carbaryl in rats. Data from Bayer 2004a, average of 4 animals at each sample time.

The ^{14}C data were reported in ppm (Bayer 2004a). The PBPK model tracks ^{14}C based on chemical species, resulting in units of mmol/L. The model results were converted to ppm by multiplying by the molecular weight of carbaryl for comparison to the data.

The rat PBPK model shows similar consistency with oral studies, conducted near the NOAEL level of 1 mg/kg (U.S. EPA) and also at 8.45 mg/kg. One exception is that brain ^{14}C concentrations are over-predicted (Figure 9).

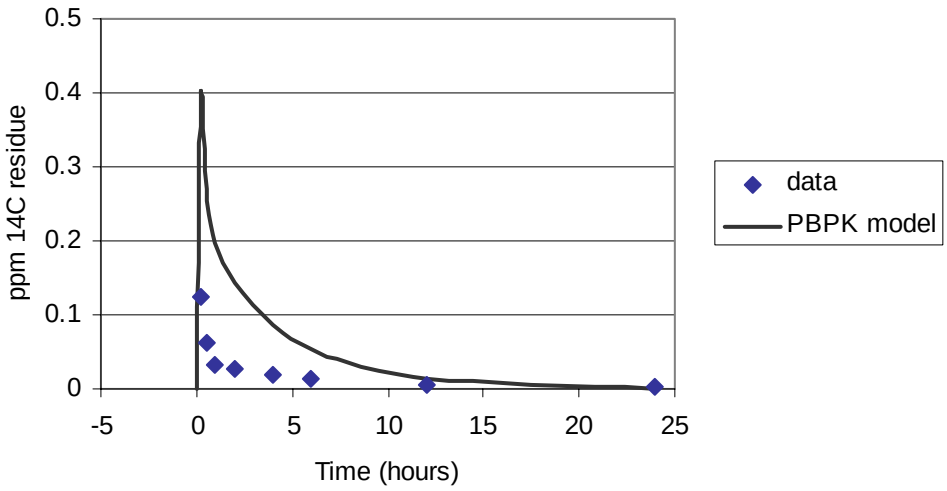

Figure 9. Brain ^{14}C concentration after oral dose of 1 mg/kg carbaryl in rats. Data from Bayer 2004a, average of 4 animals at each sample time.

By reducing the partition coefficient for carbaryl and its major metabolites to less than or equal to one (Table 5), the low dose data were better simulated. The equal partitioning between blood and brain (partition coefficient = 1) is inconsistent with the known physical properties of carbaryl, so the partition coefficient values were not reduced to less than 1.

Carbaryl was measured for the higher dose oral study, where brain concentrations of the parent compound were reasonably simulated (Figure 10), while blood concentrations were predicted but not detected (Figure 11).

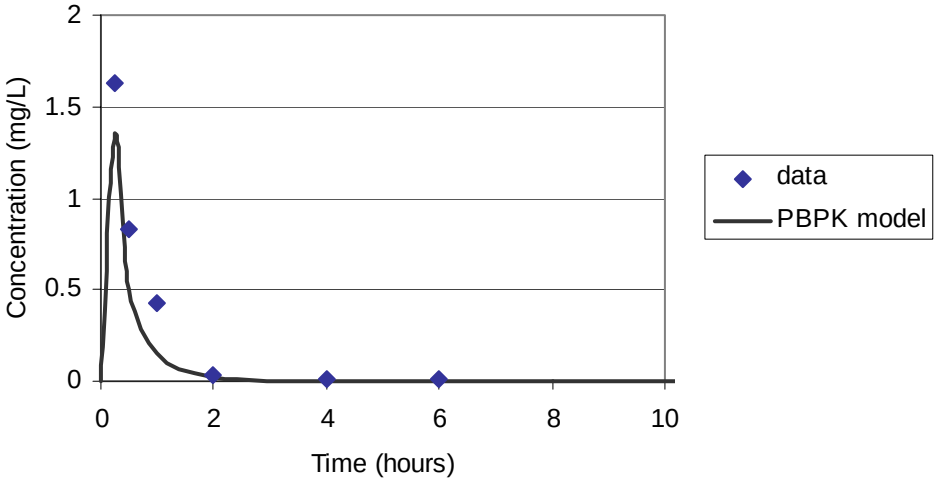

Figure 10. Brain carbaryl concentration after oral dose of 8.45 mg/kg carbaryl in rats. Data from Bayer 2004a, average of 4 animals at each sample time.

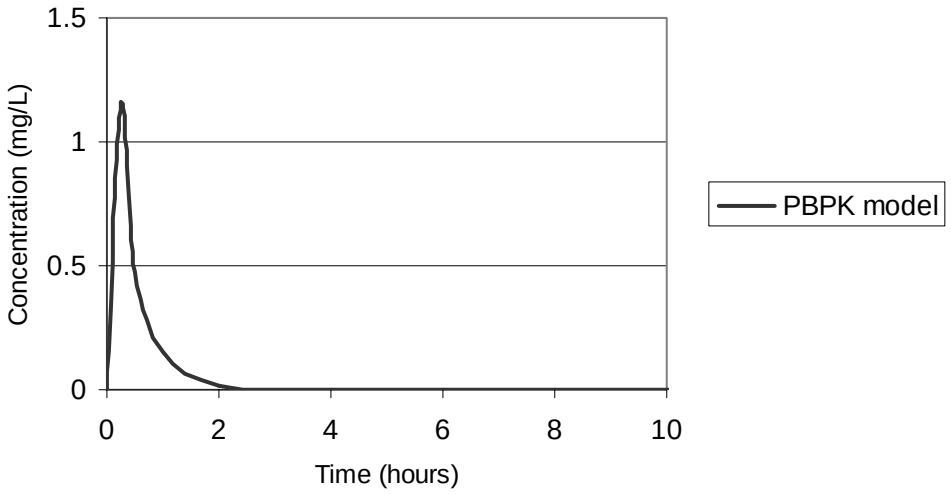

Figure 11. Blood carbaryl concentration after oral dose of 8.45 mg/kg carbaryl in rats. Carbaryl was not detected in blood at 15 minutes, approximately the time of the PBPK model predicted peak (Bayer 2004a).

Dermal exposure studies in rats of 1.74 mg/20 cm^2 (Knaak *et al.* 1984) and 0.793 mg/12.5 cm^2 (Cheng 1994) were evaluated to assess the dermal permeability of carbaryl. Representative comparisons to the data show that the model predicts the kinetics of absorption (Figures 12 and 13). Similar fits are observed with data from other dermal studies and for other compartments. Complete comparisons are in Appendix E.

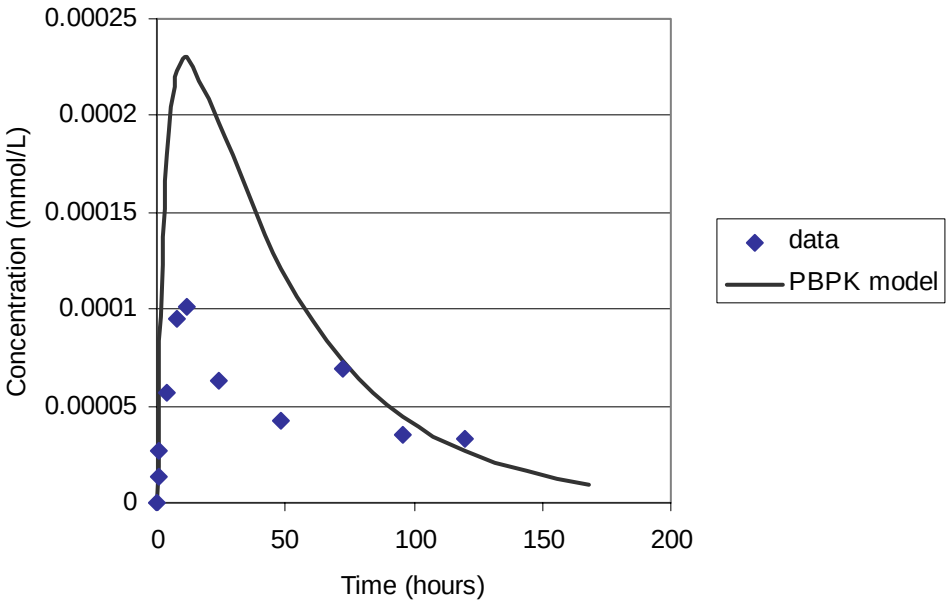

Figure 12. Blood ^{14}C concentrations following 1.74 mg/20 cm^2 carbaryl dermal application on rats. Data from Knaak *et al.* 1984, average of 3 animals at each sample time.

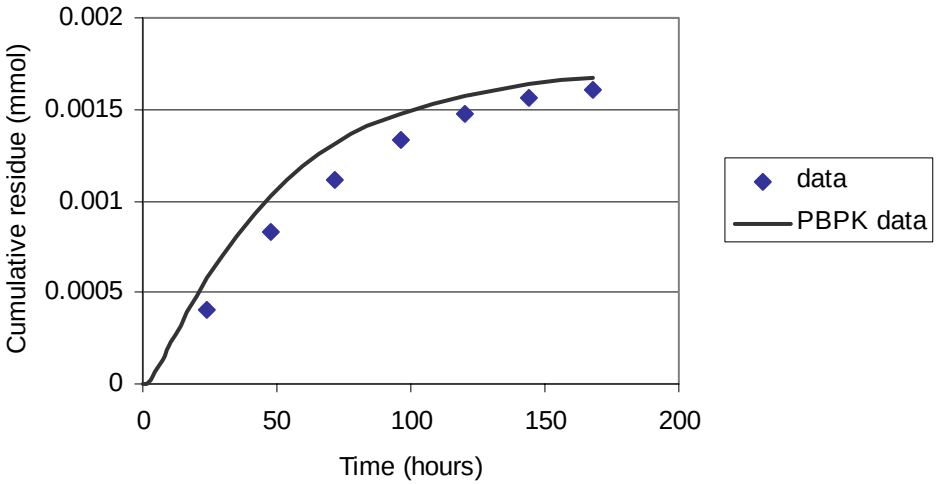

Figure 13. Cumulative ^{14}C residues in urine following 1.74 mg/20 cm^2 carbaryl dermal application on rats. Data from Knaak *et al.* 1984, pooled urine from 3 animals.

A metabolism study in rats measured concentrations of specific metabolites in urine after intraperitoneal (IP) dosing of rats at 20 mg/kg (Knaak *et al.* 1965). The model simulates the results for the identified metabolites (Figure 14). The excretion of glucuronides is slower than sulfates due to enterohepatic recirculation.

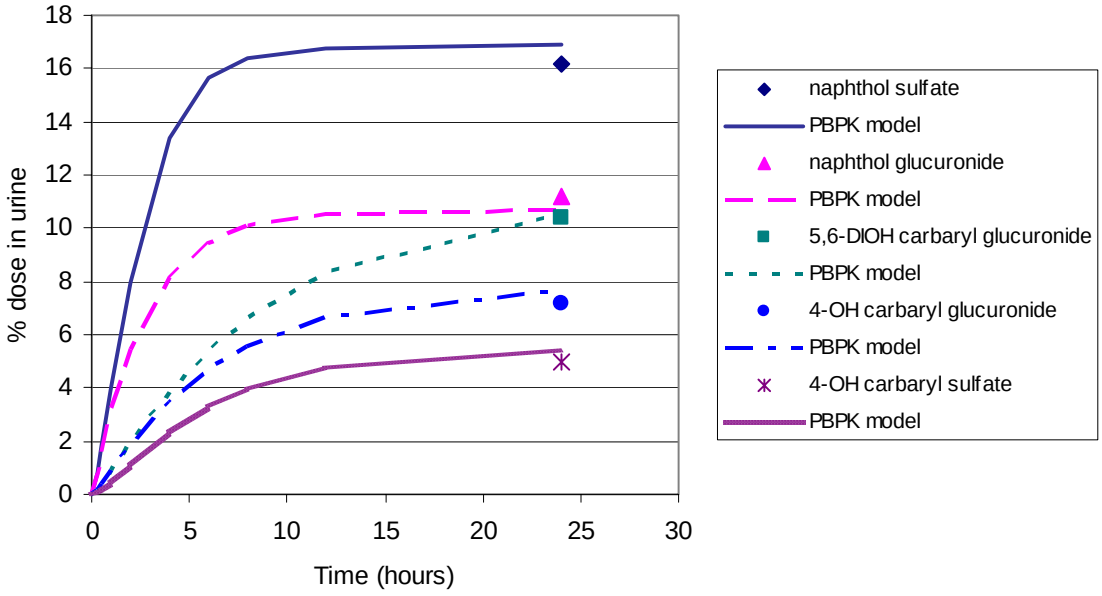

Figure 14. Excretion of metabolites following 20 mg/kg IP dosing of carbaryl in rats. Data from Knaak et al 1965, pooled urine from 3 animals.

Oral studies in rats, separate from the ones discussed above, measured the degree of cholinesterase inhibition in blood and brain (Brooks and Broxup 1995a,b). The lowest dose tested was 10 mg/kg, which resulted in measurable inhibition followed by recovery within 8 hours. These dynamics were reproduced by the model (Figures 15 and 16). The data were given by inhibition in each brain region, and were averaged for comparison to the PBPK model.

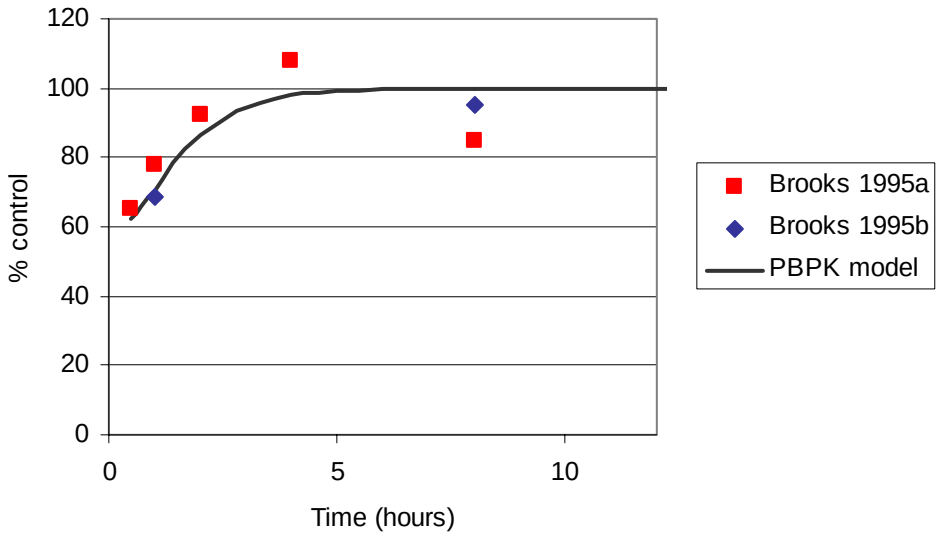

Figure 15. Blood acetylcholinesterase inhibition after 10 mg/kg carbaryl oral dose in rats. Data are average of 12 animals (6 male, 6 female) at each sample time.

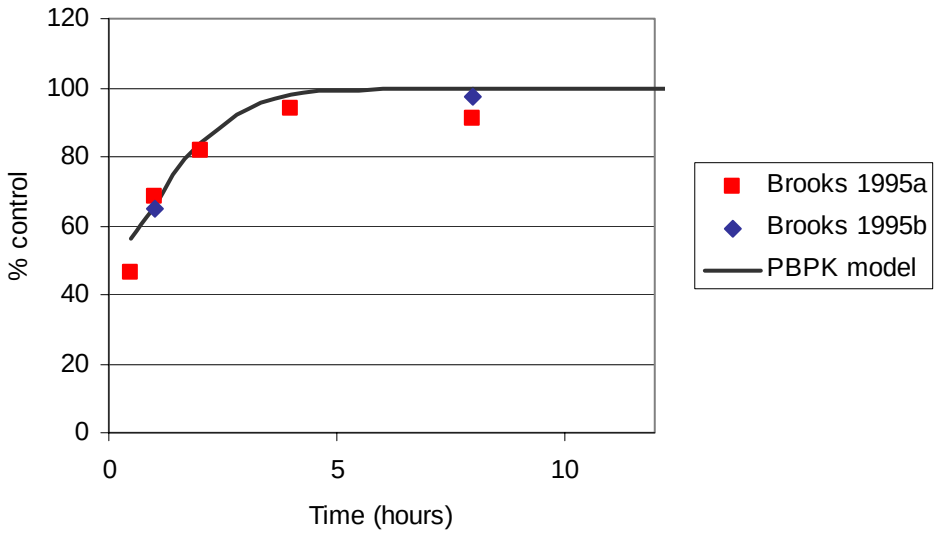

Figure 16. Brain acetylcholinesterase inhibition after 10 mg/kg carbaryl oral dose in rats. Data are average of 12 animals (6 male, 6 female) at each sample time.

A combined low dose oral and dermal exposure study in rats was conducted to simulate conditions corresponding to hypothesized repeated hand-to-mouth activities in toddlers (Bayer 2004a). Two oral doses of 0.075 mg/kg were given an hour apart, while a 0.75 mg/kg dermal dose was applied for hours 0 to 2. The

model simulations are consistent with the data, showing modest under-prediction of the blood ^{14}C data, and over-prediction of the brain ^{14}C and carbaryl concentrations (Figures 17-19).

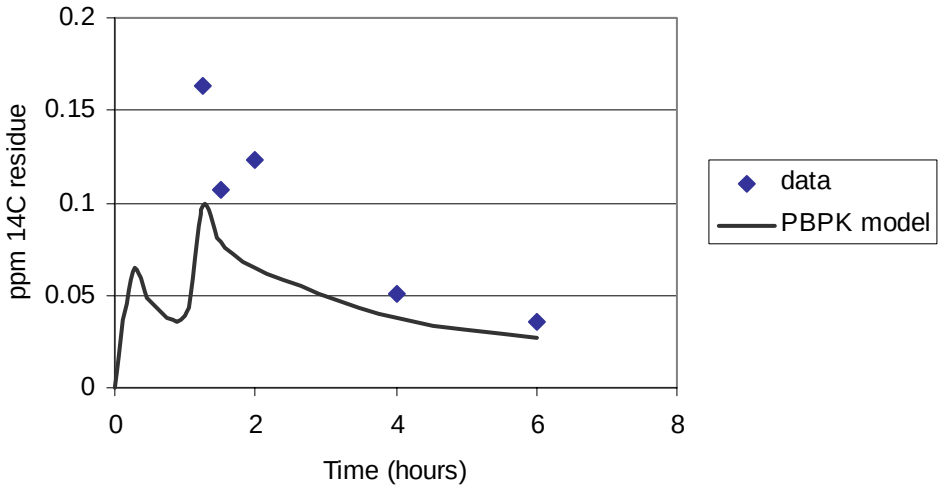

Figure 17. Blood ^{14}C concentration following dermal and repeated oral dosing of carbaryl in rats. Data from Bayer 2004a, average of 4 animals at each sample time.

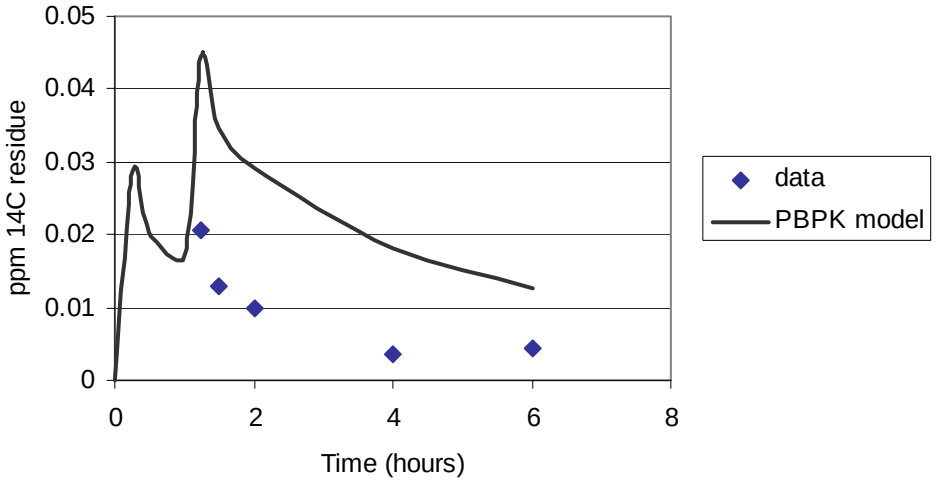

Figure 18. Brain ^{14}C concentration following dermal and repeated oral dosing of carbaryl in rats. Data from Bayer 2004a, average of 4 animals at each sample time.

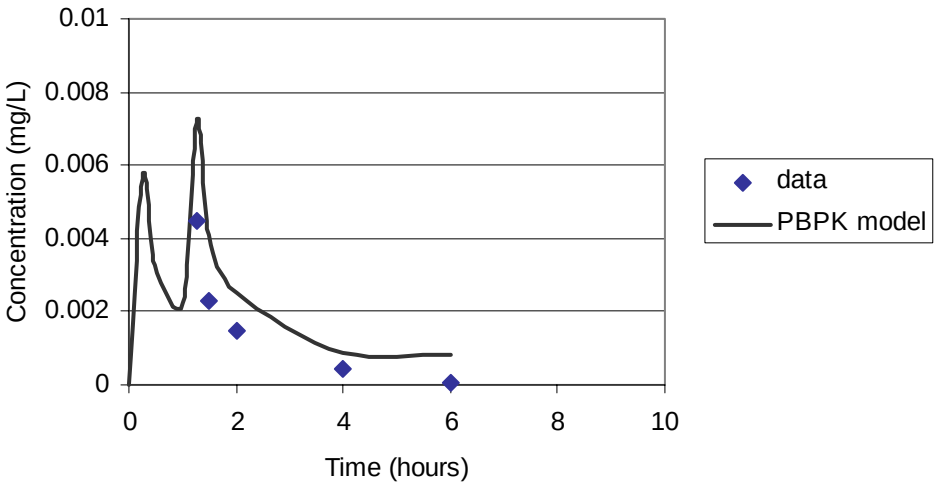

Figure 19. Brain carbaryl concentration following dermal and repeated oral dosing of carbaryl in rats. Data from Bayer 2004a, average of 4 animals at each sample time.

Additional simulations (not shown) without the dermal exposure showed results nearly identical to Figures 17 to 19. This indicates that in the hand-to-mouth exposure scenario, the oral route is the dominant route of exposure.

The rat model sufficiently captures the behavior of carbaryl, including the important dose metrics for evaluation of the post-turf application exposure scenario. The simulations are consistent with the available data across studies and measurements. Additional comparisons to data may be found in Appendix E. Exact matches of simulations to data would not be expected based on the diverse studies and experimental and animal variability. One unexpected difference is the non-detection of carbaryl in blood 15 minutes after an oral dose of 8.45 mg (Figure 11). The non-detection of carbaryl in the experimental study appears to be inconsistent with the corresponding brain carbaryl concentrations (Figure 10), and expected blood acetylcholinesterase inhibition predicted by the PBPK model and observed in a separate study under similar dosing conditions (Figure 16). Aside from that particular measurement, the model describes the absorption and distribution of carbaryl to the brain, where acetylcholinesterase inhibition – the dose metric of interest – occurs, and simulates the subsequent elimination of carbaryl and its metabolites.

3.3 Oral Exposure by Hand-to-Mouth Activities

An oral exposure scenario by hand-to-mouth activities was simulated for a 3-year-old child. The rat model was converted to an age-specific human model by implementing the appropriate physiological parameters (Section 2.2.1) and scaling the kinetic constants (Section 2.2.3) for a 3-year-old child.

Starting at time 0, two hours of hand-to-mouth activity occurred at 20 events/hour. The simulation duration was for 4 days from the beginning of the activity, over which the cumulative urine excretion and tissue concentrations were tracked.

3.3.1 Estimates of absorbed dose from oral exposure

The absorbed dose associated with the oral hand-to-mouth exposure is based on the biomonitoring study (Bayer 2004b, Appendix C). For the assumed scenario, a magnitude of exposure was chosen to be consistent with the observed excreted mass of carbaryl equivalents.

A total dose of 0.08 mg/kg for the hand-to-mouth events resulted in urine metabolite levels consistent with the 99.9%ile of excreted mass of carbaryl equivalents (Figure 20). Similar to the oral bolus studies, the urinary profiles of metabolites indicate significant elimination within a day.

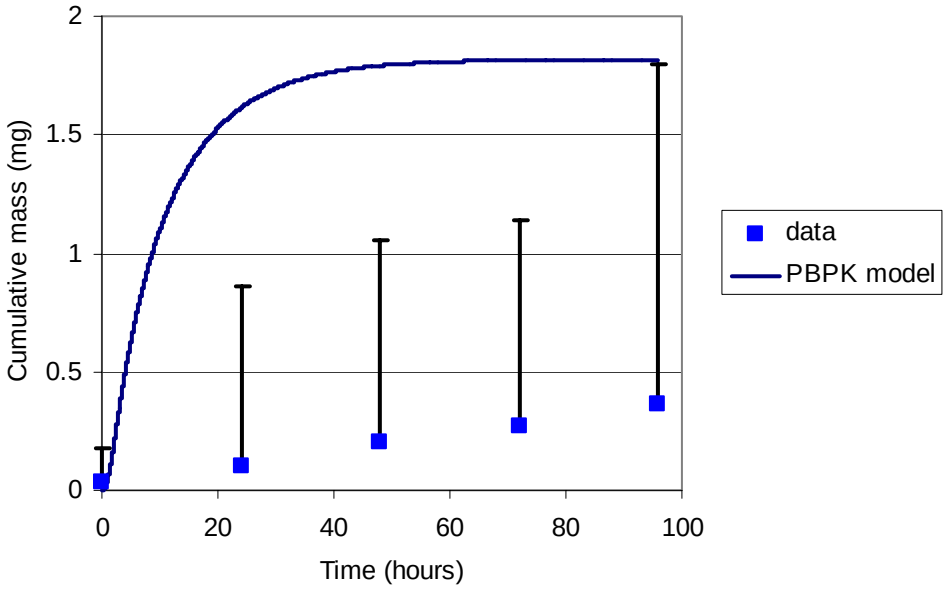

Figure 20. Cumulative excretion of carbaryl equivalents in urine from 3 year olds following turf application. The error bars represent the 99.9% range. The PBPK model assumes oral exposure through hand-to-mouth activities.

The plateau in the metabolite levels is reached earlier than in the biomonitoring study (Figure 20). As discussed in section 2.3, this simulation is a conservative scenario. By assuming that the entire absorbed dose occurs in a single 2 hour activity period, the peak tissue concentrations will be highest.

3.3.2 Estimates of blood and tissue concentrations following oral exposure

The concentration of carbaryl in blood increases over the exposure duration, then rapidly decreases, and a similar profile is observed in other tissues (Figure 21).

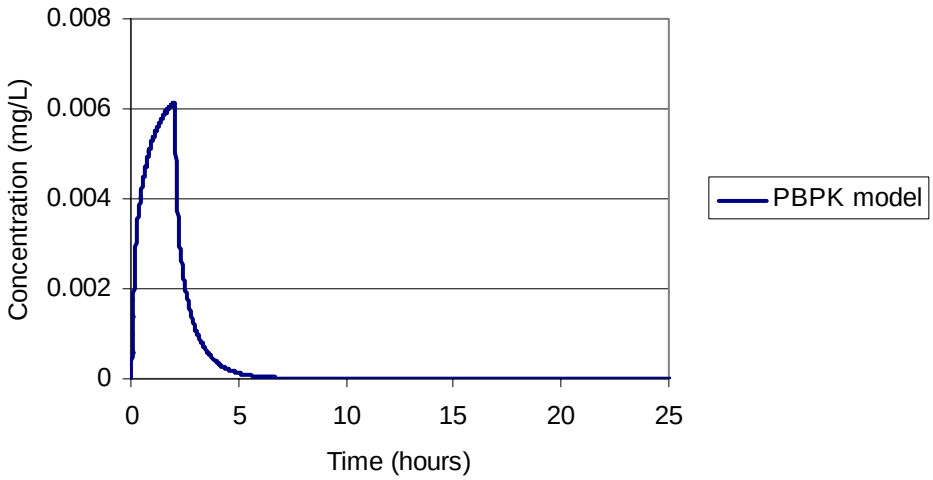

Figure 21. Carbaryl concentration in venous blood in 3 year olds following turf application. The PBPK model assumes oral exposure through hand-to-mouth activities.

The peak concentrations of carbaryl in brain and blood determine the magnitude of acetylcholinesterase inhibition (Figure 22). The scale in Figure 22 only spans from 90-100% so that the dynamics of the slight change can be visualized. The level of inhibition for the oral hand-to-mouth scenario is minimal (Table 10).

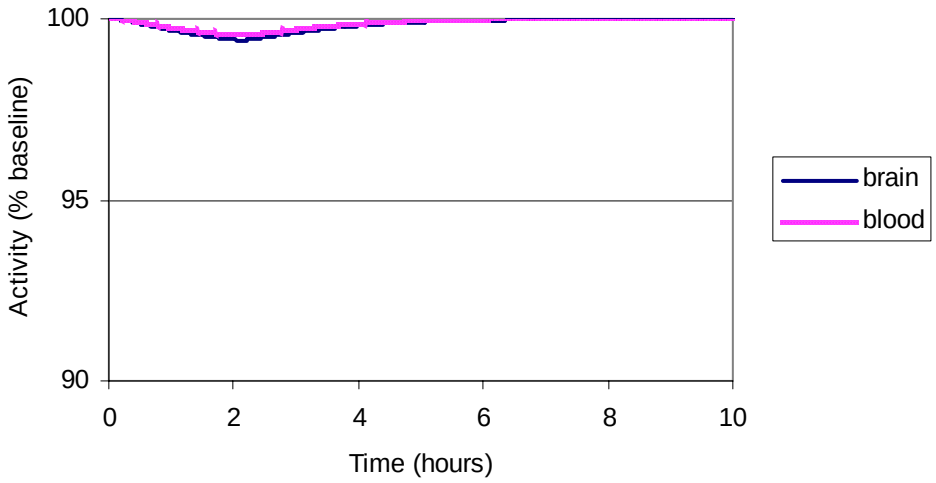

Figure 22. Acetylcholinesterase activity in brain and blood in 3 year olds following turf application. The PBPK model assumes oral exposure through hand-to-mouth activities.

Table 10. Blood and brain carbaryl concentrations and acetylcholinesterase activity.

Compartment	Peak carbaryl concentration (mg/L)	Acetylcholinesterase activity (% baseline)
Blood	0.0061	99.4
Brain	0.0061	99.5

3.4 Dermal Exposure

A dermal exposure scenario was simulated for a 9-year-old child. The rat model was converted to an age-specific human model by implementing the appropriate physiological parameters (Section 2.2.1) and scaling the kinetic constants (Section 2.2.3) for a 9-year-old child.

At time 0, a mass of carbaryl is applied on the exposed skin surface of 1000 cm^2, and is washed off after 3.55 hours. This is intended to simulate the average of transfer and rub-off activities to the lower arms and legs (including hands and feet) over the duration of activity on the treated turf. The simulation duration was for 4 days from the beginning of the activity, over which the cumulative urine excretion and tissue concentrations were tracked.

The profile of the amount of carbaryl on skin over the exposure period shows slow absorption until it is washed-off at the end of the activity (Figure 23). Since the kinetics of absorption are slow, the representation of average dermal

exposure through an initial application is a suitable approximation of the expected variable profile due to transfer and removal events.

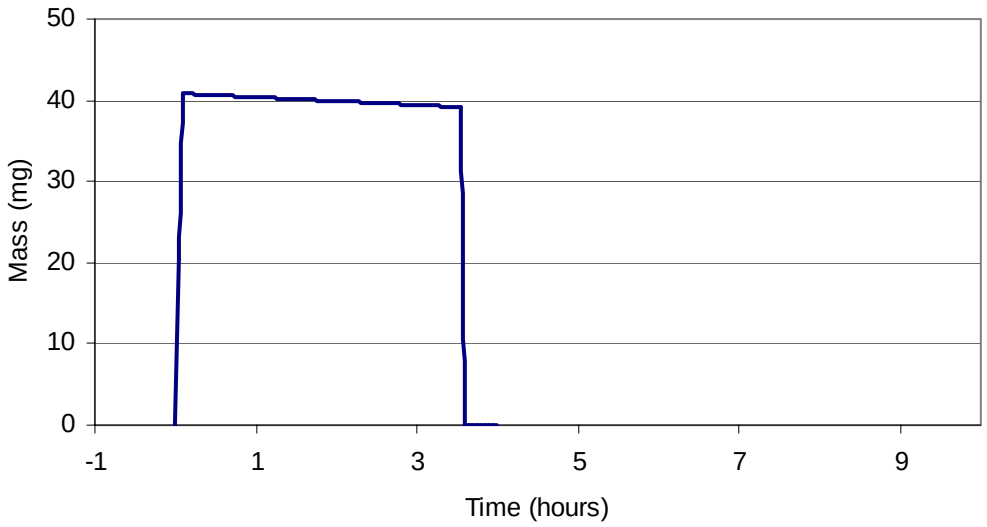

Figure 23. Modeled carbaryl mass on skin over exposure period.

3.4.1 Estimates of absorbed dose from dermal exposure

The absorbed dose associated with the dermal exposure scenario is based on the biomonitoring study (Bayer 2004b, Appendix C). For the assumed scenario, a magnitude of exposure was chosen to be consistent with the observed excreted mass of carbaryl equivalents.

A dose of 2 mg/kg was applied on the skin surface, and the total amount absorbed before wash-off is 1.69 mg, or a dose of 0.083 mg/kg. This dose resulted in urine metabolite levels consistent with the 99.9%ile of excreted mass of carbaryl equivalents (Figure 24). Similar to the oral bolus studies, the urinary profiles of metabolites indicate significant elimination within a day.

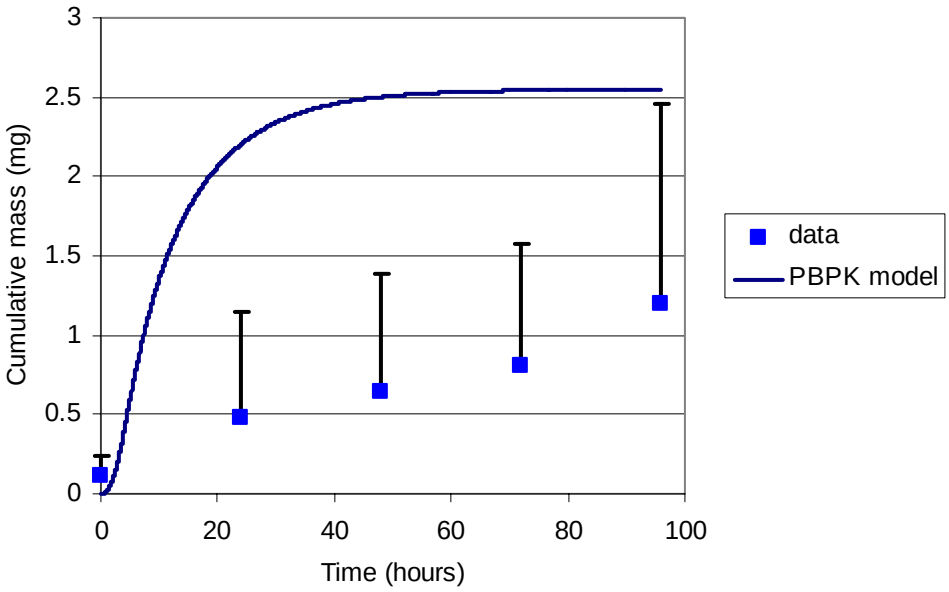

Figure 24. Cumulative excretion of carbaryl equivalents in urine from 9 year olds following turf application. The error bars represent the 99.9% range. The PBPK model assumes dermal exposure by contact with treated surfaces.

The plateau in the metabolite levels is reached earlier than in the biomonitoring study (Figure 24). As discussed in section 2.3, this simulation is a conservative scenario. By assuming that all of the absorbed dose occurs in a single activity period, the peak tissue concentrations will be highest.

3.4.2 Estimates of blood and tissue concentrations following dermal exposure

The concentration of carbaryl in blood increases over the exposure duration, then rapidly decreases, and a similar profile is observed in other tissues (Figure 25).

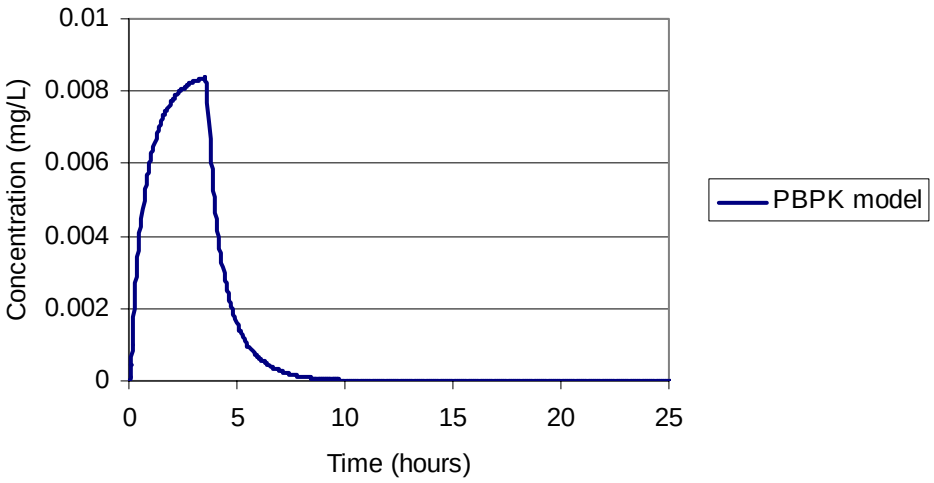

Figure 25. Carbaryl concentration in venous blood in 9 year olds following turf application. The PBPK model assumes dermal exposure by contact with treated surfaces.

The peak concentrations of carbaryl in brain and blood determine the magnitude of acetylcholinesterase inhibition (Figure 26). The scale in Figure 26 only spans from 90-100% so that the dynamics of the slight change can be visualized. The level of inhibition due to the dermal exposure scenario is minimal (Table 11).

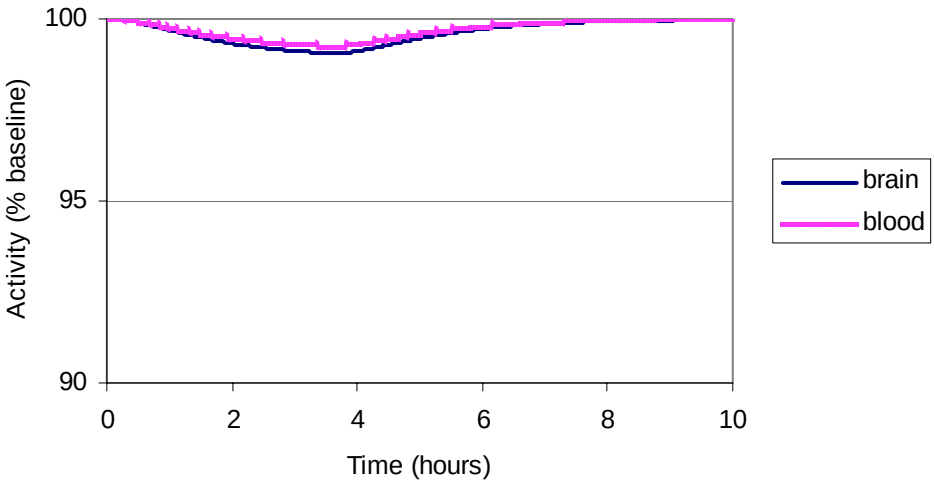

Figure 26. Acetylcholinesterase activity in brain and blood in 9 year olds following turf application. The PBPK model assumes dermal exposure by contact with treated surfaces.

Table 11. Blood and brain carbaryl concentrations and acetylcholinesterase activity.

Compartment	Peak carbaryl concentration (mg/L)	Acetylcholinesterase activity (% baseline)
Blood	0.0084	99.1
Brain	0.0084	99.2

4.0 DISCUSSION

Note: The results contained in this report are preliminary in nature and do not reflect current OPP and EPA policies regarding evaluation of inter- and intra-species extrapolation, aggregate risk, and application of the FQPA safety factor for potential sensitivity of infants and children.

For the carbaryl exposure simulation, the risk metric of interest was brain acetylcholinesterase inhibition, which is dependent on the peak brain carbaryl concentration. The exposure scenarios were for children following turf application of carbaryl. For both the oral hand-to-mouth scenario, and dermal scenario, minimal cholinesterase inhibition was predicted. This is not surprising, based on the comparison of the peak brain concentrations after exposure relative to the peak brain concentration at the rat no observed adverse effect level (NOAEL) of 1 mg/kg oral (Table 12).

Table 12. Comparison of peak concentrations after turf exposure scenarios to the rat NOAEL level

	Rat 1 mg/kg oral	Oral exposure estimate (3 yr old human)	Dermal exposure estimate (9 yr old human)
Peak brain concentration (mg/L)	0.18	0.0061	0.0084

The confidence in the model predictions, and applicability to the population in general is dependent on the behavior of the outcome metrics across model parameter ranges. The relevant range of values may span the uncertainty or variability space. The model parameters that affect the brain dose metrics are expected to be those associated with the kinetics of acetylcholinesterase inhibition, clearance of carbaryl, and transport to the brain. Parameters that fall into this category include the rate of carbaryl metabolism, blood:brain partition coefficient, blood flow rate to brain, and the rate of acetylcholinesterase inhibition. A formal sensitivity analysis was not performed and may reveal other important variables.

The range of parameter values was based on the likely variability in the human population. Where statistical distributions for the parameters could be established from the literature data, the coefficient of variation was applied relative to the best fit value used in the exposure scenarios (Sections 2.3 and 2.4) to calculate a low and high value. Otherwise, reported limits were used for the investigation. The investigated ranges of parameter values are listed in Table 13, followed by discussion of how each range was established.

Table 13. Investigated parameters and values

Parameter	Best fit	low	high	Variability basis
Blood flow to brain (% Cardiac Output)	10	6.7	12.9	Reference range
Blood:brain partition coefficient	1	0.48	1.52	Observed variability for rat blood:brain, compared with human fat:blood and rat fat:blood
Inhibition rate (mmol/hr)	250	120	530	Observed variability for rat acetylcholinesterase inhibition
Hydrolysis rate (Vmax, mmol/hr/kg)	0.071	0.022	0.22	Observed malathion variability for carboxylesterase
Total oxidation rate (Vmax, mmol/hr/kg)	0.071	0.043	0.12	Observed *in vitro*, and variability for 4-OH formation and 3A4 drugs

For the blood flow to the brain, the range is based on cited limits reported for adults (Altman and Dittmer 1974). The ratio of the high and low values relative to the mean was then applied to the mean values used in each of the child scenarios. For example, the high limit for adults was cited as 67 ml/g/min with a mean of 52 ml/g/min for a high/mean ratio of 1.29. The average % cardiac output to brain for children is 10% (Table 4), so the high investigated value was 12.9%. The additional blood flow was subtracted from the flow to rapidly perfused tissues so the blood flows to the various compartments add to 100%. The low value investigated was 6.7% of cardiac output.

Brain:blood partition coefficients have not been measured for carbaryl in humans or other species, so a distribution in humans is not available. Another chemical where similar data exists was used to estimate a realistic value for the coefficient of variation (COV) in brain:blood partition coefficients. Sato *et al.* 1977 and Simmons *et al.* 2002 measured the brain:blood partition coefficients in rats for trichloroethylene, and reported the means and standard deviations. The COV was applied relative to the fit value used in the initial model (Table 13) to

establish the low and high values to be investigated. Although the data are not human, when the COV in the fat:blood partition coefficients for trichloroethylene are compared between rats (Sato *et al.* 1977, Simmons *et al.* 2002, Koizumi 1989, Barton *et al.* 1995) and humans (Sato *et al.* 1977), the rat COV is larger providing some evidence that the values based on the rat experiments may include the likely human values. The dissimilarity between trichloroethylene and carbaryl, and the low number of subjects in the partition coefficient studies (N=5 for the human study, up to 10 in the rat studies) lowers the confidence in this analysis. However, simulations of this initial range illustrate the importance of this value and related assumptions.

The kinetics of acetylcholinesterase inhibition in the brain were measured in rats by the hydrolysis of acetylthiocholine iodide (Mortensen *et al.* 1998). They modeled the process as saturable (Michaelis-Menten) and reported the Vmax and Km values. Inhibition is modeled as a linear process for lower environmental exposures, so the variability in the quotient of Vmax/Km was calculated as an estimate of the variability of the inhibition rate constant, ki.

The metabolism of carbaryl occurs through two pathways, hydrolysis and hydroxylation (Table 7). Hydroxylation primarily occurs through P450 CYP3A4, and the kinetics were measured *in vitro* (Tang *et al.* 2002). The standard deviation of the log distribution was applied to the model *in vivo* value (Table 7) to establish the investigation range. This range is consistent with the metabolism rate ranges (Hattis, and cited references) of pharmaceuticals known to be metabolized through the CYP3A4 pathway (Flockhart), including alfentanil, diltiazem, fentanyl, haloperidol, midazolam, nifedipine, and triazolam. Carboxylesterase in involved in the hydrolysis pathway (Sogorb *et al.* 2002), so kinetic data from the metabolism of malathion were used to estimate a reasonable range. The importance of carboxylesterase may be inferred from the metabolic interactions for mixtures of carbaryl and malathion (Lechner and Abdel-Rahman 1986). Talcott *et al.* 1977, and Sams and Mason 1999 reported the malathion metabolic activity from individual human liver and serum samples, respectively. The geometric standard deviation is approximately twice as large for metabolism by serum than by liver carboxylesterase (0.25 vs. 0.11), so that value was used to establish the range to be investigated for the hydrolysis pathway for carbaryl (Table 13).

The dependence of the results on a particular parameter value can be evaluated by the change in a dose metric as that value is changed. Each parameter was changed from the best fit value to the low value or high value, while the other parameters were held at the best fit value ('low' and 'high' in Figures 27-30). The dose metrics of acetylcholinesterase inhibition and peak brain carbaryl concentrations were compared to the case where all the parameters were held at their best fit values ('all' in Figures 27-30).

The metabolism rate and brain:blood barrier partition coefficient values impact the brain carbaryl peak concentration. The implemented changes to the brain blood flow and acetylcholinesterase inhibition rates do not affect the peak concentrations for either the hand-to-mouth or dermal exposure scenarios (Figures 27 and 28).

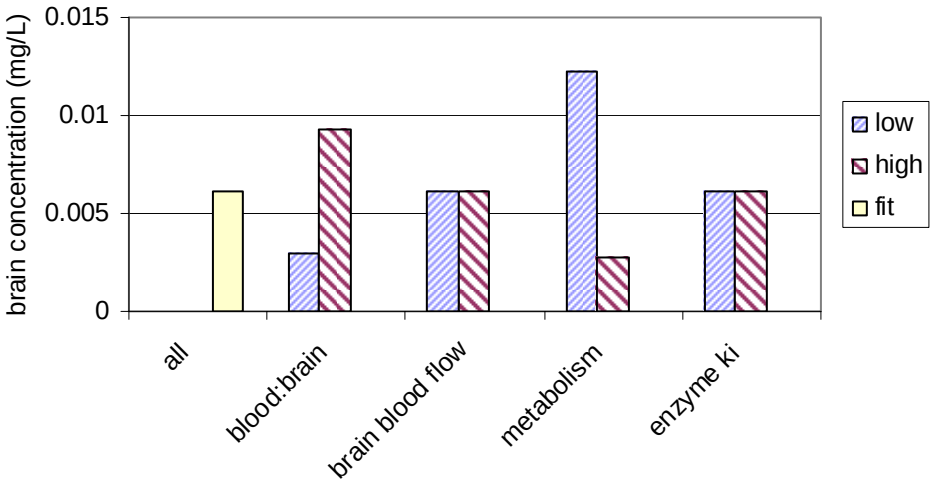

Figure 27. Brain concentrations for different parameter values in 3 year olds following turf application. The PBPK model assumes oral exposure due to hand-to-mouth activity.

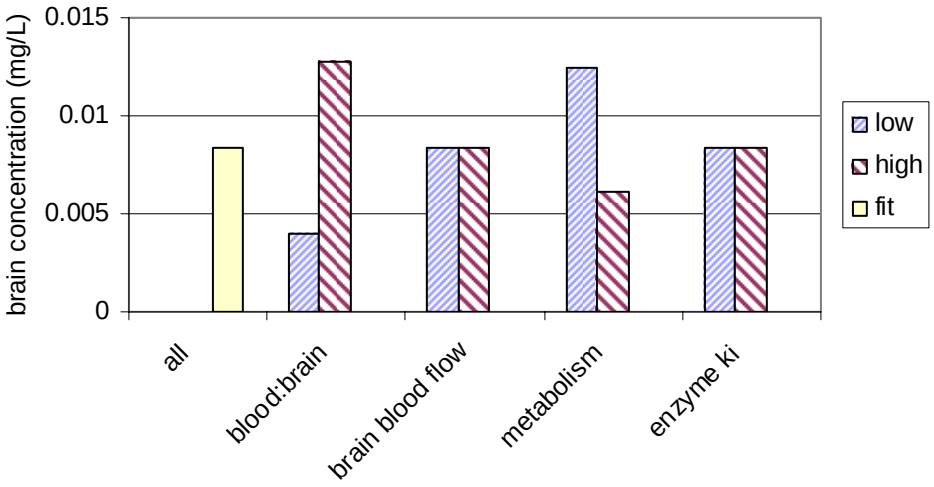

Figure 28. Brain concentrations for different parameter values in 9 year olds following turf application. The PBPK model assumes dermal exposure due to contact with treated surfaces.

Although there are modest changes to the brain concentrations, the maximum brain acetylcholinesterase inhibition levels are not affected. Effectively no

inhibition occurs for either exposure scenario when the various parameter values are applied (Figures 29 and 30).

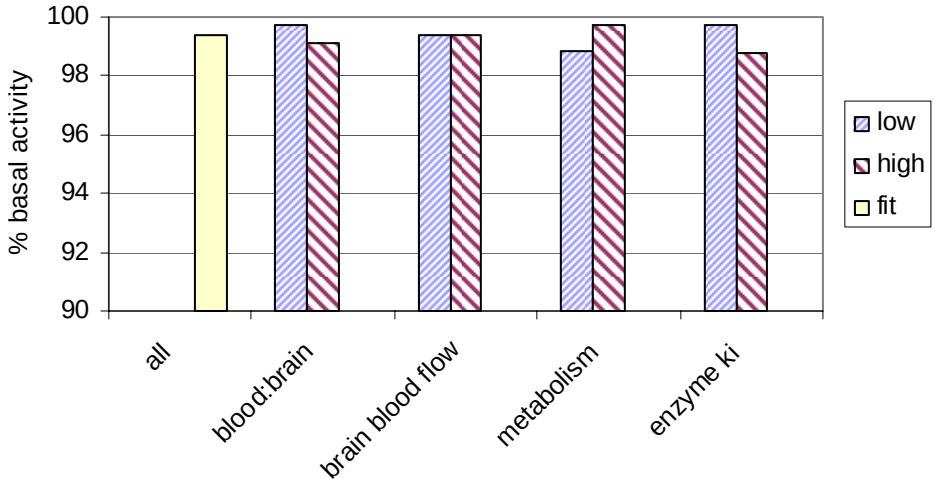

Figure 29. Maximum acetylcholinesterase inhibition for different parameter values in 3 year olds following turf application. The PBPK model assumes oral exposure due to hand-to-mouth activity.

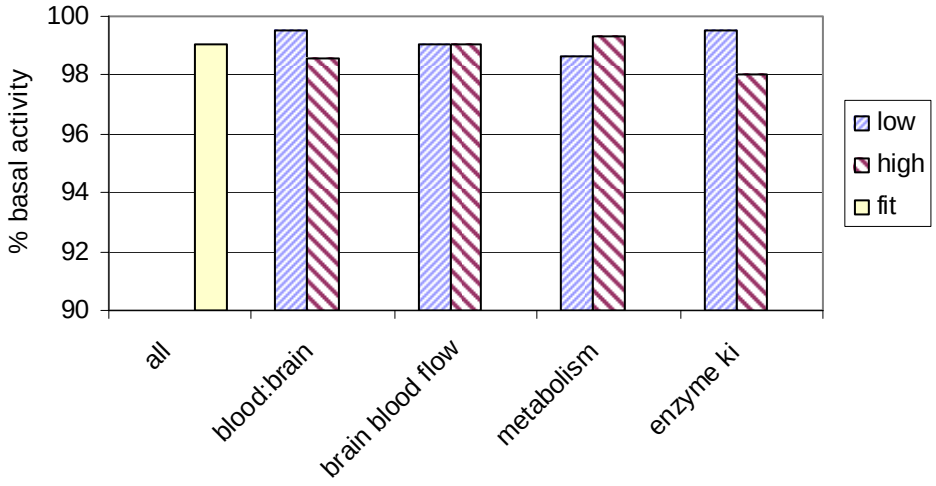

Figure 30. Maximum acetylcholinesterase inhibition for different parameter values in 9 year olds following turf application. The PBPK model assumes dermal exposure due to contact with treated surfaces.

The parameter investigations illustrate the uncertainty in and variability captured by the model for the results in Section 3. The parameters that affect the metrics of interest also highlight important experimental measurements that would increase confidence in the model. Measurements and accurate representation of

distribution of carbaryl to the brain, and of its metabolism in humans, and the associated variability, would reduce uncertainty in the model predictions.

Established methods exist for measuring tissue:blood partition coefficients for non-volatile chemicals (Jepson *et al.* 1994). However, if the active transport mechanisms of the blood-brain barrier are the cause of the low effective partition coefficient value, the model structure would need to be expanded to include them; a perfusion limited description of distribution may not capture the important distribution behavior. The involvement of active transporters may also affect the assumptions for extrapolating the model to children. The partitioning behavior is assumed to be constant for children 3 years and older, but the development of the active transport systems of the blood:brain barrier would need to be considered.

Metabolism in humans remains difficult to estimate, although the *in vitro* studies with specific enzymes provide a basis (Tang *et al.* 2002). The extrapolation to the human *in vivo* scenario remains an area of research (Lipscomb *et al.* 1998). Metabolic studies in adults will likely be applicable, since the P450 metabolic enzyme profile, and metabolism of the few studied substrates, in children older than 1 year is similar to adults (Ginsberg *et al.* 2004).

PBPK modeling techniques offer the promise of interpreting this type of exposure. However, the reliability of the output from such a model is dependent on the necessary input information. Continued development and testing of the model with quality data is necessary to refine the input parameters and values. In this regard, physiological and pharmacokinetic (PK) data are gleaned from *in vivo* and *in vitro* studies as reported in the literature to establish key values for PK parameters and the time course for disposition of the compounds in the body. This is an iterative process. It is anticipated that further refinements will continue to improve and evolve as more reliable data become available. Therefore, the results reported herein reflect the current state of reliability with the understanding that further anticipated refinements may influence the conclusions.

5.0 REFERENCES

Agata Y, Hiraishi S, Misawa H, Hirota H, Nowatari M, Hiura K, Fujino N, Oguchi K, and Horiguchi Y. (1994) Regional Blood Flow Distribution and Left Ventricular Output during Early Neonatal Life: A Quantitative Ultrasonographic Assessment. Pediatric Research. Vol 36, pp.805-810.

Ahdaya, S., Guthrie, F.E. Stomach absorption of intubated insecticides in fasted mice, Toxicol. 22, 311-317 (1982).

Altman, P.L, Dittmer, D.S. Biology Data Book, 2nd ed. Vol. III. Federation of American Societies for Experimental Biology, Washington, DC (1974).

Barton, H. A., J. R. Creech, C. S. Godin, G. M. Randall, C. S. Seckel (1995). "Chloroethylene mixtures: pharmacokinetic modeling and *in vitro* metabolism of vinyl chloride, trichloroethylene, and trans-1,2-dichloroethylene in rat." Toxicol. Appl. Pharmacol. 130: 237-247.

Bayer 2004a: Metabolism and Pharmacokinetics of [^{14}C] Carbaryl in Rats. Bayer CropScience. Bayer reports 201025 and 201026.

Bayer 2004b: Application of carbaryl pharmacokinetic data in the estimation of potential post-application health risk associated with broadcast lawn care products. Infoscientific, Inc.

Bayer 2004c. Measurement of Pesticide Exposure of Suburban Residents Associated with the Residential Use of Carbaryl. ABC Laboratories.

Benson, W.H., Dorough, H.W. Comparitive Ester Hydrolysis of Carbaryl and Ethiofencarb in Four Mammalian Species, Pesticide Biochem. Physiol. 21, 199-206 (1984).

Boot, AM, Bouquet,J, de Ridder MAJ, Krenning, EP, and de Muicnk Keizer-Schrama, S. (1997). Determinants of body composition measured by dual-energy X-ray absorptiometry in Dutch children and adolescents. Am J Clin Nutr. 66:232-8.

Brooks, W., and Broxup, B. (1995a). An acute study of the time course cholinesterase inhibition by orally administered carbaryl technical. MRID 438452-02.

Brooks, W., and Broxup, B. (1995b). A time of peak effects study of a single orally administered dose of carbaryl, technical grade, in rats. MRID 438452-03.

Casper, H.H., Peaks, J.C., Dinusson, W.E. Gastric Absorption of a Pesticide (1-Naphthyl *N*-Methylcarbamate) in the Fasted Rat, Pesticide Biochem Physiol. 2, 391-396 (1973).

Cheng,T. (1994). Dermal Absoprtion of ^{14}C-Carbaryl (80S) in Male Rats (Preliminary and Definitite Phases). MRID 433297-01.

Cool, M., Jankowski, K. A Survey of the Metabolism of Carbamate Insecticides in Insecticides, Hutson, D.H, Roberts, T.R. Eds. John Wiley and Sons, Ltd., New York, NY, 1985.

Corley, RA, Mendrala, AL, Smith, FA, Staats, DA, Gargas, M.L., Conolly, R.B., Andersen, M.E., and Reitz, R.H. (1990) Development of a Physiologically Based Pharmacokinetic Model for Chloroform. Toxicol Appl Pharmacol. 103: 512-527

Fisher, J. W., M. L. Gargas, B. C. Allen and M. E. Andersen (1991). "Physiologically based pharmacokinetic modeling with trichloroethylene and its metabolite, trichloroacetic acid, in the rat and mouse." Toxicol. Appl. Pharmacol. 109: 183-195.

Fisher, JW, Mahle,D., and Abbas,R. 1998. A Human Physiologically Based Pharmacokinetic Model for Trichloroethylene and Its Metabolites, Trichloroacetic Acid and Free Trichloroethanol. Toxicol. Appl. Pharmacol. 152: 339-359.

Flockhart Table, Cytochrome P450 Drug-Interaction Table, http://medicine.iupui.edu/flockhart/table.htm

Ginsberg, G., Hattis, D., Sonawane, B. Incorporating Pharmacokinetic Differences between Children and Adults in Assessing Children's Risk to Environmental Toxicants. Toxicol. Appl. Pharmacol. 198, 164-183 (2004).

Hassan, A., Zayed, S.M.A.D., Abdel-Hamid, F.M. Metabolism of Carbamate Drugs I: Metabolism of 1-Naphthyl-*N*-Methyl Carbamate (Sevin) in the Rat, Biochem. Pharamacol. 15, 2045-2055 (1966).

Hattis, D. Human Interindividual Variability in Parameters Related to Susceptibility for Toxic Effects, http://www2.clarku.edu/faculty/dhattis/

Hetnarski, B.; O'Brien, R. D. Electron-donor and affinity constants and their application to the inhibition of acetylcholinesterase by carbamates. Journal of Agricultural and Food Chemistry 1975, 23, 709-713.

International Commission on Radiological Protection (ICRP) "Annals of the ICRP: Basic Anatomical and Physiological Data for Use in Radiological Protection: Reference Values" Volume 32(3-4), Publication 89. Elsevier Science Ltd. New York, NY (2002).

International Life Science Institute, Risk Science Institute (ILSI-RSI) (1994) “Physiological Parameters for PBPK Models” Report. December.

Jepson, G.W., Hoover, D.K., Black, R.K., McCafferty, J.D., Mahle, D.A., Gearhart, J.M. A Partition Coefficient Determination Method for Nonvolatile Chemicals in Biological Tissues. Fund. Appl. Toxicol. 22, 519-524 (1994).

Keys, D. A., J. V. Bruckner, S. Muralidhara and J. W. Fisher (2003). "Tissue dosimetry expansion and cross-validation of rat and mouse physiologically based pharmacokinetic models for trichloroethylene." Toxicol Sci 76(1): 35-50.

Knaak, J.B., Tallant, M.J., Bartley, W.J., Sullivan, L.J. The Metabolism of Carbaryl in the Rat, Guinea Pig, and Man, J. Agr. Food Chem. 13, 537-543 (1965).

Knaak, J.B., Yee, K., Ackerman, C.R., Zweig, G., Fry, D.M., Wilson, B.W. Percutaneous Absorption and Dermal Dose-Cholinesterase Response Studies with Parathion and Carbaryl in the Rat, Toxicol. Appl. Pharmacol. 76, 252-263 (1984).

Koizumi A. (1989) “Potential of physiologically based pharmacokinetics to amalgamate kinetic data of trichloroethylene and tetrachloroethylene obtained in rats and man.” Br J Ind Med. 46(4): 239-49.

Krishna, J.G., Casida, J.E. Fate in Rats of the Radiocarbon from Ten Variously Labeled Methyl- and Dimethyl- Carbamate-C14 Insecticide Chemicals and Their Hydrolysis Products, J. Agr. Good Chem. 14, 98-105 (1966).

Kuhr, R.J., Dorough, H.W. Carbamate Insecticides: Chemistry, Biochemistry, and Toxicology. CRC Press, Cleveland, OH, 1976.

Lechner, D.W., Abdel-Rahman, M.S. Kinetics of Carbaryl and Malathion in Combination in the Rat. J Toxicol. Environ. Health 18, 241-256 (1986).

Lipscomb, J. C., J. W. Fisher, P. D. Confer, J. Z. Byczkowski (1998). “*In vitro* to *in vivo* extrapolation for trichloroethylene metabolism in humans.” Toxicol. Appl. Pharmacol. 152: 376-387.

Liu, X., Tu, M., Kelly, R.S., Chen, C., Smith, B.J. Development of a Computational Approach to Predict Blood-Brain Barrier Permeability. Drug Metab. Dispos. 32: 132-139 (2004).

Marshall, T.C., Dorough, H.W. Biliary Excretion of Carbamate Insecticides in the Rat, Pesticide Biochem. Physiol. 11, 56-63 (1979).

Milner, R., "Cranial Capacity." The Encyclopedia of Evolution: Humanity's Search For Its Origins. New York: Holt, 1990: 98

Mortensen, S.R., Hooper, M.J., Padilla, S. Rat Brain Acetylcholinesterase Activity: Developmental Profile and Maturational Sensitivity to Carbamate and Organophosphorous Inhibitors. Toxicol. 125: 13-19 (1998).

Payne, M.P., Kenny, L.C. Comparison of Models for the Estimation of Biological Partition Coefficients. J Toxicol. Environ. Health, Part A. 65: 897-931 (2002).

Poulin P, Theil FP. A priori prediction of tissue:plasma partition coefficients of drugs to facilitate the use of physiologically based pharmacokinetic models in drug discovery. J Pharm Sci 89:16-35 (2000).

Poulin P, Theil FP. Prediction of pharmacokinetics prior to *in vivo* studies. 1. Mechanism-based prediction of volume of distribution. J Pharm Sci 91:129-156 (2002).

Poulin P, Krishnan, K. A mechanistic algorithm for predicting blood:air partition coefficients of organic chemicals with the consideration of reversible binding in hemoglobin. Toxicol Appl Pharmacol 136:131-137 (1996).

Roberts TR. Hutson DH (1999). Metabolic Pathways of Agrochemicals, Part 2: Insecticides and Fungicides. The Royal Society of Chemistry, 15-24.

Sams, C., Mason, H.J. Detoxification of Organophosphates by A-Esterases in Human Serum. Human Experimental Toxicol. 18, 653-658 (1999).

Sato A., T. Nakajima, Y. Fujiwara, and N. Murayama (1977) “A pharmacokinetic model to study the excretion of trichloroethylene and its metabolites after an inhalation exposure.” Br J Ind Med. 34(1): 56-63.

Schmitz L, Koch H, Bein G, and Brockmeier K. (1998). Left Ventricular Diastolic Function in Infants, Children, and Adolescents. Reference Values and Analysis of Morphologic and Physiologic Determinants of Echocardiographic Doppler Flow Signals During Growth and Maturation. Journal of the American College of Cardiology. Vol 32, pp. 1441-1448

Shah, P.V., Monroe, R.J., Guthrie, F.E. Comparative Rates of Dermal Penetration of Insecticides in Mice, Toxicol. Appl. Pharmacol. 59, 414-423 (1981).

Simmons J.E., W. K. Boyes, P. J. Bushnell, J.H. Raymer, T. Limsakun, A. McDonald, Y.M. Sey, and M. V. Evans (2002). “A physiologically based pharmacokinetic model for trichloroethylene in the male long-evans rat.” Toxicol Sci. 69(1): 3-15.

Sogorb, M.A., Carrera, V., Benabent, M., Vilanova, E. Rabbit Serum Albumin Hydrolyzes the Carbamate Carbaryl, Chem. Res. Toxicol. 15, 520-526 (2002).

Sullivan, L.J., Eldridge, J.M., Knaak, J.B., Tallant, M.J. 5,6-Dihydro-5,6-dihidroxycarbaryl glucuronide as a significant metabolite of carbaryl in the rat, J. Agric. Food Chem. 20, 980-985 (1972).

Struble, C. (1994). Metabolism of ^{14}C-carbaryl in rats (preliminary and definitive phases). MRID 43332101, Rhone Poulenc.

Talcott, R.E., Mallipudi, N.M., Fukuto, T.R. Malathion Carboxylesterase Titer and Its Relationship to Malathion Toxicity. Toxicol. Appl. Pharmacol. 50, 501-504 (1977).

Tang, J., Cao, Y., Rose, R.L., Hodgson, E. *In vitro* Metabolism of Carbaryl by Human Cytochrome P450 and its Inhibition by Chlorpyrifos, Chemico-Bio. Interact. 141, 229-241 (2002).

U.S. EPA 2002. Exposure Related Dose Estimating Model (ERDEM) for Assessing Human Exposure and Dose. EPA/600/X-04/060.

U.S. EPA 2003. HED Phase 5 Occupational and Residential Exposure Assessment.

Appendix A. Model

1.0 Descriptions of Exposure

Exposure occurs at the boundary of the body or test system. It is of considerable interest to the U.S. EPA to limit, reduce and in specific instances eliminate exposure. Humans become exposed to chemical and biological substances, physical energy and radiation through the activities they perform routinely in everyday life or occupationally as part of certain policies, practices or procedures. Exposure can occur accidentally as a random event, or during an occupationally related task or as a result of a purposeful action such as a (terrorist) attack.

Humans may become incidentally and unknowingly exposed. Exposure to particles and gasses in the air we breathe may be unavoidable. Dermal contact with surfaces residues may be unforseen and unrecognizable. Ingestion of particles and residues in food may be unintended and unsuspected. Under certain conditions, exposure can be limited or reduced through education, managerial oversight, regulatory responsiveness, and use of proper personal protection devices (Ness, 1994).

When exposure is perceived as unavoidable, we may wish to describe exposure events in time and space under certain recognizable exposure scenarios. This may be accomplished more easily for occupationally related exposures where policies, practices and procedures have been established than for those that occur randomly or incidentally. However, regardless of the nature of the exposure, exposure follows along recognized pathways, e.g., inhalation, ingestion, and dermal, and routes, respiratory, oral, percutaneous.

ERDEM was designed to examine three pathways of exposure, inhalation, ingestion and dermal, and eight routes of entry into the in silico test system. Experimental pathways and routes of entry were included (Appendix A Section 1.1) along with what might be perceived as naturally occurring unscheduled or not experimentally controlled pathways and routes (Appendix A Section 1.2). This approach greatly enhanced the database to include laboratory animal and clinical studies in addition to environmental field studies. For example, enteral administration is represented by intraperitoneal injection (IP) of chemical into the GI tract via the Portal Blood (Liver for the Stomach/Intestine Gastro-Intestinal model).

1.1 Experimental Pathways and Routes of Entry

1.1.1 Intraperitoneal Injection

Intraperitoneal Injections into the Portal Blood may be given for multiple chemicals for up to nine scenarios starting at time T_{INP_j}, and repeated at the

interval T_{INP,TT_j}. The amount of chemical to be injected is calculated from the concentration of the chemical times the Body Volume. The amount injected decreases at an exponential rate. All injections start before the simulation start time (T0). When the scheduled event occurs to start the injection, the amount is calculated as:

$$A_{INP,J_{i,j}} = A_{INP,CUR,J_{i,j}} + C_{INP,J_{i,j}} V_B,$$

where $A_{INP,CUR,J_{i,j}}$ is the amount remaining to be absorbed from the previous interval. The amount of the *i*th chemical from the *j*th exposure remaining to be absorbed is:

$$A_{INP,CUR,J_{i.j}} = A_{INP,J_{i,j}} e^{-MIN(K_{INP,ABS,J_{i,j}}\Delta T, K_{INP,LIM_i})}$$

where $\Delta T = T - T_{INP,STL,J_j}$, T_{INP,STL,J_j} is the start time for the last IP Injection for the *j*th exposure, and MIN is the mean minimum of the two terms. The amount of the *i*th chemical remaining to be absorbed for all exposures is:

$$A_{INP,CUR_i} = \sum_{j=1}^{N_{INP,EXP}} A_{INP,CUR,J_{i,j}}$$

and the rate of change of the amount of chemical injected into the Portal Blood is given by:

$$\frac{dA_{INP_i}}{dt} = \sum_{j=1}^{N_{INP,EXP}} K_{INP,ABS,J_{i,j}} A_{INP,CUR,J_{i,j}}$$

At the start of the next injection interval, the IP amount remaining to be absorbed is accumulated for each chemical; the elapsed IP simulation time is reset to zero, and the next injection occurrence is scheduled.

1.1.2 Intramuscular Administration

Parenteral administration is represented by intramuscular injection (IM) in the muscle (Slowly Perfused Tissue). Intramuscular Injections may be given for multiple chemicals and up to nine scenarios starting at time T_{INM_j}, and repeat at the interval T_{INM,TT_j}. The amount of chemical to be injected is calculated from the concentration of the chemical times the Body Volume. The amount injected decreases at an exponential rate. All injections that start before the simulation start time (T0) and before the simulation end time are scheduled. When the scheduled event occurs, to start the injection the amount is calculated as:

$$A_{INM,J_{i.j}} = A_{INM,CUR,J_{i,j}} + C_{INM,J_{i,j}} V_B.$$

where $A_{INM,CUR,J_{i,j}}$ is the amount remaining to be absorbed from the previous interval. The amount of the *i*th chemical from the *j*th exposure remaining to be absorbed is:

$$A_{INM,CUR,J_{i,j}} = A_{INM,J_{i,j}} e^{-MIN\left(K_{INM,ABS,J_{i,j}}\Delta T, K_{INM,LIM_i}\right)}$$

where $\Delta T = T - T_{INM,STL,J_j}$, T_{INM,STL,J_j} is the start time for the last IM Injection for the *j*th exposure, and MIN means find the minimum of the two terms. The amount of the *i*th chemical remaining to be absorbed for all exposures is:

$$A_{INM,CUR_i} = \sum_{j=1}^{N_{INM,EXP}} A_{INM,CUR,J_{i,j}}$$

and the rate of change of the amount of chemical injected into the Slowly Perfused Tissue (muscle) is given by:

$$\frac{dA_{INM_i}}{dt} = \sum_{i=1}^{N_{INM,EXP}} K_{INM,ABS,J_{i,j}} A_{INM,CUR,J_{i,j}}$$

At the start of the next injection interval, the IM amount remaining to be absorbed for each chemical is reset to zero and scheduled for the next injection occurrence.

1.1.3 Intravascular Administration

There are two forms of intravascular administration into the Venous Blood, Bolus Intravenous Injection or Infusion.

1.1.3.1 Infusion into the Venous Blood

Infusion is the direct insertion of chemical into the Venous Blood at time T_{INF_j} for a period of time, T_{INF,D_j}, which can be repeated at the interval, T_{INF,TT_j}. There can be many chemicals in each infusion, each with its own concentration. The rate of change of the amount of the ith chemical infused into the Venous Blood versus time is given by:

$$\frac{dA_{INF,VB_i}}{dt} = \sum_{j=1}^{N_{INF}} C_{INF_{i,j}} Q_{INF_j}.$$

The flow rate, Q_{INF_j}, is independent of the chemical. There is one flow rate for each exposure. However, the concentration of the *i*th chemical in the *j*th exposure, $C_{INF_{i,j}}$, can be different for each chemical. The total amount of the *i*th chemical passed to the Venous Blood by Infusion is:

$$A_{INF,VB_{Ti}} = \int_{T_0}^{t} \frac{dA_{INF,VB_i}}{dt} dt.$$

1.1.3.1 Bolus Intravenous Injections

Bolus Dose Intravenous (IV) Injections start at a given time, T_{BIV_j}, and may be repeated at an input interval, T_{RIG,TT_j}. Bolus Dose Intravenous Injections (IVs) injected before simulation start time are not modeled. Those that occur at simulation start time (*T0*) are modeled as true Bolus Doses into the Venous

Blood. The equation for the initial values for the amount of chemical in the Bolus IV Dose and in the Venous Blood are given by:

$$A_{BIV_{T0i}} = \sum_{j=1}^{NBIG} A_{BIV_{i,j}}$$

$$A_{VB_{T0i}} = A_{BIV_{T0i}}$$

for the exposures that start at simulation start time. A Bolus Dose IV that occurs after the simulation start time is simulated with a rate input normally having a time duration of one-quarter of a communication interval or one-quarter of a maximum integration step, whichever is less. The equation for the *j*th exposure for the *i*th chemical then takes the form:

$$\frac{dA_{BIV_{i,j}}}{dt} = \frac{A_{BIV_{i,j}}}{T_{BIV_E} - T_{BIV_B}}$$

and for all exposures to the ith chemical at time t:

$$\frac{dA_{BIV_i}}{dt} = \sum_{j=1}^{N_{BIV}} \frac{dA_{BIV_{i,j}}}{dt}.$$

$$A_{BIV_{Ti}} = \int_{T_0}^{t} \frac{dA_{BIV_i}}{dt} dt + A_{BIV_{T0i}}$$

1.1.4 Inhalation Administration

There are two types of inhalation, Open or Closed Chamber Inhalation. Open Chamber Inhalation is assumed.

The subjects in each simulation are in a closed chamber or an open chamber. They cannot be mixed. If the simulation uses an open chamber then:

A. If no exposure is defined then the simulation starts with an open chamber with no concentration of chemical.
B. There is no change in the concentration of chemical in an open chamber due to exhaled air.
C. If one or more open chamber exposures are defined and none are designated the starting exposure then exposure number one is the exposure starting the simulation.
D. Any number of chemicals can have a concentration in an Open Chamber exposure.
E. The simulation cannot switch in the middle from Open to Closed Chamber Inhalation.

If the simulation uses a closed chamber then:

F. There must be a Closed Chamber exposure defined to start the simulation.
G. Only one Closed Chamber exposure can be active at once.

H. Any number of chemicals can be assigned a concentration for a Closed Chamber exposure.
I. The chemicals in the exhaled air change the concentration of each chemical in the closed chamber.
J. If Closed Chamber Inhalation is chosen then the whole simulation will be with a closed chamber.
K. Open Chamber Inhalation can be approximated with an extremely large closed chamber.

The input concentration for an Open Chamber is in units of parts per million. The input for Closed Chamber Inhalation can be the amount (mass units), or the concentration (units of parts per million). The Open Chamber concentration for the *i*th chemical in mass per unit volume is calculated from:

$$C_{INH_i} = \sum_{j=1}^{N_{INH,EXP}} C_{AIR,J_{i,j}} C_{AIR,1PPM_i},$$

For Closed Chamber Inhalation the volume of the chamber is required. The volume of the air in the chamber is calculated by subtracting the volume of the number of subjects:

$$V_{CC,GAS_j} = V_{CC_j} - N_{SBJ} V_B$$

If the input into the Closed Chamber is a concentration then it is given in parts per million and converted to mass per unit volume units. But, if the input is an amount, then the amount is converted to concentration by:

$$C_{INH_i} = \frac{A_{CC,J_{i,j}}}{V_{CC,GAS_j}}.$$

There are two types of lung included in ERDEM, Static Lung and Breathing Lung. The inhalation pathway involves entry through the Open or Closed Chamber Static Lung or the Breathing Lung. The lung equations are not included in this report since inhalation exposures were not considered. Details may be found in the ORD\NERL APM report “Exposure Related Dose Estimating Model (ERDEM) for Assessing Human Exposure and Dose” (U.S. EPA 2002).

1.2 Implementation of the Exposure Time Histories for Rate Ingestion, Inhalation, and Skin Surface Exposures.

Exposure time histories have been implemented in ERDEM for rate ingestion, open chamber Inhalation, and skin surface exposure time histories. There can be up to nine time histories for each exposure type (except for skin surface exposure which can have up to five exposures), but only one for each chemical. The time histories may be repeated periodically. Each time history will have a start time and duration interval. Any exposure can be expressed as an exposure time history.

Each exposure route has most of these variables:

I. Concentration of chemical in a volume of food, water, or air;
II. Volume of the food, water or air;
III. Flow rate - volume per unit time;
IV. Start time of exposure, duration of exposure, and interval between exposures.

If an exposure starts on or before the simulation start time, then the simulation starts with the exposure in effect. Otherwise, there is an event to start and one to terminate the exposure. There can be overlapping exposures of the same type in most cases (not for Closed Chamber Inhalation exposures). If the exposure is an exposure time history, then only one chemical can be modeled and there can be only one exposure time history of a particular type in any one simulation.

1.2.1 Ingestion Into the Stomach and the Stomach Lumen

Rate ingestion input is a time history of the time and the amount per unit time (concentration times flow rate) of the chemical. Linear interpolation is used to obtain intermediate values.

1.2.1.1 Bolus Dose Ingestion

Bolus dose ingestion occurs when chemical is taken into the Gastro-Intestinal tract very rapidly; for instance in one big bite or drink. Bolus dose inputs that occur at simulation start time (T_0) are modeled as true bolus doses. The initial value for the integration in the stomach or stomach lumen is the sum of all exposures that start at simulation start time. The equation is:

$$A_{BIG_{T0i}} = A_{BIG_{T0i}} + \sum_{j=1}^{NBig} C_{BIG_{i,j}} V_{BIG_j}$$

for all exposures to the *i*th chemical at time T_0.

Bolus dose inputs with start time T_{BIGj} that are greater than the simulation start time and before the simulation stop time are simulated by rate inputs that start at the scheduled bolus dose start time with a duration of 1/4 of a communication interval, or 1/4 of a maximum integration interval, whichever is less. The bolus dose for the jth exposure can be repeated at the input interval, $T_{BIG,TTj}$. The approximation of a bolus dose input via a rate input of a relatively short duration produces results very similar to those achieved with an actual bolus dose while allowing a more accurate evaluation of amounts and concentrations via numerical integration. The equation for the *j*th exposure for the *i*th chemical then takes the form:

$$\frac{dA_{BIG_{i,j}}}{dt} = \frac{C_{BIG_{i,j}} V_{BIG_j}}{T_{BIG_E} - T_{BIG_B}}$$

and for all exposures to the *i*th chemical at time t:

$$\frac{dA_{BIG_i}}{dt} = \sum_{j=1}^{N_{BIG}} \frac{dA_{BIG_{i,j}}}{dt}.$$

The variable $A_{BIG_{T0i}}$ is the initial value in the numerical integrations for the total amount of the ith chemical in the bolus dose ingestion, and the amount in the stomach or stomach lumen:

$$A_{BIG_{Ti}} = \int_{T_0}^{t} \frac{dA_{BIG_i}}{dt} dt + A_{BIG_{T0i}}$$

1.2.1.2 Rate Ingestion

The Rate Ingestion for each exposure starts at a given time, T_{RIG_j}, occurs over a duration of time, T_{RIG,D_j}, and may be repeated at an input interval, T_{RIG,TT_j}. The concentration of the chemical in the food or drink and the flow rate are required inputs. The product results in the rate of change of chemical in the stomach or stomach lumen versus time. Overlapping exposures are allowed. The rate of change of the *i*th chemical in rate ingestion versus time is given by:

$$\frac{dA_{RIG_i}}{dt} = \sum_{j=1}^{N_{RIG}} C_{RIG_{i,j}} Q_{RIG_j}.$$

Thus there is one flow rate for each exposure. But the concentration of each chemical in the *j*th exposure may be different. The numerical integration to obtain the total amount of the *i*th chemical passed to the stomach by Rate Ingestion is:

$$A_{RIG,ST_{Ti}} = \int_{T_0}^{t} \frac{dA_{RIG_i}}{dt} dt + A_{RIG0_i}$$

1.2.2 Inhalation Exposure

Inhalation exposure input follows a time history and concentration in Parts Per Million (PPM) of chemical. Linear interpolation is used to obtain intermediate values. The inhalation pathway involves entry through the Open or Closed Chamber Static Lung or the Breathing Lung. The lung equations are not included in this report since inhalation exposures were not considered. Details may be found in the ORD\NERL APM report “Exposure Related Dose Estimating Model (ERDEM) for Assessing Human Exposure and Dose” (U.S. EPA 2002).

1.2.3 Dermal Exposure

There are two types of dermal exposure modeled in ERDEM, one for chemicals in an aqueous vehicle, most often a water based diluent, and chemicals as a dried residue or adsorbed onto particles as a dry source.

1.2.3.1 Skin Surface Exposure to a Chemical in an Aqueous Vehicle

Skin Surface exposure input follows a time history where a surface area of the skin (square centimeters) becomes exposed to a chemical in an aqueous vehicle as a concentration (mass per centimeter cubed). This concentration and area of the skin are used to compute the rate of change of the amount of chemical absorbed. Linear interpolation is used to obtain intermediate values. The skin surface is exposed to chemical in an aqueous vehicle (water) at time T_{SKW_j} for a period of time, T_{SKW,D_j}, which can be repeated at the interval, T_{SKW,TT_j}. Skin surface (water) exposures progress from a simulation start time and end at a scheduled termination time point.
The concentration of the *i*th chemical at the skin surface is found from summing the concentrations from each of the up to five exposure scenarios:

$$C_{SKS_i} = \sum_{j=1}^{N_{SKW,EXP}} C_{SKW,J_{i,j}}$$

The rate of change of chemical in the epidermis due to the concentration C_{SKS_i} on the skin surface is given by:

$$\frac{dA_{SKW,DR_i}}{dt} = C_{SKS_i} K_{SKS,DR,PRM_i} A_{SK} .$$

1.2.3.2 Skin Surface Exposure to Transfer from a Dry Surface

A chemical exists on a surface represented as a mass per unit area. It is transferred to the skin of a subject represented by a transfer coefficient. A short exposure period would represent a bolus.

The rate of change of chemical on the dermis due to a dry exposure is:

$$\frac{dA_{sks,ex_i}}{dt} = A_{surf_i} K_{sks,rt_i}$$

Integrating this equation gives the total applied dose.

The rate of loss of chemical from the skin surface due to evaporation is given by:

$$\frac{dA_{sks,ev_i}}{dt} = (1.0 - \delta_{wof}) A_{sks_i} (\delta_{ev1} K_{sks,ev1_i} + \delta_{ev2} K_{sks,ev2_i})$$

where
$\delta_{wof} = 1$ if a wash-off is in progress, and zero otherwise,
$\delta_{ev1} = 1$ if the first evaporation rate constant is active, and zero otherwise,
$\delta_{ev2} = 1$ if the second evaporation rate constant is active and zero otherwise.

The rate that the ith chemical moves from the skin surface into the dermis is given by:

$$\frac{dA_{sks,dr_i}}{dt} = K_{sks,dr,prm_i} A_{sk} C_{sks_i}$$

where $C_{sks_i} = \frac{A_{sks_i}}{V_{sk}}$

If no wash-off is in progress, then the rate of change of the amount of the *i*th chemical on the skin is given by the rate of application minus the rate of chemical moving into the dermis minus the rate of loss due to evaporation:

$$\frac{dA_{sks_i}}{dt} = \frac{dA_{sks,ex_i}}{dt} - \frac{dA_{sks,dr_i}}{dt} - \frac{dA_{sks,ev_i}}{dt}.$$

If a wash-off is in progress, then:

$$\frac{dA_{sks_i}}{dt} = -\frac{dA_{sks,wof_i}}{dt}$$

where the wash-off is scheduled at time t_{wof} for one time step, Δt, to remove all chemical on the dermis:

$$\frac{dA_{sks,wof_i}}{dt}(t_{wof}) = \frac{A_{sks_i}}{\Delta t}(t_{wof}).$$

1.3 Variable Definitions

Bolus Dose Ingestions:

A_{BIG_i} = The amount of the *i*th chemical in all of the Bolus Dose Ingestions at time t,

$A_{BIG_{T0i}}$ = The total amount of the *i*th chemical in the Bolus Dose at simulation start time,

$C_{BIG_{i,j}}$ = The concentration of the *i*th chemical in the *j*th Bolus Dose,

N_{BIG} = The number of Bolus Dose Ingestion exposures,

T_{BIG_B} = The time that the Bolus Dose Ingestion starts,

T_{BIG_E} = The time that the Bolus Dose Ingestion ends, and

V_{BIG_j} = The volume of the *j*th Bolus Dose.

Rate Ingestions:

A_{RIG0_i} = The initial value for the *i*th chemical in the Rate Ingestions,

$A_{RIG,ST_{Ti}}$ = The total amount of the *i*th chemical passing from Rate Ingestions to the Stomach at time t,

$C_{RIG_{i,j}}$ = The concentration of the *i*th chemical in the *j*th Rate Ingestion exposure,

$\frac{dA_{RIG_i}}{dt}$ = The rate of change of the *i*th chemical in the Rate Ingestions at time t,

N_{RIG} = The number of Rate Ingestion exposures, and

Q_{RIG_j} = The flow rate for the *j*th Rate Ingestion.

Infusions:

$A_{INF,VB_{Ti}}$ = The total amount of the *i*th chemical in Infusions to Venous Blood at time t,

$\frac{dA_{INF,VB_i}}{dt}$ = The rate of change of the *i*th chemical in Infusions versus time at time t,

$C_{INF_{i,j}}$ = The concentration of the *i*th chemical in the *j*th Infusion,

Q_{INF_j} = The Infusion flow rate for the *j*th exposure.

Bolus Dose Intravenous Injection (Bolus IV):

$A_{BIV_{i,j}}$ = The amount of the *i*th chemical in the *j*th Bolus Dose IV,

$A_{BIV_{T0i}}$ = The total amount of the *i*th chemical in the Bolus Dose IV at simulation start time,

N_{BIV} = The number of Bolus Dose IV exposures,

T_{BIV_B} = The time that the Bolus Dose IV starts,

T_{BIV_E} = The time that the Bolus Dose IV ends.

Intraperitoneal Injection:

$A_{INP,CUR,J_{i,j}}$ = The amount of the *i*th chemical remaining to be absorbed from the previous interval for the *j*th IP scenario,

$A_{INP,J_{i,j}}$ = The amount of the *i*th chemical currently in the IP Injection for the jth scenario,

A_{INP_i} = The amount of the *i*th chemical currently in the IP Injection,

$C_{INP,J_{i,j}}$ = The concentration of the *i*th chemical in the IP Injection for the *j*th scenario,

$\frac{dA_{INP_i}}{dt}$ = The rate of change of the amount of the *i*th chemical in the IP Injection,

$K_{INP,ABS,J_{i,j}}$ = The first order absorption rate constant for the *j*th set of IP Injections of the *i*th chemical,

K_{INP,LIM_i} = The factor to limit the minimum amount of the *i*th chemical from IP Injections remaining to be absorbed.

V_B = Volume of the Body of each subject.

Intramuscular Injection:

$A_{INM,CUR,J_{i,j}}$ = The amount of the *i*th chemical remaining to be absorbed from the previous interval for the *j*th IM Injection scenario,

$A_{INM,J_{i,j}}$ = The amount of the *i*th chemical currently in the IM Injection for the *j*th scenario,

A_{INM_i} = The amount of the *i*th chemical currently in the IM Injection,

$C_{INM,J_{i,j}}$ = The concentration of the *i*th chemical in the IM Injection for the *j*th scenario,

$\frac{dA_{INM_i}}{dt}$ = The rate of change of the amount of the *i*th chemical in the IM Injection,

$K_{INM,ABS,J_{i,j}}$ = The first order absorption rate constant for the *j*th set of IM Injections and the *i*th chemical,

K_{INM,LIM_i} = The factor to limit the minimum amount of the *i*th chemical from IM Injections remaining to be absorbed.

Skin Surface Exposure (Water):

A_{SK} = Area of the skin covered by the solution containing the chemical,

$A_{SKW,DR}$ = The amount of the *i*th chemical that has moved from the skin surface to the Dermis,

$\frac{dA_{SKW,DR_i}}{dt}$ = The rate of change in the amount of the *i*th chemical moving from the skin surface to the Dermis,

C_{SKS} = The concentration of the *i*th chemical on the skin surface due to all overlapping exposures,

$C_{SKW,J_{i,j}}$ = The concentration of the *i*th chemical for the *j*th exposure on the skin surface,

K_{SKS,DR,PRM_i} = The permeation coefficient for the *i*th chemical from Skin Surface to Dermis.

Inhalation:

$A_{CC.J_{i,j}}$ = The amount of the *i*th chemical in the *j*th Closed Chamber,

$C_{AIR,1\ PPM_i}$ = The concentration of *i*th chemical in air for one part per million at one atmosphere and 25º C. This is used to convert concentration in PPM to mass per unit volume.

$C_{AIR,J_{i,j}}$ = The concentration of the *i*th chemical in the *j*th exposure in parts per million.

C_{INH} = The concentration of the *i*th chemical in inhaled air, units of mass per unit volume.

N_{SBJ} = The number of subjects in the *j*th Closed Chamber,

V_{CC_j} = The volume of the Closed Chamber for the *j*th inhalation exposure,

V_{CC,GAS_i} = The volume of the gas in the chamber adjusted for the volume of the subjects.

2.0 Chemical Disposition In Silico

Absorption involves entry of a drug or chemical into the body. We have observed that a chemical may enter directly into the GI tract from intraperitoneal injection (Appendix A Section 1.1.1) or more naturally from ingestion of food or from purposeful (pica or geophagia) or accidental non-dietary ingestion of filth and extraneous matter.

Intravascular parenteral administration directly into the blood stream, intravenously or intra-arterially, was considered as an exposure route because this route of administration is important for laboratory or clinical testing (Appendix A Section 1.1.1). This approach was also developed for intramuscular injection (Appendix A Section 1.1.2) as an avenue of comparison with other parenteral routes of exposure, especially dermal.

Once the drug or chemical enters the blood stream, its disposition in blood and other fluids, e.g. cerebrospinal fluid (CSF), organs and tissues determines its access to the site or sites of action. Drug and chemical disposition involves distribution from blood and fluids to tissues and organs, metabolism in liver and other organs of metabolism, and elimination in exhaled breath, fluids, e.g. milk, and excreta.

2.1 Distribution of Chemical from Blood to Tissues, Organs and in Fluids

2.1.1.1 Binding in the Arterial Blood

The binding in the arterial blood is of the Michaelis-Menten form but is an equilibrium relationship so that the amount of the *i*th chemical that is bound is calculated rather than the rate. The equation is

$$A_{AB,B_i} = K_{AB,MxB_i} \frac{C_{AB_i} V_{AB}}{(K_{AB,DB_i} + ABS(C_{AB_i}))}$$

2.1.1.2 Calculation of Free Chemical in the Arterial Blood

The free chemical in the arterial blood is calculated by subtracting the amount bound from the total amount as follows:

$$A_{AB,F_i} = A_{AB_i} - A_{AB,B_i}$$

2.1.2 The Venous Blood

The venous blood contains chemical output from the compartments and input to the static lung or the breathing lung. The chemical output to blood from the GI walls is passed to the portal blood.

2.1.2.1 Binding in the Venous Blood

The binding in the venous blood is of the Michaelis-Menten form but an equilibrium relationship so that the amount of the *i*th chemical that is bound is calculated rather than the rate. The equation is:

$$A_{VB,B_i} = K_{VB,MxB_i} \frac{C_{VB_i} V_{VB}}{(K_{VB,DB_i} + ABS(C_{VB_i}))}$$

2.1.2.2 Calculation of Free Chemical in the Venous Blood

The free chemical in the venous blood is calculated by subtracting the amount bound from the total amount as follows:

$$A_{VB,F_i} = A_{VB_i} - A_{VB,B_i}$$

2.1.3 Distribution in Tissues

2.1.3.1 Distribution in the Residual Carcass

The rate of change of the ith chemical in the carcass is given by the rate that chemical enters from the arterial blood, and in the chylomicrons from the lymph pool (when the four walled GI model is used), and exits via the venous blood. Elimination is modeled and the rate of elimination of the *i*th chemical is subtracted. Chemical may be metabolized and the rate of metabolism further reduces the rate of increase of the chemical in the carcass. Other metabolites may metabolize to the *i*th chemical and their rate of formation is added. The equation is:

$$V_{CR}\frac{dC_{CR_i}}{dt} = Q_{B,CR}C_{AB,F_i} + K_{LP,CR_i}A_{LP_i} - Q_{B,CR}\frac{C_{CR,F_i}}{R_{CR,VB_i}} - \frac{dA_{CR,E_i}}{dt} - \sum_{j=1}^{N_{M_j}}\frac{dA_{CR,M_{i,j}}}{dt} - \sum_{I_{C,l,m}=i}\frac{dA_{CR,M_{l,m}}}{dt},$$

where the variable $I_{C,l,m}$ is the circulating compound that is the *m*th metabolite of the *l*th circulating compound. The equations for metabolism are presented in Section 2.2 of Appendix A. Binding and elimination equations are presented below.

2.1.3.1.1 Binding in the Carcass

The binding in the carcass is of the Michaelis-Menten form but is an equilibrium relationship so that the amount of the *i*th chemical that is bound is calculated rather than the rate. The equation is

$$A_{CR,B_i} = K_{CR,MxB_i}\frac{C_{CR_i}V_{CR}}{(K_{CR,DB_i} + ABS(C_{CR_i}))}$$

2.1.3.1.3 Calculation of Free Chemical in the Carcass

The free chemical in the carcass is calculated by subtracting the amount bound from the total amount as follows:

$$A_{CR,F_i} = A_{CR_i} - A_{CR,B_i}$$

2.1.3.1.4 Elimination in the Carcass

There are two types of elimination currently implemented in ERDEM: a linear form in which the rate of elimination is proportional to the amount of the free *i*th chemical in the Carcass, and a saturable Michaelis-Menten form. The linear form is

$$\frac{dA_{CR,E_i}}{dt} = K_{CR,E_i} A_{CR,F_i}$$

and the saturable form for elimination is:

$$\frac{dA_{CR,E_i}}{dt} = V_{m,CR,E_i} \frac{C_{CR,F_i}}{(K_{mM,CR,E_i} + ABS(C_{CR,F_i}))}$$

2.1.3.2 Distribution in Fat Tissue

The rate of change of the *i*th chemical in the fat tissue is given by the rate that chemical enters from the arterial blood and the chylomicrons from the lymph pool and exits via the venous blood. Elimination is modeled and the rate of elimination of the *i*th chemical is subtracted. Chemical may be metabolized and the rate of metabolism further reduces the rate of increase of the chemical in the fat tissue. Other metabolites may metabolize to the *i*th chemical and their rate of formation is added. The equation is:

$$V_{FT} \frac{dC_{FT_i}}{dt} = Q_{B,FT} C_{AB,F_i} + K_{LP,FT_i} A_{LP_i} - Q_{B,FT} \frac{C_{FT,F_i}}{R_{FT,VB_i}} - \frac{dA_{FT,E_i}}{dt} - \sum_{j=1}^{N_{M_j}} \frac{dA_{FT,M_{i,j}}}{dt} - \sum_{I_{C,l,m}=i} \frac{dA_{FT,M_{l,m}}}{dt},$$

where the variable $I_{C,l,m}$ is the circulating compound that is the *m*th metabolite of the *l*th circulating compound. The equations for metabolism are presented in Section 2.2 in Appendix A. Binding and elimination equations are presented below.

2.1.3.2.1 Binding in Fat Tissue

The binding in the fat is of the Michaelis-Menten form but is an equilibrium relationship so that the amount of the *i*th chemical that is bound is calculated rather than the rate. The equation is:

$$A_{FT,B_i} = K_{FT,MxB_i} \frac{C_{FT_i} V_{CR}}{(K_{FT,DB_i} + ABS(C_{FT_i}))}$$

2.1.3.2.2 Calculation of Free Chemical in Fat Tissue

The free chemical in the fat tissue is calculated by subtracting the amount bound from the total amount as follows:

$$A_{FT,F_i} = A_{FT_i} - A_{FT,B_i}$$

2.1.3.2.3 Elimination in Fat Tissue

There are two types of elimination currently implemented in ERDEM: a linear form in which the rate of elimination is proportional to the amount of the free *i*th chemical in the Fat, and a saturable Michaelis-Menten form. The linear form is:

$$\frac{dA_{FT,E_i}}{dt} = K_{FT,E_i} A_{FT,F_i}$$

and the saturable form for elimination is:

$$\frac{dA_{FT,E_i}}{dt} = V_{m,FT,E_i} \frac{C_{FT,F_i}}{(K_{mM,FT,E_i} + ABS(C_{FT,F_i}))}$$

2.1.3.3 Distribution in Slowly Perfused Tissue

The rate of change of the *i*th chemical in the slowly perfused tissue is given by the rate that the chemical is input from intramuscular injections, from the lymph pool as chylomicrons and as input from the arterial blood that exits via the venous blood. Elimination is modeled and the rate of elimination of the *i*th chemical is subtracted. Chemical may be metabolized and the rate of metabolism further reduces the rate of increase of the chemical in the slowly perfused tissue. Other metabolites may metabolize to the *i*th chemical and their rate of formation is added. The equation is:

$$V_{SL} \frac{dC_{SL_i}}{dt} = Q_{B,SL} C_{AB,F_i} + K_{LP,SL_i} A_{LP_i} + \frac{dA_{INM_i}}{dt} - Q_{B,SL} \frac{C_{SL,F_i}}{R_{SL,VB_i}} - \frac{dA_{SL,E_i}}{dt} - \sum_{j=1}^{N_{Mj}} \frac{dA_{SL,M_{i,j}}}{dt} - \sum_{I_{C,l,m}=i} \frac{dA_{SL,M_{l,m}}}{dt},$$

where the variable $I_{C,l,m}$ is the circulating compound that is the *m*th metabolite of the *l*th circulating compound. The equations for metabolism are presented in

Section 2.2 of Appendix A. Binding and elimination equations are presented below.

2.1.3.3.1 Binding in the Slowly Perfused Tissue

The binding in the slowly perfused tissue is of the Michaelis-Menten form but is an equilibrium relationship so that the amount of the *i*th chemical that is bound is calculated rather than the rate. The equation is:

$$A_{SL,B_i} = K_{SL,MxB_i} \frac{C_{SL_i} V_{SL}}{(K_{SL,DB_i} + ABS(C_{SL_i}))}$$

2.1.3.3.2 Calculation of Free Chemical in the Slowly Perfused Tissue

The free chemical in the slowly perfused tissue is calculated by subtracting the amount bound from the total amount as follows:

$$A_{SL,F_i} = A_{SL_i} - A_{SL,B_i}$$

2.1.3.3.3 Elimination in the Slowly Perfused Tissue

There are two types of elimination currently implemented in ERDEM: a linear form in which the rate of elimination is proportional to the amount of the free *i*th chemical in the Slowly Perfused Tissue, and a saturable Michaelis-Menten form. The linear form is:

$$\frac{dA_{SL,E_i}}{dt} = K_{SL,E_i} A_{SL,F_i}$$

and the saturable form for elimination is:

$$\frac{dA_{SL,E_i}}{dt} = V_{m,SL,E_i} \frac{C_{SL,F_i}}{(K_{mM,SL,E_i} + ABS(C_{SL,F_i}))}$$

2.1.3.4 Distribution in Rapidly Perfused Tissue

The rate of change of the *i*th chemical in the rapidly perfused tissue is given by the rate that chemical enters from the lymph pool as chylomicrons and from the arterial blood and exits via the venous blood. Elimination is modeled and the rate of elimination of the *i*th chemical is subtracted. Chemical may be metabolized and the rate of metabolism further reduces the rate of increase of the chemical in the rapidly perfused tissue. Other metabolites may metabolize to the *i*th chemical and their rate of formation is added. The equation is:

$$V_{RP}\frac{dC_{RP_i}}{dt} = Q_{B,RP}C_{AB,F_i} + K_{LP,RP_i}A_{LP_i} - Q_{B,RP}\frac{C_{RP,F_i}}{R_{RP,VB_i}} - \frac{dA_{RP,E_i}}{dt} - \sum_{j=1}^{N_{M_j}}\frac{dA_{RP,M_{i,j}}}{dt} - \sum_{I_{C,l,m}=i}\frac{dA_{RP,M_{l,m}}}{dt},$$

where the variable $I_{C,l,m}$ is the circulating compound that is the *m*th metabolite of the *l*th circulating compound. The equations for metabolism are presented in Section 2.2 of Appendix A. Binding and elimination equations are presented below.

2.1.3.4.1 Binding in the Rapidly Perfused Tissue

The binding in the rapidly perfused tissue is of the Michaelis-Menten form but is an equilibrium relationship so that the amount of the *i*th chemical that is bound is calculated rather than the rate. The equation is:

$$A_{RP,B_i} = K_{RP,MxB_i}\frac{C_{RP_i}V_{RP}}{(K_{RP,DB_i} + ABS(C_{RP_i}))}$$

2.1.3.4.2 Calculation of Free Chemical in the Rapidly Perfused Tissue

The free chemical in the Rapidly Perfused Tissue is calculated by subtracting the amount bound from the total amount as follows:

$$A_{RP,F_i} = A_{RP_i} - A_{RP,B_i}$$

2.1.3.4.3 Elimination in the Rapidly Perfused Tissue

There are two types of elimination currently implemented in ERDEM: a linear form in which the rate of elimination is proportional to the amount of the free *i*th chemical in the Rapidly Perfused Tissue and a saturable Michaelis-Menten form. The linear form is:

$$\frac{dA_{RP,E_i}}{dt} = K_{RP,E_i}A_{RP,F_i}$$

and the saturable form for elimination is:

$$\frac{dA_{RP,E_i}}{dt} = V_{m,RP,E_i}\frac{C_{RP,F_i}}{(K_{mM,RP,E_i} + ABS(C_{RP,F_i}))}$$

2.1.4 Distribution of Chemical in Organs

2.1.4.1 Distribution of Chemical from Blood to the Brain

The rate of change of the ith chemical in the brain is given by the rate that chemical enters from the arterial blood and in the chylomicrons from the lymph pool (when the four walled gastro-intestinal model is used), and exits via the venous blood. The blood/brain barrier is modeled by properly choosing the partition coefficients. Elimination of chemical from brain is modeled and the rate of elimination of the ith chemical is subtracted. Chemical may be metabolized and the rate of metabolism further reduces the rate of increase of the chemical in the brain. Other metabolites may metabolize to the ith chemical and their rate of formation is added. The equation is:

$$V_{BN}\frac{dC_{BN_i}}{dt} = Q_{B,BN}C_{AB,F_i} + K_{LP,BN_i}A_{LP_i} - Q_{B,BN}\frac{C_{BN,F_i}}{R_{BN,VB_i}} - \frac{dA_{BN,E_i}}{dt} - \sum_{j=1}^{N_{M_j}}\frac{dA_{BN,M_{i,j}}}{dt} - \sum_{I_{C,l,m}=i}\frac{dA_{BN,M_{l,m}}}{dt},$$

where the variable $I_{C,l,m}$ is the index to the circulating compound that is the *m*th metabolite of the *l*th circulating compound. The equations for metabolism are presented in Section 2.2 of Appendix A. Binding and elimination equations are presented below.

2.1.4.1.1 Binding in the Brain

The binding in the Brain is of the Michaelis-Menten form but is an equilibrium relationship so that the amount of the ith chemical that is bound is calculated rather than the rate. The equation is:

$$A_{BN,B_i} = K_{BN,MxB_i}\frac{C_{BN_i}V_{BN}}{(K_{BN,DB_i} + ABS(C_{BN_i}))}$$

2.1.4.1.2 Calculation of Free Chemical in the Brain

The free chemical in the Brain is calculated by subtracting the amount bound from the total amount as follows:

$$A_{BN,F_i} = A_{BN_i} - A_{BN,B_i}$$

2.1.4.1.3 Elimination from the Brain

There are two types of elimination currently implemented in ERDEM: a linear form in which the rate of elimination is proportional to the amount of the free *i*th chemical in the Brain and a saturable Michaelis-Menten form. The linear form is:

$$\frac{dA_{BN,E_i}}{dt} = K_{BN,E_i} A_{BN,F_i}$$

and the saturable form for elimination is:

$$\frac{dA_{BN,E_i}}{dt} = V_{m,BN,E_i} \frac{C_{BN,F_i}}{(K_{mM,BN,E_i} + ABS(C_{BN,F_i}))}$$

2.1.4.2 Distribution of Chemical to the Liver

2.1.4.2.1 Stomach/Intestine Model of Distribution to the Liver

The liver compartment has the *i*th chemical input from the stomach and intestine following intraperitoneal injections. Input from the arterial blood is also included. The *i*th chemical is moved from the liver to venous blood where it may be lost due to elimination. Additional chemical is bound in the liver using an equilibrium process. Chemical may be metabolized and the rate of metabolism further reduces the rate of increase of the chemical in the Liver. Other metabolites may metabolize to the *i*th chemical and their rate of formation is added. The equation is:

$$V_{LV} \frac{dC_{LV_i}}{dt} = \frac{dA_{ST,PB_i}}{dt} + \frac{dA_{IN,PB_i}}{dt} + \frac{dA_{INP_i}}{dt} + Q_{B,LV} C_{AB,F_i} - Q_{B,LV} \frac{C_{LV,F_i}}{R_{LV,VB_i}} -$$

$$\frac{dA_{LV,E_i}}{dt} - \sum_{j=1}^{N_{M_j}} \frac{dA_{LV,M_{i,j}}}{dt} - \sum_{I_{C,l,m}=i} \frac{dA_{LV,M_{l,m}}}{dt},$$

where the equations for the input to portal blood from the stomach and the intestine are respectively:

$$\frac{dA_{ST,PB_i}}{dt} = K_{ABS,ST,PB_i} A_{ST_i},$$

and

$$\frac{dA_{IN,PB_i}}{dt} = K_{ABS,IN,PB_i} A_{IN_i},$$

where the variable $I_{C,l,m}$ is the circulating compound that is the *m*th metabolite of the *l*th circulating compound. The equations for metabolism are presented in the Section 2.2 of Appendix A. Binding and elimination equations are presented below.

2.1.4.2.2 Gastro-Intestinal Model of Distribution to the Liver

The liver compartment for the complete GI tract has the *i*th chemical input from the portal blood (from intraperitoneal injections) and lymph pool as chylomicrons in addition to the input from the Arterial Blood. The *i*th chemical is moved from the liver to the venous blood to the bile which is passed to the Duodenum Lumen, and may be lost due to elimination. Additional chemical is bound in the Liver using an equilibrium process. Chemical may be metabolized and the rate of metabolism further reduces the rate of increase of the chemical in the Liver. Other metabolites may metabolize to the *i*th chemical and their rate of formation is added. The equation is:

$$V_{LV}\frac{dC_{LV_i}}{dt} = Q_{B,LV}\left(C_{AB,F_i} - \frac{C_{LV,F_i}}{R_{LV,VB_i}}\right) + Q_{PB,LV}\left(C_{PB_i} - \frac{C_{LV,F_i}}{R_{LV,VB_i}}\right) -$$

$$\frac{dA_{LV,E}}{dt} + K_{LP,LV_i}A_{LP_i} - Q_{BL}\frac{C_{LV,F_i}}{R_{BL,DUL_i}} - \sum_{j=1}^{N_{M_j}}\frac{dA_{LV,M_{i,j}}}{dt} - \sum_{I_{C,l,m}=i}\frac{dA_{LV,M_{l,m}}}{dt}$$

The intraperitoneal injection in this case is passed to the portal blood.

2.1.4.2.3 Binding in the Liver

The binding in the liver is of the Michaelis-Menten form but is an equilibrium relationship so that the amount of the *i*th chemical that is bound is calculated rather than the rate. The equation is:

$$A_{LV,B_i} = K_{LV,MxB_i}\frac{C_{LV_i}V_{LV}}{(K_{LV,DB_i} + ABS(C_{LV_i}))}$$

2.1.4.2.4 Calculation of Free Chemical in the Liver

The free chemical in the liver is calculated by subtracting the amount bound from the total amount as follows:

$$A_{LV,F_i} = A_{LV_i} - A_{LV,B_i}$$

2.1.4.2.5 Elimination in the Liver

There are two types of elimination currently implemented in ERDEM: a linear form in which the rate of elimination is proportional to the amount of the free *i*th chemical in the Liver and a saturable Michaelis-Menten form. The linear form is:

$$\frac{dA_{LV,E_i}}{dt} = K_{LV,E_i}A_{LV,F_i}$$

and the saturable form for elimination is:

$$\frac{dA_{LV,E_i}}{dt} = V_{m,LV,E_i} \frac{C_{LV,F_i}}{(K_{mM,LV,E_i} + ABS(C_{LV,F_i}))}$$

2.1.4.3 Absorption and Distribution in the Stomach

The stomach has the *i*th chemical input by bolus ingestion (a plug of food or drink) and rate ingestion (food or drink input over time), with chemical output to portal blood via the liver to the intestine. The equation for the rate of change of *i*th chemical in the stomach is:

$$\frac{dA_{ST_i}}{dt} = \frac{dA_{BIG_i}}{dt} + \frac{dA_{RIG_i}}{dt} - K_{ABS,ST,PB_i} A_{ST_i} - K_{ST,IN_i} A_{ST_i},$$

where the bolus ingestion and the rate ingestion exposures are discussed in Section 1.2.1 of Appendix A.

2.1.4.4 The Intestine

The rate of change of the *i*th chemical in the intestine is given by the rate of input from the stomach and the rate of output to the portal blood via the liver to feces. The equation is:

$$\frac{dA_{IN_i}}{dt} = K_{ST,IN_i} A_{ST_i} - K_{ABS,IN,PB_i} A_{IN_i} - K_{IN,FEC_i} A_{IN_i}$$

2.1.4.5 The Kidney

The rate of change of the ith chemical in the kidney is given by the rate that chemical enters from the arterial blood and in the chylomicrons from the lymph pool (when the four walled GI model is used), and exits via the venous blood and the urine. Chemical may be metabolized and the rate of metabolism further reduces the rate of increase of the chemical in the kidney. Other metabolites may metabolize to the ith chemical and their rate of formation is added. The equation is:

$$V_{KD} \frac{dC_{KD_i}}{dt} = Q_{B,KD} C_{AB,F_i} + K_{LP,KD_i} A_{LP_i} - Q_{B,KD} \frac{C_{KD,F_i}}{R_{KD,VB_i}} - \frac{dA_{KD,URN_i}}{dt} - \sum_{j=1}^{N_{M_j}} \frac{dA_{KD,M_{i,j}}}{dt} - \sum_{I_{C,l,m}=i} \frac{dA_{KD,M_{l,m}}}{dt},$$

2.1.4.5.2 Calculation of Free Chemical in the Kidney

The free chemical in the kidney is calculated by subtracting the amount bound from the total amount as follows:

$$A_{KD,F_i} = A_{KD_i} - A_{KD,B_i}$$

2.1.4.5.3 Elimination in the Kidney

There are two types of urine elimination currently implemented in ERDEM: a linear form in which the rate of elimination is proportional to the amount of the free *i*th chemical in the Kidney and a saturable Michaelis-Menten form. The linear form is:

$$\frac{dA_{KD,URN_i}}{dt} = K_{KD,URN_i} A_{KD,F_i}$$

and the saturable form for elimination is:

$$\frac{dA_{KD,URN_i}}{dt} = V_{m,KD,URN_i} \frac{C_{KD,F_i}}{(K_{mM,KD,URN_i} + ABS(C_{KD,F_i}))}$$

2.1.4.6 The Spleen

The rate of change of the *i*th chemical in the spleen is given by the rate that chemical enters from the arterial blood, and in the chylomicrons from the lymph pool (when the four walled GI model is used), and exits via the portal blood (or into the liver if the stomach/intestine GI is used). Elimination is modeled and the rate of elimination of the *i*th chemical is subtracted. Chemical may be metabolized and the rate of metabolism further reduces the rate of increase of the chemical in the spleen. Other metabolites may metabolize to the *i*th chemical and their rate of formation is added. The equation is:

$$V_{SP} \frac{dC_{SP_i}}{dt} = Q_{B,SP} C_{AB,F_i} + K_{LP,SP_i} A_{LP_i} - Q_{B,SP} \frac{C_{SP,F_i}}{R_{SP,PB_i}} - \frac{dA_{SP,E_i}}{dt} - \sum_{j=1}^{N_{M_j}} \frac{dA_{SP,M_{i,j}}}{dt} - \sum_{I_{C,l,m}=i} \frac{dA_{SP,M_{l,m}}}{dt},$$

where the variable $I_{C,l,m}$ is the circulating compound that is the *m*th metabolite of the *l*th circulating compound. The equations for metabolism are presented in Section 2.2 of Appendix A. Binding and elimination equations are presented below.

2.1.4.6.1 Binding in the Spleen

The binding in the spleen is of the Michaelis-Menten form but is an equilibrium relationship so that the amount of the *i*th chemical that is bound is calculated rather than the rate. The equation is:

$$A_{SP,B_i} = K_{SP,MxB_i} \frac{C_{SP_i} V_{SP}}{(K_{SP,DB_i} + ABS(C_{SP_i}))}$$

2.1.4.6.2 Calculation of Free Chemical in the Spleen

The free chemical in the spleen is calculated by subtracting the amount bound from the total amount as follows:

$$A_{SP,F_i} = A_{SP_i} - A_{SP,B_i}$$

2.1.4.6.3 Elimination in the Spleen

There are two types of elimination currently implemented in ERDEM: a linear form in which the rate of elimination is proportional to the amount of the free *i*th chemical in the Spleen and a saturable Michaelis-Menten form. The linear form is:

$$\frac{dA_{SP,E_i}}{dt} = K_{SP,E_i} A_{SP,F_i}$$

and the saturable form for elimination is:

$$\frac{dA_{SP,E_i}}{dt} = V_{m,SP,E_i} \frac{C_{SP,F_i}}{(K_{mM,SP,E_i} + ABS(C_{SP,F_i}))}$$

2.1.4.7 The Dermal Tissue

The dermal dissue receives the ith chemical by permeation through the skin and from the arterial blood and is released to the venous blood according to the equation:

$$V_{DR} \frac{dC_{DR_i}}{dt} = \frac{dA_{SKS,DR_i}}{dt} + K_{LP,DR_i} A_{LP_i} + Q_{B,DR} C_{AB,F_i} - Q_{B,DR} \frac{C_{DR_i}}{R_{DR,VB_i}}$$

where

$$\frac{dA_{SKS,DR_i}}{dt} = C_{SKS_i} K_{PRM,SKS,DR_i} AREA_{SK}$$

2.2 Metabolism in Selected Tissues and Organs

The term metabolism refers to any reaction that produces a new compound. The term *Metabolite* could be replaced with a term such as *Reactant.* ERDEM has been designed to handle multiple circulating compounds. It is assumed that ***all metabolites are circulating and the metabolism structure is the same in all compartments***. The metabolism parameters, however, can be different in each compartment. The equations implemented in ERDEM are presented for the following areas:

- Enzyme Destruction and Re-synthesis

Maximum rate of change of metabolite formation, taking enzyme destruction and re-synthesis into consideration, is calculated.

- Maximum Rate of Metabolite Formation

The maximum rate of formation of the metabolite is found for the liver by scaling for species and body volume. The maximum rate for other compartments is scaled from the Liver value.

- Saturable and Linear Metabolites

Equations and parameters are presented for calculating the rate of metabolite formation.

- Inhibition

A metabolite or circulating compound may work in such a manner as to inhibit the formation of another metabolite. There are four types of inhibition modeled here, competitive inhibition, mixed inhibition, strictly non-competitive inhibition, and uncompetitive inhibition.

Equations are presented for the liver metabolism with circulating metabolites in section 2.2.6 of Appendix A. The other compartments use similar equations. The metabolism parameters, maximum velocity (V_{max}) and the Michaelis-Menten constant (K_m) could be different in each compartment, or the V_{max} for metabolism in other compartments may be calculated relative to that used in the Liver. If the units of volume are changed, the units of the input V_{max} cannot be changed. Also, the units of the volume of the body used for the scaling conversion cannot be changed. In other words, there can be no volume unit conversion before the calculation of the scaled version of the V_{max}.

An input reference body volume is assumed (currently one unit) and the V_{max} input is assumed to be in units of amount per unit time. The calculation of V_{max} then always works. A volume unit change is applied both to the reference body

volume as well as the current body volume. This then would be consistent for the scaling of the V_{max} for elimination as will the maximum binding value in the calculation of the amount bound. This ratio of body volumes will be used throughout the scaling processes in ERDEM.

2.2.1 Implementation Outline

If a circulating compound is metabolized, then one or more metabolites are defined. These may be linear, saturable, or be affected by one of four types on inhibition. Each of these metabolites is itself considered to be circulating.

The user will input the circulating compound number for each metabolite. The number of metabolites for each circulating compound is used as the input. These metabolites are also assumed to be circulating. The user will input metabolism parameters using i,j with “i” being the index to the circulating compound and “j” being the metabolite counter for the metabolites of circulating compound i. The user will need to input set, print, display and plot statements using the index i.

The individual metabolite amounts are calculated in the compartmental calculations for the individual chemical. The metabolism section for each compartment calculates two sums. The first is the sum of all rates of metabolite formation of the *i*th circulating compound. The second is the sum of the rate of formation of all metabolites that are the same as the *i*th circulating compound. These rate sums are integrated in the circulating compound section for each compartment.

2.2.2 Variable Names for Metabolism Parameters

Table 2.1 presents variable names, with a short description, that are used globally in all compartments. The variables used in the metabolism calculations are shown in Table 2.2 (the liver compartment for example). Those variables that now have one or two indices but have unchanged names are not listed.

Table 2.2.2: Metabolism Variables Used in All Compartments.

Variable Name	Variable Description	Notes
CH_NM_SH(I)	Chemical Short Name for *i*th circulating compound. In SET statements use CH_NM_SH(1,I)	Eight characters, used in error statements.
CH_NM_LG(I)	Chemical Long Name for *i*th circulating compound.	Thirty characters for use in descriptive text.
N_M(I)	Number of metabolites of the *i*th circulating compound.	A two digit integer. Maximum value is six. NM_i
I_CMPD(I,J)	Number of the circulating compound that is the *j*th metabolite of the *i*th circulating compound.	For j=1 to N_M(i) In eqns: $I_{c,i,j}$
TYPE_M(I,J)	Type of the *j*th metabolite (equation(s) to use) of the *i*th circulating compound. In SET statements use TYPE_M(1,I,J).	Up to three characters to specify equation(s) to use.

Table 2.2.3: Variables Used in Metabolism Calculations (Liver Example)

Variable Name (Used in Program)	Variable Description	Variable Name (in Documents)
A_LV_F(I)	Amount of the *i*th chemical that is free.	A_{LV,F_i}
C_LV_F(I)	Concentration of the *i*th circulating compound that is free.	C_{LF,F_i}
A_LV_M_SUM(I)	Sum of the amounts of Liver metabolite of the *i*th chemical. (mg)	A_{M,LV,SUM_i}
A_LV_MC_SUM(I)	Sum of amounts of Liver metabolite that are the same as the ith chemical. (mg)	A_{MC,LV,SUM_i}
DA_LV_M(I,J)	Rate of formation for the *k*th Liver metabolite for the *i*th chemical. (mg/H)	$\frac{dA_{M,LV_{i,j}}}{dt}$
DA_LV_M_SUM(I)	Sum of rates of formation for all Liver metabolites of the *i*th chemical. (mg/H).	$\frac{dA_{M,LV,SUM_i}}{dt}$
DA_LV_MC_SUM(I)	Sum of rates of formation of all metabolites that are the same chemical as the *i*th circulating compound. (mg/H)	$\frac{dA_{MC,LV,SUM_i}}{dt}$

Variable Name (Used in Program)	Variable Description	Variable Name (in Documents)
DCM_M_LV(I,J)	Maximum rate of change of *k*th Liver metabolite concentration for the *i*th chemical. (mg/L/H).	$V_{Mx_0,LV_{i,j}}$
DRM_LV_MEDR(I, J)	Rate of change of the maximum *j*th Liver metabolite metabolic rate including enzyme destruction and resynthesis for the *i*th chemical.	$\frac{dV_{Mx,LV,edr_{i,j}}}{dt}$
K_LV_ML(I,J)	The rate constant for the Linear form of the metabolism calculation.	$K_{ML,LV_{i,j}}$
K_MD1_LV(I,J)	First dissociation constant for the inhibitor to formation of the *j*th Liver metabolite of the *i*th chemical.	$K_{MD1,LV_{i,j}}$
K_MD2_LV(I,J)	Second dissociation constant for the inhibitor to formation of the *j*th Liver metabolite of the *i*th chemical.	$K_{MD2,LV_{i,j}}$
K_MM_LV(I,J)	Michaelis-Menten constant for *j*th Liver metabolite of *i*th chemical. (mg/L)	$K_{mm,LV_{i,j}}$
K1_MER(I,J)	First order rate of *j*th Liver metabolite enzyme resynthesis for *i*th chemical. (1/H)	$K_{1M,er_{i,j}}$
K2_MED(I,J)	Second order rate of *j*th Liver metabolite enzyme destruction for the *i*th chemical. (L/MG)	$K_{2M,ed_{i,j}}$
VM_M_LV(I,J)	Maximum rate of *j*th Liver metabolite metabolism for the *i*th chemical. (MG/H)	$V_{Mx,LV_{i,j}}$
VM_MEDR_LV(I,J)	Maximum rate of *j*th Liver metabolite metabolism after taking enzyme change into account for the *i*th chemical. (MG/H)	$V_{Mx,LV,edr_{i,j}}$

2.2.3 Calculation of Maximum Rate of Change of Metabolism

The equation for the maximum rate of change of metabolism in the Liver for the jth metabolite of the ith chemical is given by

$$V_{Mx,LV_{i,j}} = V_{M_{x_0},LV_{i,j}}\left(\frac{V_B}{V_{ref}}\right)^{r_m}$$

where

V_B = volume of the body,

V_{ref} = reference volume for $V_{Mx_0,LV_{i,j}}$

r_m = power of the volume of the body for interspecies scaling.

2.2.4 Calculations when including Enzyme Destruction and Re-synthesis

The equation for the rate of change of maximum metabolic rate in the liver including enzyme destruction and re-synthesis for the *j*th metabolite of the *i*th circulating compound is given by:

$$\frac{dV_{Mx,LV,edr_{i,j}}}{dt} = K_{1M,er_{i,j}}(V_{Mx,LV_{i,j}} - V_{Mx,LV,edr_{i,j}}) - K_{2M,ed_{i,j}} V_{Mx,LV,edr_{ij}} \frac{dA_{M,LV_{i,j}}}{dt} / V_{LV}$$

where the variable definitions are given in Table 2.2.3, and V_{LV} = the volume of the Liver. The value of the maximum metabolic rate taking enzyme destruction and re-synthesis into consideration is obtained by integration as:

$$V_{Mx.LV,edr_{i,j}} = \int \frac{dV_{Mx,LV,edr_{i,j}}}{dt} dt + V_{Mx,LV_{i,j}}.$$

2.2.5 The Rate of Formation of Saturable and Linear Metabolite in the Liver

The rate of formation of theth metabolite, when saturable, in the liver from the *i*th circulating compound is given by:

$$\frac{dA_{M,LV_{i,j}}}{dt} = V_{Mx,LV,edr_{i,j}} \frac{C_{LV,F_i}}{\left(K_{mm,LV_{i,j}} + \left|C_{LV,F_i}\right|\right)}$$

where the indices *i*, and *j* are defined above and parameters are defined in Table 2.2.3. For those metabolites which the user wants to be strictly linear, then the linear form of the equation would apply. The rate of formation of a linear metabolite in the liver is:

$$\frac{dA_{M,LV_{i,j}}}{dt} = K_{ML,LV_{i,j}} A_{LV,F_i}.$$

The sum of the rates of formation of the metabolites for the *i*th circulating compound can be calculated according to where the rate of formation of metabolites determines the loss in the rate of increase of amount in the liver for the *i*th circulating compound:

$$\frac{dA_{M,LV,SUM_i}}{dt} = \sum_{j=1}^{N_M} \frac{dA_{M,LV_{i,j}}}{dt},$$

2.2.6 Circulating Compounds which are Metabolites

The rates of formation of metabolites, in this case in the liver, which are the same as one of the circulating compounds are summed and then added to the rate of increase of the amount of the circulating compound. This is accomplished by assuming that every metabolite could be any of the circulating compounds. An index $I_{c,i,j}$ is saved for each metabolite. If the *j*th metabolite of the ith circulating compound is the same compound as the *k*th circulating compound, then the index *k* for the circulating compound is saved in $I_{c,i,j}$ otherwise the index $I_{c,i,j}$ is set to zero. If the index is non-zero, then the rate of formation of that metabolite is added to a sum for that circulating compound. The rate of formation of a circulating metabolite may be linear or saturated (with inhibition if applicable) as described in Section 2.2.5 of Appendix A. The rate equation the becomes

$$\frac{dA_{MC,LV,SUM_k}}{dt} = \sum_{I_{c,i,j}=k} \frac{dA_{M,LV_{i,j}}}{dt}$$

where $\frac{dA_{M,LV_{i,j}}}{dt}$ = the contribution to the rate of change of the *k*th chemical in the Liver from the rate of formation of the *j*th metabolite of the *i*th chemical.

2.2.7 Inhibition in the Metabolism Process

Compounds elsewhere in the metabolism chains for any of the circulating compounds may inhibit the formation of a given metabolite. There are four kinds of inhibition addressed here. They are defined by the formulas for an apparent V_{max}, and an apparent Michaelis-Menten constant K_{mm} (See Table 2.2.7).

$$\frac{dA_{M,LV_{i,J}}}{dt} = V_{\max,App_{i,J}} \frac{C_{LV,F_i}}{(K_{mm,App_{i,j}} + |C_{LV,F_i}|)},$$

where $V_{max,App}$ and $K_{mm,App}$ are taken from Table 2.2.7 for the inhibition case that applies.

Table 2.2.7 Parameter Formulas for Four Types of Inhibition of Metabolism

Type of Inhibition	$V_{max,App}$	$K_{mm,App}$
Competitive Inhibition	$V_{Mx,LV,edr_{i,j}}$	$K_{mm,LV_{i,j}}(1+C_{LV,F_{Ii,j}}/K_{MD1,LV_{i,j}})$
Mixed Inhibition	$\frac{V_{Mx,LV,edr_{i,j}}}{(1+C_{LV,F_{Ii,j}}/K_{MD2,LV_{i,j}})}$	$K_{mm,LV_{i,j}}\frac{(1+C_{LV,F_{Ii,j}}/K_{MD1,LV_{i,j}})}{(1+C_{LV,F_{Ii,j}}/K_{MD2,LV_{i,j}})}$
Pure non-competitive Inhibition	$\frac{V_{Mx,LV,edr_{i,j}}}{(1+C_{LV,F_{Ii,j}}/K_{MD2,LV_{i,j}})}$	$K_{mm,LV_{i,j}}$
Uncompetitive Inhibition	$\frac{V_{Mx,LV,edr_{i,j}}}{(1+C_{LV,F_{Ii,j}}/K_{MD2,LV_{i,j}})}$	$\frac{K_{mm,LV_{I,i,j}}}{(1+C_{LV,F_{Ii,j}}/K_{MD2,LV_{i,j}})}$

where $I_{i,j}$ = zero or the index to the chemical that is the inhibitor to the *j*th metabolite of the *i*th circulating compound.

2.2.8 Metabolism in the other Organs and Tissues

2.2.8.1 Metabolism in the Brain

The brain metabolism equations are the same as those for the liver except that the equation for the V_{max} is given as a function of the Liver value from the equation:

$$V_{Mx,BN_{i,j}} = V_{Mx,LV_{i,j}} R_{M,BN,LV_{i,j}} \frac{V_{BN}}{V_{LV}}$$

where $R_{M,BN,LV_{i,j}}$ is a scaling factor for V_{max} in the Brain for the *j*th metabolite of the *i*th chemical.

2.2.8.2 Metabolism in the Kidney

The kidney metabolism equations are the same as those for the liver except that the equation for the V_{max} is given as a function of the liver value from the equation:

$$V_{Mx,KD_{i,j}} = V_{Mx,LV_{i,j}} R_{M,KD,LV_{i,j}} \frac{V_{KD}}{V_{LV}}$$

where $R_{M,KD,LV_{i,j}}$ is a scaling factor for V_{max} in the Kidney for the *j*th metabolite of the *i*th chemical.

2.2.8.3 Metabolism in the Carcass

The carcass metabolism equations are the same as those for the liver except that the equation for the V_{max} is given as a function of the Liver value from the equation:

$$V_{Mx,CR_{i,j}} = V_{Mx,LV_{i,j}} R_{M,CR,LV_{i,j}} \frac{V_{CR}}{V_{LV}}$$

where $R_{M,CR,LV_{i,j}}$ is a scaling factor for V_{max} in the Carcass for the *j*th metabolite of the *i*th chemical.

2.2.8.4 Metabolism in the Fat

The fat metabolism equations are the same as those for the liver except that the equation for the V_{max} is given as a function of the liver value from the equation:

$$V_{Mx,FT_{i,j}} = V_{Mx,LV_{i,j}} R_{M,FT,LV_{i,j}} \frac{V_{FT}}{V_{LV}}$$

where $R_{M,FT,LV_{i,j}}$ is a scaling factor for V_{max} in the Fat for the *j*th metabolite of the ith chemical.

2.2.8.5 Metabolism in the Slowly Perfused Tissue

The slowly perfused tissue metabolism equations are the same as those for the Liver except that the equation for the V_{max} is given as a function of the Liver value from the equation:

$$V_{Mx,SL_{i,j}} = V_{Mx,LV_{i,j}} R_{M,SL,LV_{i,j}} \frac{V_{SL}}{V_{LV}}$$

where $R_{M,SL,LV_{i,j}}$ is a scaling factor for V_{max} in the slowly perfused tissue for the *j*th metabolite of the *i*th chemical.

2.2.8.6 Metabolism in the Rapidly Perfused Tissue

The rapidly perfused tissue metabolism equations are the same as those for the liver except that the equation for the V_{max} is given as a function of the liver value from the equation:

$$V_{Mx,RP_{i,j}} = V_{Mx,LV_{i,j}} R_{M,RP,LV_{i,j}} \frac{V_{RP}}{V_{LV}}$$

where $R_{M,RP,LV_{i,j}}$ is a scaling factor for V_{max} in the rapidly perfused tissue for the *j*th metabolite of the *i*th chemical.

2.2.8.7 Metabolism in the Spleen

The spleen metabolism equations are the same as those for the liver except that the equation for the V_{max} is given as a function of the liver value from the equation:

$$V_{Mx,SP_{i,j}} = V_{Mx,LV_{i,j}} R_{M,SP,LV_{i,j}} \frac{V_{SP}}{V_{LV}}$$

where $R_{M,SP,LV_{i,j}}$ is a scaling factor for V_{max} in the spleen for the *j*th metabolite of the *i*th chemical.

2.3 References

U.S. EPA 2002. Exposure Related Dose Estimating Model (ERDEM) for Assessing Human Exposure and Dose. EPA/600/X-04/060.

Appendix B. QA

1.0 Quality Assurance for Data and Compartment Models

The purpose of this section is to identify the sources and quality of input data. The data fall into 7 general categories, as described in Table B1. Data deemed of the highest quality were gleaned from publications in peer reviewed journals available in the open literature or from reports conducted under Good Laboratory Practices (GLP) protocols (Category I). These data were used in accordance with the purpose intended by the measurement such as urinary metabolite data from studies designed to quantify and identify urinary metabolites according to specific protocols involving methods for which quality assurance requirements were set a priori. Secondary data (Category II) may be defined as environmental, exposure, or health data developed for another purpose such as dermal absorption parameters involving structurally related chemicals. Secondary data may be viewed as inputs to the ERDEM model for the purpose of estimating absorbed dose, tissue concentrations, and urine eliminations.

Many diverse types of data, including physical data, chemical data, and physiological data may also be used for PBPK modeling (Categories III and IV). These data are taken from a variety of sources including databases, peer-reviewed publications, and estimation techniques. For example, these data might include organ volumes modeled as compartments designed to reasonably represent the flow of chemical within the blood as well as clearance from these compartments. Data from non peer reviewed sources, such as government documents or internal reports (Category V), are evaluated against peer reviewed data. These data may be chemical specific for a single purpose such as the clinical use of congeneric compound having similar physicochemical properties as the target chemical. Estimates may also be gleaned or inferred from a method or statistical process (Categories VI or VII). The method or process may be standardized (ASTM) but the resultant data presented to support the method may not be intended for any other purpose other than to explain the accuracy and precision of the method. Estimates gleaned from statistical processes, such as Quantitative Structure Activity Relationships (QSAR), may also represent a means to test a mechanism rather than predict biological activity. In all of these cases, however, estimates must be accompanied by supporting statistics that express the level of uncertainty surrounding the method or process.

The sources of all data contained within this report have been documented by reference or footnote describing the source of the data. Chemical reactions are modeled as metabolism. A general summary of the models and data utilized in PBPK modeling are presented in the following tables. The data fall into 7 general categories, as described in Table B1. The sources of the major data utilized are categorized and described in Table B2. The compartment models utilized are categorized and described in Tables B3 and B4.

Table B1. Categories of Data Sources and Models

Category	Description
I	Taken from peer reviewed literature or GLP report, used for the purpose intended by the measurement
II	Taken from peer reviewed literature or GLP report, used for the purpose other than intended by the measurement
III	Taken from peer-reviewed database compiled for the purposes in which it is being used
IV	Taken from non peer-reviewed database compiled for the purposes other than those for which it is being used
V	Taken from other non peer-reviewed source
VI	Estimated based on peer-reviewed method or data
VII	Estimated based on non peer-reviewed method

Table B2: Quality and Sources of Data Used in the ERDEM Human Carbaryl Model

Variables		Category	Description	Citation
Cardiac Output		VI	The data from Agata et al (1994) and Schmitz et al (1998) and a curve was fitted to it (Appendix D)	Agata, et al (1994), Schmitz, et al (1998), Rosenthal and Bush (1998)
Body Weight		II	Studies to determine the distribution of body weights by age for humans	Burmaster and Crouch (1997) and Exposure Factors Handbook, Tables 7.2
Body Compartment Blood Flow percentages		I	Values of percentages are modified with the addition of the skin model.	Fisher *et al.* (1998).
Body Compart-ment Volumes	Dermis	V	Value used for PBPK modeling of chloroform	Corley *et al.* (1990)
	Fat	II	Values for children aged 4-21 years	Boot, *et al.*, (1997)
	Liver Kidney	I	Values taken from Reference Man	ICRP 2002
	GI Tract	I	Values taken from reference	ILSI 1994

Variables		Category	Description	Citation
	Rapidly Perf	VI	Modified as necessary for additional of dermal model	Fisher *et al.* (1998)
	Slowly Perf	III	Estimated from the fat content	Fisher *et al.* (1998)
	Brain	II	Measurements	Milner (1990)
Skin Permeation Coefficients		VI	Utilized experimental results for rats	Table 1
Gastrointestinal Absorption Rates		VI	Utilized experimental results for rats; scaled by body weight for rat and human	Table 1
Tissue to Blood Partition Coefficients		VI	Combination of QSAR (Appendix D) and experimental results	Poulin and Theil (2000), Table 1
Metabolism Constants for Saturable Metabolism		VI	Utilized experimental results for rats; scaled by body weight for rat and human.	Table 1
Urine Elimination Rate Constants		VI	Utilized experimental results for rats; scaled by body weight for rat and human.	Table 1
Acetylcholinesterase inhibition		VI	Based on *in vitro* study; refined from rat *in vivo* experiments	Hetnarski and O'Brien 1975; Table 1

Table B3: Categories of Compartment Model Approaches

Category	Description
A	Widely accepted modeling approach
B	Approach similar to commonly used and accepted approaches, but adapted to satisfy project specific requirements
C	Novel approach addressing specific requirements of estimating absorption and dose.

Table B4: Quality of Compartment Models

Model	Cat.	Description
Brain	A	The blood-brain barrier is not modeled. A permeation coefficient determines the amount of chemical remaining in the brain and that passed to the venous blood. Metabolism is modeled as a saturable Michaelis-Menten process.
Dermis	B	Chemical is placed on the skin over a short application period and then a permeation coefficient is used to determine absorption into the skin
Kidney	A	A permeation coefficient determines the amount of chemical remaining in the kidney and that passed to the venous blood. Urine elimination is modeled with a urine rate constant, or saturable Michaelis-Menten constants.
Fat, Liver, Rapidly Perfused Slowly Perfused	A	A permeation coefficient determines the amount of chemical remaining in the compartment and that passed to the venous blood. Metabolism in the liver is modeled as a saturable Michaelis-Menten process
Blood	A	The arterial blood enters a compartment, a permeation coefficient determines the amount of chemical remaining in the compartment and that passed to the venous blood. Metabolism in the blood is modeled as a saturable Michaelis-Menten process
Stomach/ Intestine	A	Modeled with rate constants from stomach to intestine, stomach to portal blood, intestine to portal blood, and intestine to feces.

2.0 Quality Assurance for the Exposure Related Dose Estimating Model (ERDEM)

2.1 Quality Assurance of the ERDEM Models

There are many different methods of checking the quality of the ERDEM Model. The key is to never assume that everything is working properly. Continuous checking and testing are required. The inputs to the model must be checked and rechecked. The outputs from model runs must be carefully checked.

.

2.2 Code review

The model code is written in the Advanced Continuous Simulation Language (ACSL). It is reviewed periodically, when any problems occur, or when changes

are to be made. The input variable initializations are checked, those variables that are sent from one compartment to the next are checked, the warnings of improper data input are checked, the initialization and setting of exposure events, and the equations in the derivative section are checked.

2.3 Mass balance checks.

During any model run, mass balance checks are automatically performed by compartment, for each chemical, and an overall mass balance ratio check is performed. Failure of these checks can be due to improper coding of an equation, or could be the result of lack of input exposures, or faulty inputs. The following is an example of the mass balance ratios by compartment for trichloroacetic acid. Values on the order of 10^{-14} are expected because the model is run in double precision:

MASS BALANCE DIFFERENCE RATIOS (ADIF/AINPUT): R_AB_DIF(2)= 0.2371175E-15
R_AL_DIF= 0.000000 R_BN_DIF=-0.1746669E-15 R_CC_DIF= 0.000000
R_CN_DIF= 0.000000 R_CNL_DIF= 0.000000 R_CP_DIF= 0.9002710E-17
R_CR_DIF= 0.000000 R_DR_DIF=-0.1091668E-15 R_DU_DIF= 0.000000
R_DUL_DIF= 0.000000 R_FT_DIF= 0.000000 R_IN_DIF= 0.000000
R_KD_DIF=-0.1164446E-15 R_LD_DIF= 0.000000 R_LG_DIF= 0.1035248E-15
R_LP_DIF= 0.000000 R_LV_DIF=-0.1064165E-17 R_OV_DIF= 0.000000
R_PB_DIF= 0.000000 R_PU_DIF= 0.000000 R_RP_DIF= 0.000000
R_SI_DIF= 0.000000 R_SIL_DIF= 0.000000 R_SL_DIF= 0.000000
R_SP_DIF= 0.000000 R_ST_DIF= 0.000000 R_STL_DIF= 0.000000
R_SW_DIF= 0.000000 R_TS_DIF= 0.000000 R_UD_DIF= 0.000000
R_VB_DIF= 0.000000

2.4 Proper Operation with Inputs for Known Chemicals and Their Known Metabolism Paths

An example of proper operation with inputs for MTBE is shown in Figure 1. Plots of the concentration of MTBE in the liver, kidney, and venous blood are shown for a continuous inhalation in an environment with 400 ppb of MTBE. A basic set of such model runs are performed that are repeatable so that if the model is changed, then these sets of data can be rerun and output results checked against earlier results. Compartments are checked for proper circulation of chemicals and proper metabolism and elimination.

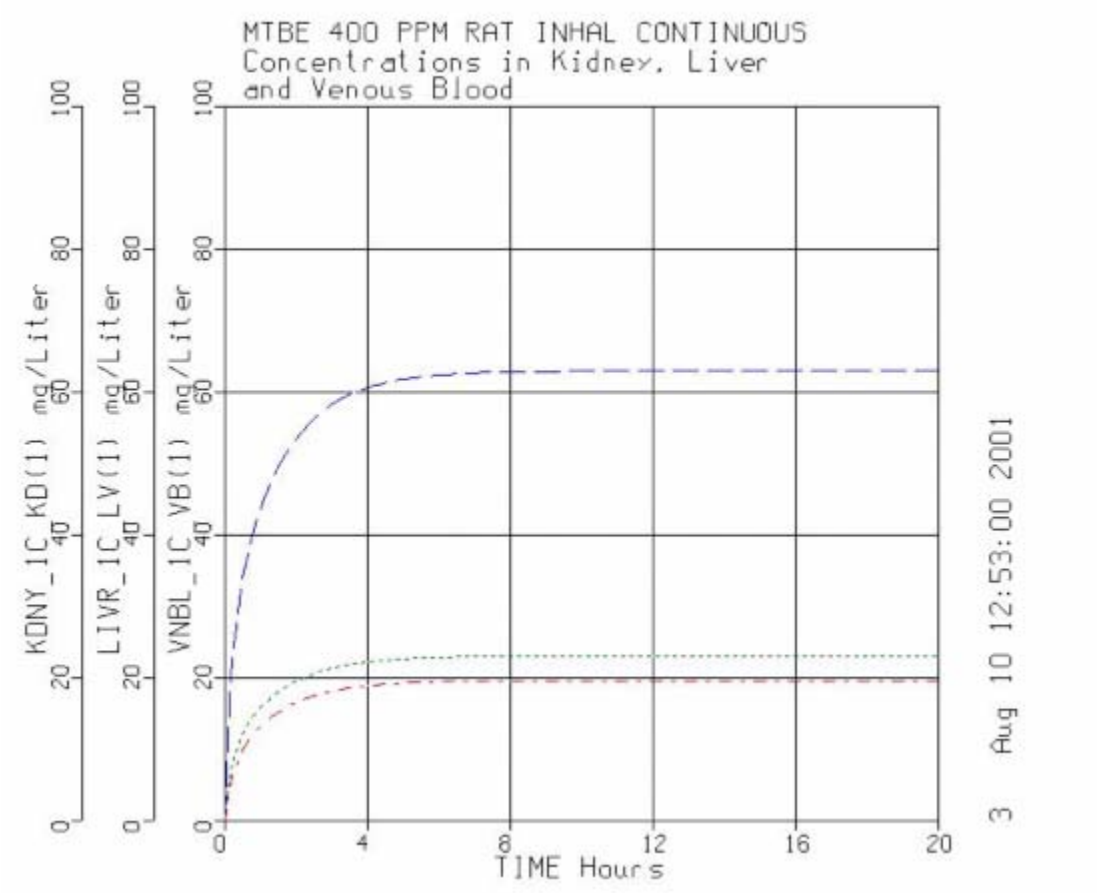

Figure B1: Concentrations of MTBE in Kidney, Liver, and Venous Blood for Continuous Exposure at 400 ppm.

2.5 Comparisons of Model Runs with Experimental Results

The results of a PBPK/PD model mean very little unless some measure of confidence in the results may be obtained. One way to do this is to test the model against experimental data. The ERDEM model has been compared with results of at least three different sets of chemicals and experimental data sets other than carbaryl:

- Fisher et al, 1998, with trichloroethylene on human volunteers.
- Comparison of ERDEM runs with methyl tertiary-butyl ether (MTBE) experimental results for humans, rats, and mice.
- Comparison with radio-labeled isofenphos and parathion.

These model runs with ERDEM validate the model for each special case. Each new chemical and demographic group require separate comparison with experimental data.

2.6 Proper Use of an ERDEM Model

In order to gain confidence in the results of model runs, the user of an ERDEM model must consider the following:

- The source for the values of input parameters to the ERDEM model must be specified, even if an approximation. If the model is functioning as designed but the input values are improper, then it is the same as if the model itself did not work properly.

- Mistakes in the setting of input values, even though they are well chosen, will cause improper model operation.

- Part of quality assurance for given sets of model runs is review of the outputs for various organs and determining that they are reasonable.

- The user must check for error messages output by the model engine when processing improper inputs.

- The ERDEM model checks input values and outputs warnings and even may abort the model run when illegal values are input. The user should check all warnings.

- The user must check output results for reasonableness.

- The absorbed dose from the various exposures, the amounts eliminated, the amounts metabolized, and the amount of chemical eliminated due to enzyme inhibition should all be checked. These are supplied as part of the output printed at the completion of a model run.

- The relative and absolute error limits must be set according to guidelines available in the Front End.

The mass balance ratios for each compartment, each chemical and total mass balance must be on the order of 10^{-14} or less.

Appendix C. Biomonitoring Study Data Analysis

1.1 Study Description

The Bayer biomonitoring study is described elsewhere (Bayer 2004c). The following is taken directly from the abstract of Bayer 2004c:

"The purpose of this study was to characterize the potential absorbed doses of carbaryl to homeowners and residents during and following the residential application of carbaryl by measuring urinary pesticide metabolite levels in the applicator, spouse, and children of representative families that use pesticides. Non-professional adult and child volunteers were used to measure carbaryl absorbed doses in homeowners and their families during and after application of Sevin® GardenTech Ready-To-Spray, a formulation of carbaryl. Sites were selected in Missouri and California. Ten families were monitored in Missouri and 13 families were monitored in California.

"The formulated product, Sevin® GardenTech Ready-To-Spray (22.5% a.i. wt/wt), is a liquid formulation of Sevin®, for use on lawns, gardens, and ornamentals for insect control.

"Application of the test substance was performed by an adult at each site. The applicator sprayed approximately 4,000 to 10,000 ft^2 of lawn and/or approximately 400 to 1,000 ft^2 of garden or ornamentals on the property or residence. The test substance was applied at the recommended label rate at the Missouri sites (average of 4.8 lb a.i./A with a range of 2.5 to 6.5 lb a.i./A). The test substance was applied at an average rate of 30.0 lb a.i./A (range of 2.0 to 160 lb a.i./A) for the California sites. The method of application was a hose end sprayer. With two exceptions, the families consisted of the applicator, spouse, and a minimum of one child between the ages of 4 to 17 years old. The Missouri Site 10 family consisted of a 3.5 years-old child. The California Site 8 family consisted of an applicator and one child. The total number of participants in the study was 106 (23 applicators, 22 spouses, 6 adult residents, 42 children 4-12 years-old, and 13 children 13-17 years-old).

"The average time required to apply the test substance and clean-up for the Missouri sites was 42 minutes (range of 30 to 80 min). The average amount of GardenTech Ready-To-Spray applied was 45 oz which is equivalent to 451 g a.i (range of 332 to 613 g a.i.). The average time required to apply the test substance and clean-up for the California sites was 25 minutes (range of 5 to 60 min). The amount of GardenTech Ready-To-Spray applied was 32 oz at each site, which is equivalent to 255 g a.i. The application of the liquid formulation to the lawn, vegetable garden, and ornamental flowers was selected to represent an upper-bound exposure potential for carbaryl residential uses.

"Activities outside the residence in or near the treated areas for the applicator, spouse, and children were monitored the day of application (day 0), and days 1, 2, and 3 post-application. Activities such as mowing, trimming, weeding, planting, applying fertilizer, working in gardens, working on buildings, hanging clothes, and playing were documented for each individual participant and the approximate time of potential exposure.

"Urine samples were collected from participants beginning two days before (day 2) the application through three days after application (day 3). Each urine sample was a 24-hour composite, resulting in six 24-hour urine samples from each participant (days -2, -1, 0, 1, 2, and 3). The day 0 sample collection period began with the first void after the application and ended 24 hours later. The presence of 1-naphthol in the urine can result from non-carbaryl sources of exposure. The two days of pre-application monitoring were intended to provide information on background levels of 1-naphthol among the study participants. No correction has been made for pre-application 1-naphthol levels. The conversion of urinary 1-naphthol to carbaryl based on carbaryl pharmacokinetic data inherently assumes that all 1-naphthol present in the urine derived from carbaryl and is an inherent source of overestimation of the carbaryl-specific levels of 1-naphthol.

"Urine samples were analyzed for 1-naphthol using "Method for the HPLC Analysis of 1-Naphthol, Caffeine, and Cotinine in Urine." The LOQ for 1 naphthol was determined to be 0.01 ppm. The average recovery for the 0.01 ppm level was 71.5 ± 0.14%. The average recovery for the 0.1 ppm level was 80.9 ± 0.89%. The average recovery for the 1 ppm level was 84.3 ± 0.93%.

"Method recoveries were corrected for any analyte determined in the corresponding controls.

"In both the Missouri and California participants there were levels of 1-naphthol detected in the Days –2 and –1 urine samples. The 1-naphthol likely resulted from exposure to non-carbaryl sources of 1-naphthol and potentially from dietary residues of carbaryl. For the Missouri sites the pre-application 1-naphthol levels (corrected to carbaryl residues) found in the urine ranged from 4.5 to 0.005 µg/kg body weight in the applicator, 5.8 to 0.005 µg/kg body weight in the spouses, 1.2 to 0.005 µg/kg body weight in children 13 to 17 years old, and 12.5 to 0.005 µg/kg body weight in children 4 to 12 years old. For California the pre-application 1-naphthol levels (corrected to carbaryl residues) found in the urine ranged from 1.5 to 0.005 µg/kg body weight in the applicator, 3.7 to 0.005 µg/kg body weight in the spouses, 2.0 to 0.005 µg/kg body weight in adult residents, 1.4 to 0.005 µg/kg body weight in children 13 to 17 years old, and 2.2 to 0.005 µg/kg body weight in children 4 to 12 years old.

"For the Missouri sites, carbaryl residue levels found in urine from applicators on day-0 ranged from 21.7 to 0.26 µg/kg body weight. Carbaryl residue levels found

in urine from spouses on day 0 ranged from 4.9 to 0.005 µg/kg body weight. Carbaryl residue levels found in urine from children 4 - 12 years old on day-0 ranged from 61 to 0.15 µg/kg body weight. Carbaryl residue levels found in urine from children 13 - 17 years old on day 0 ranged from 12.6 to 0.25 µg/kg body weight. Maximum carbaryl residue levels found were 21.7 µg in applicators, 4.9 µg in spouses, 61 µg in children 4 -12, and 12.6 µg in children 13 - 17."

1.2 Data Analysis

As mentioned in section 2.3 of the main text, only the Missouri data were considered for this assessment based on the inconsistencies with the labeling instructions at the California sites. The 1-naphthol levels were converted to carbaryl equivalents based on the following:

- Molecular weight conversion (201.2/144.2= 1.4)
- Metabolic selectivity, where 40% of carbaryl is assumed to be excreted as 1-naphthol species

Therefore, the mass of 1-naphthol in urine was multiplied by 3.5 (1.4 / 0.40) to estimate the equivalent mass of carbaryl absorbed.

Repeated measurement analysis of variance, rm-ANOVA (with a preferable balance design), was selected for the analysis of study data because of dependence of each subsequent within-subjects measurement on the previous measurements (as an individual-subject variation constraint, see Winer, 1976; BMDP, 1979; and Kleinbaum *et al.*, 1998). In the Bayer and EPA studies, the data were nested with states by sites; the dependent variables were the repeated measures of urine volume (mL), creatinine concentration (g/L), corrected excretion of 1-naphthol (µg/mL), and total excretion of 1-naphthol (µg). Their children age grouping critera produced an unbalance rm-ANOVA design. The rationale for both age groupings was not explained as shown in the following:

1. Bayer Age-Grouping
   - applicator, others, and (2-level) children such as 4-12; 13-17
2. EPA Age-Grouping
   - applicator, others, and (4-level) children such as 4-5; 6-10; 11-15; 16-17

Consideration was given to the unbalanced nature of Bayer and EPA age grouping, and adjustments were made according to child development and learning (Bredekamp, 1983; American Academy of Pediatrics and the American Red Cross, 1990). This adjustment produced four groups: 4-5 years of age described as preschoolers (n=7), 6-8 years for elementary school aged (n=7), 9-12 years for older elementary school aged (n=9) and 13-16 for junior high school and high school aged (n=7) for the Missouri data (Table C1). This balance sample size improvement allows us to perform the traditional rm-ANOVA with a

better suitability for the balance design assumption. Then, the balance rm-ANOVA was considered the more appropriate design for the Missouri data.

Table C1. Children sample size distributions in three groupings, Bayer, EPA, and Current

	Age group			
Study	I	II	III	IV
Bayer	Age: 4-12	Age: 13-17		
	n=23	*n=7*		
EPA	Age:4-5	Age: 6-10	Age: 11-15	Age: 16-17
	n=7	*n=13*	*n=8*	*n=2*
Current	Age: 3-5	Age: 6-8	Age: 9-12	Age: 13-17
	n=7	*n=7*	*n=9*	*n=7*

The results generated by SPSS software were summarized into the upper confidence interval plots produced by R software for the cumulative excreted mass of carbaryl equivalents (Figure C1).

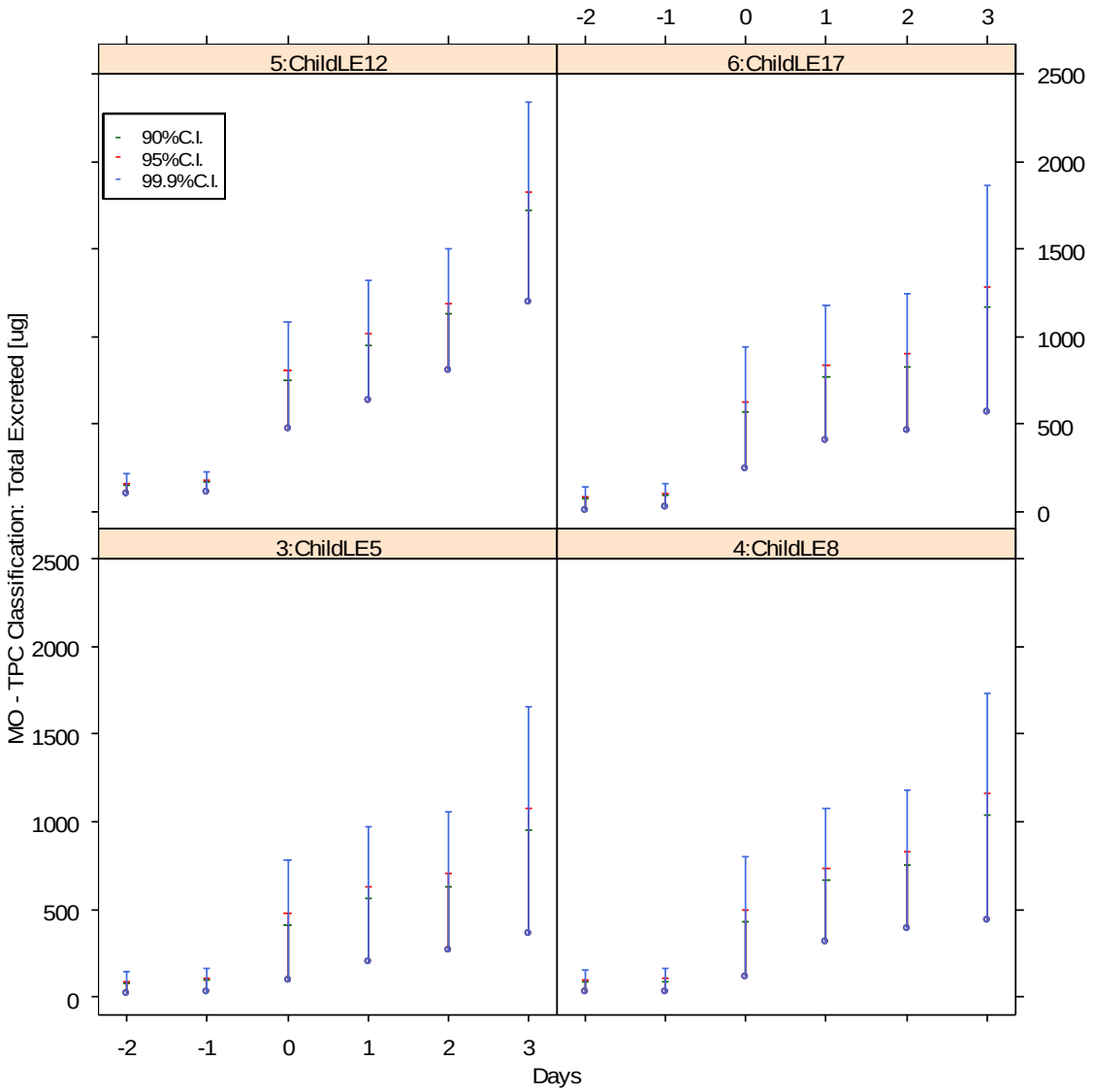

Figure C1. Confidence interval plot by age group of cumulative excreted mass of carbaryl equivalents.

Table C2. Confidence Intervals by Age Group

STATE	Confidence	FACTOR	Days	Mean	StdError	Lower Bound	Upper Bound
MO	95%C.I.	3:ChildLE5	-2	19.624	34.733	-51.771	91.02
MO	***95%C.I.***	***3:ChildLE5***	***-1***	***33.259***	***34.91***	***-38.501***	***105.018***
MO	95%C.I.	3:ChildLE5	0	98.071	185.091	-282.388	478.531
MO	95%C.I.	3:ChildLE5	1	204.743	207.305	-221.379	630.864
MO	95%C.I.	3:ChildLE5	2	270.686	211.814	-164.705	706.077
MO	95%C.I.	3:ChildLE5	3	359.876	348.674	-356.834	1076.585
MO	95%C.I.	4:ChildLE8	-2	28.014	34.733	-43.381	99.41
MO	***95%C.I.***	***4:ChildLE8***	***-1***	***32.376***	***34.91***	***-39.384***	***104.135***
MO	95%C.I.	4:ChildLE8	0	114.589	185.091	-265.871	495.048
MO	95%C.I.	4:ChildLE8	1	311.174	207.305	-114.947	737.296
MO	95%C.I.	4:ChildLE8	2	391.65	211.814	-43.741	827.041
MO	95%C.I.	4:ChildLE8	3	439.743	348.674	-276.967	1156.452
MO	95%C.I.	5:ChildLE12	-2	101.478	30.632	38.513	164.443
MO	***95%C.I.***	***5:ChildLE12***	***-1***	***116.189***	***30.788***	***52.903***	***179.475***
MO	95%C.I.	5:ChildLE12	0	473.983	163.235	138.449	809.517
MO	95%C.I.	5:ChildLE12	1	639.794	182.826	263.991	1015.598
MO	95%C.I.	5:ChildLE12	2	807.406	186.803	423.427	1191.384
MO	95%C.I.	5:ChildLE12	3	1196.506	307.501	564.427	1828.584
MO	95%C.I.	6:ChildLE17	-2	13.457	34.733	-57.938	84.853
MO	***95%C.I.***	***6:ChildLE17***	***-1***	***32.971***	***34.91***	***-38.788***	***104.731***
MO	95%C.I.	6:ChildLE17	0	250.114	185.091	-130.346	630.574
MO	95%C.I.	6:ChildLE17	1	412.171	207.305	-13.95	838.293
MO	95%C.I.	6:ChildLE17	2	463.029	211.814	27.638	898.419
MO	95%C.I.	6:ChildLE17	3	570.257	348.674	-146.452	1286.967

The assessment focused on evaluating conservative scenarios, so the 99.9%ile was used to establish the magnitude of exposure. The group LE5 was simulated to evaluate hand-to-mouth exposure, and the LE12 group was used since they showed the highest biomarker levels. The older group is assumed to be exposed by the dermal route.

1.3 References

American Red Cross. Safely Checklist from The American Red Cross Child Care Course, Health & Safety Units. The American Red Cross, 1990.

BMDP Statistical Software Manual 1979. Berkeley: University of California Press.

Bredekamp S. Guide to accreditation by the National Academy of Early Childhood Programs. National Association for the Education of Young Children, Washington, DC, 1985.

Kleinbaum, D. G., Kupper, L. L., Muller, K. E., and Nizam, A. (1998) "Applied Regression Analysis and Other Multivariable Methods," 3rd Ed. Pacific Grove: Duxbury Press.

Winer, B. J.(1971). "Statistical Principles in Experimental Design," 2nd Ed. New York: McGraw-Hill.

Appendix D. Cardiac Output and Partition Coefficients

1.0 Calculation of Cardiac Output for Children as a function of age and growth

Cardiac output measurements used in the simulations were obtained from Rosenthal and Bush (1998). Pulmonary blood flow was determined in a small number of boys and girls of different ages. The neonatal values were obtained from Agata et al, (1994). Values for children 0.5 to 19 years of age were obtained from Schmitz et al, (1998). These final two studies were selected because they combined information for both males and females and the total number of subjects was larger than in other studies surveyed. The values used for the simulations represent averages for each age group and gender.

1.1 Methods and Results

The average value of 96 hours after birth was selected as the starting value for neonates. This value was selected because there was a steady decline in cardiac output after birth, reaching a steady state value at 96 hours. These data were plotted with the data from Schmitz et al, (1998) and a regression equation was obtained (Figure D1)

Cardiac output (liters/hour) = $174.64\ x^{0.2989}$, where x is age in years.

This equation was used to calculate the average cardiac output for children ages 3, 9, and 18 years. The calculation is the same for both boys and girls. After the calculation, cardiac outputs were rounded to 3 significant digits (Table D1). These values were used in the simulations for boys and girls.

Table D1. Cardiac Output for Children by Age

Age (Years)	**Cardiac Output (Liters/Hour)**
3	242
9	337
18	414

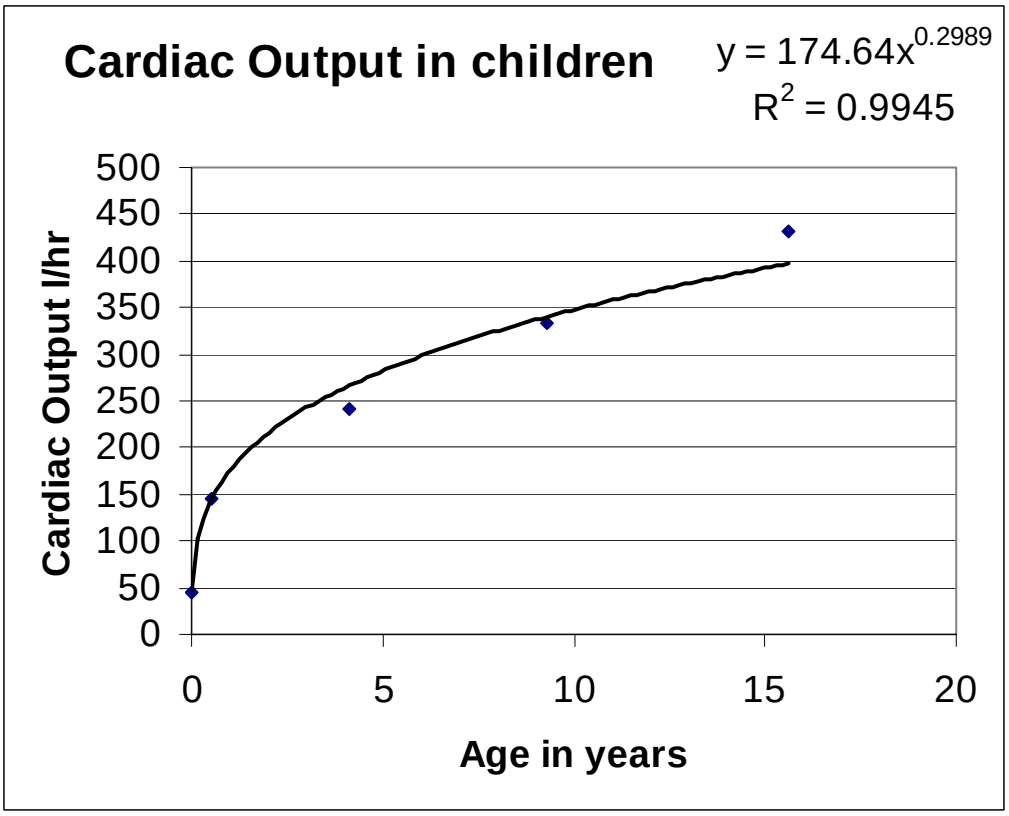

Figure D1. Cardiac Output Data and the Fitted Equation for Children

1.2 References

Agata Y, Hiraishi S, Misawa H, Hirota H, Nowatari M, Hiura K, Fujino N, Oguchi K, and Horiguchi Y. (1994) Regional Blood Flow Distribution and Left Ventricular Output during Early Neonatal Life: A Quantitative Ultrasonographic Assessment. Pediatric Research. Vol 36, pp.805-810.

Rosenthal M. and Bush A. (1998) . Haemodynamics in children during rest and exercise: methods and normal values. Eur Respir J. Vol 11: pp. 854-865.

Schmitz L, Koch H, Bein G, and Brockmeier K. (1998). Left Ventricular Diastolic Function in Infants, Children, and Adolescents. Reference Values and Analysis of Morphologic and Physiologic Determinants of Echocardiographic Doppler Flow Signals During Growth and Maturation. Journal of the American College of Cardiology. Vol 32, pp. 1441-1448.

2.0 Estimation of human tissue: plasma partition coefficients (Pt:p) for carbaryl and metabolites

Tissue: plasma partition coefficients (Pt:p) are physiochemical input parameters. The Pt:p represent the relative distribution of a chemical between tissues and plasma at equilibrium. *In vitro* and *In vivo* methods are available for direct estimation of the Pt:ps; however, these methods are often resource and time intensive, requiring equilibrium conditions and the use of appropriate analytical methods. In recent years, algorithms have been developed for predicting Pt:p based on the chemical's n-octanol-water partition coefficient (Kow) and the relative distribution of lipids in tissue and plasma (Poulin and Theil 2002, Poulin and Krishnan 1995, Haddad *et al.* 2000;).

The basis of this approach is that the solubility of a chemical in tissue (e.g., plasma) may be approximated by its additive solubility in lipid and water (Poulin and Krishnan 1995). Lipid solubility is approximated by the Kow. The quantitative relation between Kow and Pt:p may be used to predict tissue distribution based on the following equation:

$$\text{Pt:p, nonadipose}^* = \frac{\text{Kow (Vnlt + 0.3Vpht) + [Vwt + 0.7Vpht]}}{\text{Kow (Vnlp + 0.3Vphp) + [Vwt + 0.7Vphp]}} \quad (\textbf{D1})$$

where V is the fractional tissue volume content of neutral lipids (nl), phospholipids (ph) and water (w), t is tissue, p is plasma (Table D2).

Table D2. Human physiological parameters for volumes used in estimating $P_{t:p}$ (Poulin and Theil 2002)

Tissue	Tissue (Vt)[a]	Water (Vw)	Vnl	Vpl
Adipose	0.120	0.180	0.790	0.002
Bone	0.086	0.439	0.074	0.001
Brain	0.020	0.770	0.051	0.057
Gut	0.017	0.718	0.049	0.016
Heart	0.005	0758	0.012	0.017
Kidney	0.004	0.783	0.021	0.016
Liver	0.026	0.751	0.035	0.025
Lung	0.008	0.811	0.003	0.009
Muscle	0.400	0.760	0.024	0.007
Skin	0.037	0.718	0.028	0.011
Spleen	0.003	0.788	0.020	0.020
Plasma	0.042	0.945	0.004	0.002

a. Fraction of Body weight (L/Kg) for 70 kg human

Equation **D1** is limited to non-adipose tissue because Kow does not properly estimate the hydrophobic interactions of chemicals and ionized lipids found in adipose tissue (Poulin and Theil 2002). Alternatively, Kob, based on the olive oil:buffer partition coefficient, takes into account partitioning of nonionized and ionized species:

$$Pt{:}p,\ adipose^{*} = \frac{Kob\ (Vnlt + 0.3Vpht) + [Vwt + 0.7Vpht]}{Kob\ (Vnlp + 0.3Vphp) + [Vwt + 0.7Vphp]} \qquad (\mathbf{D2})$$

However, experimental data for Kob are much more limited than for Kow. It is therefore convenient to compute this parameter from Kow (Leo *et al.* 1971) :

$$\text{Log Kob} = 1.115 \times \log \text{Kow} - 1.35,\ n=104,\ r=0.99 \qquad (\mathbf{D3})$$

Both equations **D1** and **D2** tend to overestimate the Pt:p to the extent that protein binding in tissue and plasma is not taken into consideration. Protein binding may be considered in the PBPK model as an equilibrium reaction, distinguishing the relative amount of bound compound from free. On the other hand, if not large, it may be taken directly into account in the estimated partition coefficient. Poulin and Theil (2002) indicate that equation **D1** may be multiplied by the ratio of the

fraction of unbound protein the plasma to the fraction of unbound protein in tissue (fup/fut).

$$\text{Pt:p, nonadipose} = \text{Pt:p, nonadipose*} \times (\text{fup/fut}) \qquad (\mathbf{D4})$$

The fraction unbound in tissue (fut) may be estimated from fup, based on assumptions of the relative distribution of typical binding proteins between plasma and tissue (ie., albumin, globulins, and lipoproteins). According to Poulin and Theil (2000), mammalian systems tend toward a value of 0.5; hence,

$$\text{fut} = 1/(1+\{[(1-\text{fup})/\text{fup}] \times 0.5\}) \qquad (\mathbf{D5})$$

A 10% protein binding in plasma (fup=0.9) is assumed to obtain a ratio where fup/fut =0.95. Thus, the bias in Pt:p is -5% for 10% protein binding. However, the error for adipose tissue is 1:1 since the adjustment is greater (fup/1) with the assumption of no protein binding in adipose tissue:

$$\text{Pt:p, adipose} = \text{Pt:p, adipose*} \times \text{fup} \qquad (\mathbf{D6})$$

The predicted Pt:p may be checked for plausibility, provided that experimental data exist for the steady state volume of distribution. Each tissue contributes to the total experimental volume of distribution as follows: Vt x Pt:p. Hence, the predicted volume of distribution (Vdss) may be computed as follows:

$$\text{Predicted Vdss} = \Sigma\,(\text{Vt} \times \text{Pt:p}) + \text{Vp} \qquad (\mathbf{D7})$$

All estimates of Pt:p assume no protein binding, hence fup/fut=1 and fup=1. Assuming 20% protein binding in the plasma, these methods overestimate Pt:p by 10% in non-adipose tissue.

2.1 Estimation of LogP (Log_{10}[Kow]) for carbaryl and metabolites

Experimental values for LogP were used for carbaryl and naphthol (Table D3). Because experimental LogP were not available for the other metabolites of carbaryl, LogP were estimated using the semi-empirical neural network approach (see http://www.logp.com./) and are listed in Table D3. The prediction for carabyl using this method was logP= 2.35, consistent with the experimental value of 2.36.

2.2 Estimation of LogD (Log_{10}[Kob]) for carbaryl and metabolites

Log D was estimated for carbaryl using equation **D3** giving a value of Log_{10}[Kob]= 1.284. Equation **D3** assumes that the compound is neutral. For acid or base compounds, ionizability was taken into account. Common metabolites of carbaryl tend to be acidic. Adjustments based on Hendersen-Hasselbalch

equations take into consideration ionized species. Equation **D8** employs the neutral LogD and the pKa to estimate LogD for monoprotic acids (see Table D3).

$$\text{LogD(monoprotic acid)} = \text{LogD(neutral)} - \log(1 + 10^{\text{pH-pKa}}) \quad (\textbf{D8})$$

The pKa for acid metabolites were predicted using (http://ibmlc2.chem.uga.edu/sparc/index.cfm) and physiological pH was employed. The pKa values of the compounds are predicted using approximately 300 Hammett and Taft equations.

Table D3. Physiochemical properties of carbaryl and its metabolites

Compound	MW	Structure	pKa	Log(Kow), experiment	Log(Kow), predicted	Log(Kob), pH 7.4
Carbaryl	201.2		12.02	2.36	2.3484	1.284
4-OH carbaryl	217.2		9.2		1.8682	0.73
3,4 DIOH carbaryl	235.2		12.66		0.2516	-1.0694
5,6 DIOH carbaryl	235.2		12.16		-0.007	-1.357805
Naphthol	144.2		9.4	2.85	2.6888	1.82775
3,4 DIOH naphthol	178.2		9.92		0.1867	-1.1418

Compound	MW	Structure	pKa	Log(Kow), experiment	Log(Kow), predicted	Log(Kob), pH 7.4
Naphthyl sulfate	224.2				-0.4554	-9.0745
Naphthyl glucuronide	320.3		2.78		0.8421	-4.3046
3,4 DIOH naphthyl sulfate	258.2				-3.3424	-12.1069
3,4 DIOH naphthyl glucuronide	354.3				-1.5013	-7.115
4-OH carbaryl sulfate	297.3				-1.276	-10.05
4-OH carbaryl glucuronide	393.3		2.75		0.0215	-5.2775
3,4 DIOH carbaryl sulfate	315.3				-3.1608	-12.1781

Compound	MW	Structure	pKa	Log(Kow), experiment	Log(Kow), predicted	Log(Kob), pH 7.4
3,4 DIOH carbaryl glucuronide	411.4				-0.913	-6.5872
5,6 DIOH carbaryl glucuronide	411.4				-1.1719	-6.8687

2.3 Calculation of partition coefficients

As mentioned in section 2.2.2, partition coefficients were calculated only for carbaryl and its primary metabolites, along with 3,4 DIOH naphthol. As seen in Table D3, complete chemical descriptions were available for these compounds, but the other metabolites have not been completely characterized.

To calculate the Pt:p for any non-adipose tissue, the calc entry for any tissue is divided by the calc entry for plasma. To calculate the Pt:p for adipose tissue, the calc entry for adipose is divided by the calc entry for plasma(D*vo:w). In the following tables, 'calc' refers to the numerator of equation1 for all tissues except the adipose tissue, where the numerator of equation **D2** is employed. For plasma tissue, the denominator of equation **D1** is employed except for 'plasma (D*vo:w), where the denominator of equation **D2** is employed.

Table D4. Partition coefficient calculations for carbaryl

Tissue	**HUMAN** Tissue (Vt)	Water (Vw)	Neutral Lipid (Vnl)	Phospholipids (Vpl)	Ko:w	Carbaryl -num-	$P_{t:b}$	$P_{t:p}$	$Vt*P_{t:p}$
Adipose (D*vo:w)	0.120	0.180	0.7900	0.0020	19.116	15.2946	17.107	14.90	1.782
Adipose (Ko:w)	0.120	0.180	0.7900	0.0020	229.087				
Bone	0.086	0.439	0.0740	0.0011	229.087	17.4678	10.32	9.18	0.786
Brain	0.020	0.770	0.0510	0.0565	229.087	16.3760	9.68	8.61	0.172
Gut	0.017	0.718	0.0487	0.0163	229.087	13.0062	7.69	6.83	0.117
Heart	0.005	0.758	0.0115	0.0166	229.087	4.5450	2.69	2.39	0.011
Kidney	0.004	0.783	0.0207	0.0162	229.087	6.6512	3.93	3.50	0.015
Liver	0.026	0.751	0.0348	0.0252	229.087	10.4728	6.19	5.50	0.143
Lung	0.008	0.811	0.0030	0.0090	229.087	2.1231	1.25	1.12	0.008
Muscle	0.400	0.760	0.0238	0.0072	229.087	6.7121	3.97	3.53	1.411
Skin	0.037	0.718	0.0284	0.0111	229.087	7.9947	4.73	4.20	0.156
Spleen	0.003	0.788	0.0201	0.0198	229.087	6.7673	4.00	3.56	0.009
Plasma	0.042	0.945	0.0035	0.0023	229.087	1.9030			
Plasma (D*vo:w)	0.042	0.945	0.0035	0.0023	19.116	1.0264			
Whole blood	0.077	0.820	0.0032	0.0020	229.087	1.6919			
Whole blood (D*vo/w)	0.077	0.820	0.0032	0.0020	19.116	0.8940			
Erythrocytes	0.035							**Vdss**	**4.653**

Table D5. Partition coefficient calculations for 3,4-dihydroxy carbaryl

	HUMAN		Neutral Lipid	Phospholipids			3,4-DiOH Carbaryl		
Tissue	Tissue (Vt)	Water (Vw)	(Vnl)	(Vpl)	Ko:w	-num-	$P_{t:b}$	$P_{t:p}$	$Vt*P_{t:p}$
Adipose (D*vo:w)	0.120	0.180	0.7900	0.0020	0.085	0.2488	0.303	0.26	0.031
Adipose (Ko:w)	0.120	0.180	0.7900	0.0020	1.785				
Bone	0.086	0.439	0.0740	0.0011	1.785	0.5724	0.69	0.60	0.051
Brain	0.020	0.770	0.0510	0.0565	1.785	0.9308	1.12	0.98	0.020
Gut	0.017	0.718	0.0487	0.0163	1.785	0.8251	1.00	0.86	0.015
Heart	0.005	0.758	0.0115	0.0166	1.785	0.7990	0.96	0.84	0.004
Kidney	0.004	0.783	0.0207	0.0162	1.785	0.8400	1.01	0.88	0.004
Liver	0.026	0.751	0.0348	0.0252	1.785	0.8442	1.02	0.88	0.023
Lung	0.008	0.811	0.0030	0.0090	1.785	0.8275	1.00	0.87	0.007
Muscle	0.400	0.760	0.0238	0.0072	1.785	0.8114	0.98	0.85	0.340
Skin	0.037	0.718	0.0284	0.0111	1.785	0.7824	0.94	0.82	0.030
Spleen	0.003	0.788	0.0201	0.0198	1.785	0.8483	1.02	0.89	0.002
Plasma	0.042	0.945	0.0035	0.0023	1.785	0.9540			
Plasma (D*vo:w)	0.042	0.945	0.0035	0.0023	0.085	0.9469			
Whole blood	0.077	0.820	0.0032	0.0020	1.785	0.8282			
Whole blood (D*vo/w)	0.077	0.820	0.0032	0.0020	0.085	0.8217			
Erythrocytes	0.035							**Vdss**	**0.570**

Table D6. Partition coefficient calculations for 3,4-dihydroxy carbaryl glucuronide

	HUMAN		Neutral Lipid	Phospholipids			3,4-DiOH Carbaryl Glucuronide		
Tissue	Tissue (Vt)	Water (Vw)	(Vnl)	(Vpl)	Ko:w	-num-	$P_{t:b}$	$P_{t:p}$	$Vt*P_{t:p}$
Adipose (D*vo:w)	0.120	0.180	0.7900	0.0020	0.000	0.1814	0.221	0.19	0.023
Adipose (Ko:w)	0.120	0.180	0.7900	0.0020	0.122				
Bone	0.086	0.439	0.0740	0.0011	0.122	0.4488	0.55	0.47	0.041
Brain	0.020	0.770	0.0510	0.0565	0.122	0.8178	1.00	0.86	0.017
Gut	0.017	0.718	0.0487	0.0163	0.122	0.7360	0.90	0.78	0.013
Heart	0.005	0.758	0.0115	0.0166	0.122	0.7716	0.94	0.81	0.004
Kidney	0.004	0.783	0.0207	0.0162	0.122	0.7975	0.97	0.84	0.004
Liver	0.026	0.751	0.0348	0.0252	0.122	0.7738	0.94	0.82	0.021
Lung	0.008	0.811	0.0030	0.0090	0.122	0.8180	1.00	0.86	0.007
Muscle	0.400	0.760	0.0238	0.0072	0.122	0.7682	0.93	0.81	0.324
Skin	0.037	0.718	0.0284	0.0111	0.122	0.7296	0.89	0.77	0.029
Spleen	0.003	0.788	0.0201	0.0198	0.122	0.8050	0.98	0.85	0.002
Plasma	0.042	0.945	0.0035	0.0023	0.122	0.9471			
Plasma (D*vo:w)	0.042	0.945	0.0035	0.0023	0.000	0.9466			
Whole blood	0.077	0.820	0.0032	0.0020	0.122	0.8219			
Whole blood (D*vo/w)	0.077	0.820	0.0032	0.0020	0.000	0.8214			
Erythrocytes	0.035							**Vdss**	**0.527**

Table D7. Partition coefficient calculations for 3,4-dihydroxy carbaryl sulfate

	HUMAN		Neutral Lipid	Phospholipids			3,4-DiOH Carbaryl sulfate		
Tissue	Tissue (Vt)	Water (Vw)	(Vnl)	(Vpl)	Ko:w	-num-	$P_{t:b}$	$P_{t:p}$	$Vt*P_{t:p}$
Adipose (D*vo:w)	0.120	0.180	0.7900	0.0020	0.000	0.1814	0.221	0.19	0.023
Adipose (Ko:w)	0.120	0.180	0.7900	0.0020	0.001				
Bone	0.086	0.439	0.0740	0.0011	0.001	0.4398	0.54	0.46	0.040
Brain	0.020	0.770	0.0510	0.0565	0.001	0.8096	0.99	0.86	0.017
Gut	0.017	0.718	0.0487	0.0163	0.001	0.7294	0.89	0.77	0.013
Heart	0.005	0.758	0.0115	0.0166	0.001	0.7696	0.94	0.81	0.004
Kidney	0.004	0.783	0.0207	0.0162	0.001	0.7944	0.97	0.84	0.004
Liver	0.026	0.751	0.0348	0.0252	0.001	0.7687	0.94	0.81	0.021
Lung	0.008	0.811	0.0030	0.0090	0.001	0.8173	1.00	0.86	0.007
Muscle	0.400	0.760	0.0238	0.0072	0.001	0.7651	0.93	0.81	0.323
Skin	0.037	0.718	0.0284	0.0111	0.001	0.7258	0.88	0.77	0.028
Spleen	0.003	0.788	0.0201	0.0198	0.001	0.8019	0.98	0.85	0.002
Plasma	0.042	0.945	0.0035	0.0023	0.001	0.9466			
Plasma (D*vo:w)	0.042	0.945	0.0035	0.0023	0.000	0.9466			
Whole blood	0.077	0.820	0.0032	0.0020	0.001	0.8214			
Whole blood (D*vo/w)	0.077	0.820	0.0032	0.0020	0.000	0.8214		**Vdss**	**0.525**

Table D8. Partition coefficient calculations for 5,6-dihydroxy carbaryl

	HUMAN		Neutral Lipid	Phospholipids				5,6-DiOH Carbaryl	
Tissue	Tissue (Vt)	Water (Vw)	(Vnl)	(Vpl)	Ko:w	-num-	$P_{t:b}$	$P_{t:p}$	$Vt*P_{t:p}$
Adipose (D*vo:w)	0.120	0.180	0.7900	0.0020	0.044	0.2161	0.263	0.23	0.027
Adipose (Ko:w)	0.120	0.180	0.7900	0.0020	0.984				
Bone	0.086	0.439	0.0740	0.0011	0.984	0.5129	0.62	0.54	0.046
Brain	0.020	0.770	0.0510	0.0565	0.984	0.8764	1.06	0.92	0.018
Gut	0.017	0.718	0.0487	0.0163	0.984	0.7821	0.95	0.82	0.014
Heart	0.005	0.758	0.0115	0.0166	0.984	0.7858	0.95	0.83	0.004
Kidney	0.004	0.783	0.0207	0.0162	0.984	0.8195	0.99	0.86	0.004
Liver	0.026	0.751	0.0348	0.0252	0.984	0.8103	0.98	0.85	0.022
Lung	0.008	0.811	0.0030	0.0090	0.984	0.8229	1.00	0.87	0.007
Muscle	0.400	0.760	0.0238	0.0072	0.984	0.7906	0.96	0.83	0.333
Skin	0.037	0.718	0.0284	0.0111	0.984	0.7570	0.92	0.80	0.030
Spleen	0.003	0.788	0.0201	0.0198	0.984	0.8275	1.00	0.87	0.002
Plasma	0.042	0.945	0.0035	0.0023	0.984	0.9507			
Plasma (D*vo:w)	0.042	0.945	0.0035	0.0023	0.044	0.9468			
Whole blood	0.077	0.820	0.0032	0.0020	0.984	0.8251			
Whole blood (D*vo/w)	0.077	0.820	0.0032	0.0020	0.044	0.8216			
Erythrocytes	0.035							Vdss	**0.549**

Table D9. Partition coefficient calculations for 5,6-dihydroxy carbaryl glucuronide

	HUMAN		Neutral Lipid	Phospholipids			5,6-DiOH Carbaryl glucuronide		
Tissue	Tissue (Vt)	Water (Vw)	(Vnl)	(Vpl)	Ko:w	-num-	$P_{t:b}$	$P_{t:p}$	$Vt*P_{t:p}$
Adipose (D*vo:w)	0.120	0.180	0.7900	0.0020	0.000	0.1814	0.221	0.19	0.023
Adipose (Ko:w)	0.120	0.180	0.7900	0.0020	0.067				
Bone	0.086	0.439	0.0740	0.0011	0.067	0.4448	0.54	0.47	0.040
Brain	0.020	0.770	0.0510	0.0565	0.067	0.8141	0.99	0.86	0.017
Gut	0.017	0.718	0.0487	0.0163	0.067	0.7330	0.89	0.77	0.013
Heart	0.005	0.758	0.0115	0.0166	0.067	0.7707	0.94	0.81	0.004
Kidney	0.004	0.783	0.0207	0.0162	0.067	0.7961	0.97	0.84	0.004
Liver	0.026	0.751	0.0348	0.0252	0.067	0.7715	0.94	0.81	0.021
Lung	0.008	0.811	0.0030	0.0090	0.067	0.8177	1.00	0.86	0.007
Muscle	0.400	0.760	0.0238	0.0072	0.067	0.7668	0.93	0.81	0.324
Skin	0.037	0.718	0.0284	0.0111	0.067	0.7279	0.89	0.77	0.029
Spleen	0.003	0.788	0.0201	0.0198	0.067	0.8036	0.98	0.85	0.002
Plasma	0.042	0.945	0.0035	0.0023	0.067	0.9469			
Plasma (D*vo:w)	0.042	0.945	0.0035	0.0023	0.000	0.9466			
Whole blood	0.077	0.820	0.0032	0.0020	0.067	0.8217			
Whole blood (D*vo/w)	0.077	0.820	0.0032	0.0020	0.000	0.8214			
Erythrocytes	0.035							**Vdss**	**0.526**

Table D10. Partition coefficient calculations for naphthol

Tissue	HUMAN Tissue (Vt)	Water (Vw)	Neutral Lipid (Vnl)	Phospholipids (Vpl)	Ko:w	-num-	Naphthol $P_{t:b}$	Naphthol $P_{t:p}$	$Vt*P_{t:p}$
Adipose (D*vo:w)	0.120	0.180	0.7900	0.0020	67.259	53.3563	49.542	43.47	5.198
Adipose (Ko:w)	0.120	0.180	0.7900	0.0020	707.946				
Bone	0.086	0.439	0.0740	0.0011	707.946	53.0614	15.11	13.60	1.164
Brain	0.020	0.770	0.0510	0.0565	707.946	48.9145	13.93	12.53	0.251
Gut	0.017	0.718	0.0487	0.0163	707.946	38.6682	11.01	9.91	0.169
Heart	0.005	0.758	0.0115	0.0166	707.946	12.4366	3.54	3.19	0.015
Kidney	0.004	0.783	0.0207	0.0162	707.946	18.8937	5.38	4.84	0.021
Liver	0.026	0.751	0.0348	0.0252	707.946	30.7572	8.76	7.88	0.205
Lung	0.008	0.811	0.0030	0.0090	707.946	4.8526	1.38	1.24	0.009
Muscle	0.400	0.760	0.0238	0.0072	707.946	19.1433	5.45	4.91	1.962
Skin	0.037	0.718	0.0284	0.0111	707.946	23.1889	6.60	5.94	0.220
Spleen	0.003	0.788	0.0201	0.0198	707.946	19.2368	5.48	4.93	0.013
Plasma	0.042	0.945	0.0035	0.0023	707.946	3.9022			
Plasma (D*vo:w)	0.042	0.945	0.0035	0.0023	67.259	1.2274			
Whole blood	0.077	0.820	0.0032	0.0020	707.946	3.5116			
Whole blood (D*vo/w)	0.077	0.820	0.0032	0.0020	67.259	1.0770			
Erythrocytes	0.035							Vdss	**9.271**

Table D11. Partition coefficient calculations for naphthyl sulfate

	HUMAN		Neutral Lipid	Phospholipids			Naphthyl sulfate		
Tissue	Tissue (Vt)	Water (Vw)	(Vnl)	(Vpl)	Ko:w	-num-	$P_{t:b}$	$P_{t:p}$	$Vt*P_{t:p}$
Adipose (D*vo:w)	0.120	0.180	0.7900	0.0020	0.000	0.1814	0.221	0.19	0.023
Adipose (Ko:w)	0.120	0.180	0.7900	0.0020	0.350				
Bone	0.086	0.439	0.0740	0.0011	0.350	0.4658	0.57	0.49	0.042
Brain	0.020	0.770	0.0510	0.0565	0.350	0.8334	1.01	0.88	0.018
Gut	0.017	0.718	0.0487	0.0163	0.350	0.7482	0.91	0.79	0.013
Heart	0.005	0.758	0.0115	0.0166	0.350	0.7754	0.94	0.82	0.004
Kidney	0.004	0.783	0.0207	0.0162	0.350	0.8033	0.98	0.85	0.004
Liver	0.026	0.751	0.0348	0.0252	0.350	0.7835	0.95	0.83	0.021
Lung	0.008	0.811	0.0030	0.0090	0.350	0.8193	1.00	0.86	0.007
Muscle	0.400	0.760	0.0238	0.0072	0.350	0.7741	0.94	0.82	0.327
Skin	0.037	0.718	0.0284	0.0111	0.350	0.7369	0.90	0.78	0.029
Spleen	0.003	0.788	0.0201	0.0198	0.350	0.8110	0.99	0.86	0.002
Plasma	0.042	0.945	0.0035	0.0023	0.350	0.9480			
Plasma (D*vo:w)	0.042	0.945	0.0035	0.0023	0.000	0.9466			
Whole blood	0.077	0.820	0.0032	0.0020	0.350	0.8227			
Whole blood (D*vo/w)	0.077	0.820	0.0032	0.0020	0.000	0.8214			
Erythrocytes	0.035							**Vdss**	**0.532**

Table D12. Partition coefficient calculations for naphthyl glucuronide

	HUMAN		Neutral Lipid	Phospholipids				Naphthyl glucuronide	
Tissue	Tissue (Vt)	Water (Vw)	(Vnl)	(Vpl)	Ko:w	-num-	$P_{t:b}$	$P_{t:p}$	$Vt*P_{t:p}$
Adipose (D*vo:w)	0.120	0.180	0.7900	0.0020	0.000	0.1814	0.221	0.19	0.023
Adipose (Ko:w)	0.120	0.180	0.7900	0.0020	6.952				
Bone	0.086	0.439	0.0740	0.0011	6.952	0.9565	1.13	0.98	0.084
Brain	0.020	0.770	0.0510	0.0565	6.952	1.2819	1.51	1.31	0.026
Gut	0.017	0.718	0.0487	0.0163	6.952	1.1020	1.30	1.13	0.019
Heart	0.005	0.758	0.0115	0.0166	6.952	0.8842	1.04	0.91	0.004
Kidney	0.004	0.783	0.0207	0.0162	6.952	0.9721	1.15	1.00	0.004
Liver	0.026	0.751	0.0348	0.0252	6.952	1.0631	1.25	1.09	0.028
Lung	0.008	0.811	0.0030	0.0090	6.952	0.8569	1.01	0.88	0.007
Muscle	0.400	0.760	0.0238	0.0072	6.952	0.9455	1.12	0.97	0.388
Skin	0.037	0.718	0.0284	0.0111	6.952	0.9464	1.12	0.97	0.036
Spleen	0.003	0.788	0.0201	0.0198	6.952	0.9829	1.16	1.01	0.003
Plasma	0.042	0.945	0.0035	0.0023	6.952	0.9756			
Plasma (D*vo:w)	0.042	0.945	0.0035	0.0023	0.000	0.9466			
Whole blood	0.077	0.820	0.0032	0.0020	6.952	0.8478			
Whole blood (D*vo/w)	0.077	0.820	0.0032	0.0020	0.000	0.8214		**Vdss**	**0.665**

Table D13. Partition coefficient calculations for 3,4-dihydroxy naphthol

	HUMAN		Neutral Lipid	Phospholipids				3.4 DiHydroxy Naphthol	
Tissue	Tissue (Vt)	Water (Vw)	(Vnl)	(Vpl)	Ko:w	-num-	$P_{t:b}$	$P_{t:p}$	$Vt*P_{t:p}$
Adipose (D*vo:w)	0.120	0.180	0.7900	0.0020	0.072	0.2385	0.290	0.25	0.030
Adipose (Ko:w)	0.120	0.180	0.7900	0.0020	1.538				
Bone	0.086	0.439	0.0740	0.0011	1.538	0.5541	0.67	0.58	0.050
Brain	0.020	0.770	0.0510	0.0565	1.538	0.9141	1.10	0.96	0.019
Gut	0.017	0.718	0.0487	0.0163	1.538	0.8118	0.98	0.85	0.015
Heart	0.005	0.758	0.0115	0.0166	1.538	0.7950	0.96	0.83	0.004
Kidney	0.004	0.783	0.0207	0.0162	1.538	0.8337	1.01	0.87	0.004
Liver	0.026	0.751	0.0348	0.0252	1.538	0.8338	1.01	0.87	0.023
Lung	0.008	0.811	0.0030	0.0090	1.538	0.8261	1.00	0.87	0.007
Muscle	0.400	0.760	0.0238	0.0072	1.538	0.8050	0.97	0.84	0.338
Skin	0.037	0.718	0.0284	0.0111	1.538	0.7746	0.94	0.81	0.030
Spleen	0.003	0.788	0.0201	0.0198	1.538	0.8419	1.02	0.88	0.002
Plasma	0.042	0.945	0.0035	0.0023	1.538	0.9530			
Plasma (D*vo:w)	0.042	0.945	0.0035	0.0023	0.072	0.9469			
Whole blood	0.077	0.820	0.0032	0.0020	1.538	0.8272			
Whole blood (D*vo/w)	0.077	0.820	0.0032	0.0020	0.072	0.8217		Vdss	**0.563**

Table D14. Partition coefficient calculations for 3,4-dihydroxy naphthyl glucuronide

	HUMAN		Neutral Lipid	Phospholipids				3.4 DiHydroxy naphthyl glucuronide	
Tissue	Tissue (Vt)	Water (Vw)	(Vnl)	(Vpl)	Ko:w	-num-	$P_{t:b}$	$P_{t:p}$	$Vt*P_{t:p}$
Adipose (D*vo:w)	0.120	0.180	0.7900	0.0020	0.000	0.1814	0.221	0.19	0.023
Adipose (Ko:w)	0.120	0.180	0.7900	0.0020	0.032				
Bone	0.086	0.439	0.0740	0.0011	0.032	0.4421	0.54	0.47	0.040
Brain	0.020	0.770	0.0510	0.0565	0.032	0.8117	0.99	0.86	0.017
Gut	0.017	0.718	0.0487	0.0163	0.032	0.7311	0.89	0.77	0.013
Heart	0.005	0.758	0.0115	0.0166	0.032	0.7701	0.94	0.81	0.004
Kidney	0.004	0.783	0.0207	0.0162	0.032	0.7952	0.97	0.84	0.004
Liver	0.026	0.751	0.0348	0.0252	0.032	0.7700	0.94	0.81	0.021
Lung	0.008	0.811	0.0030	0.0090	0.032	0.8175	1.00	0.86	0.007
Muscle	0.400	0.760	0.0238	0.0072	0.032	0.7659	0.93	0.81	0.324
Skin	0.037	0.718	0.0284	0.0111	0.032	0.7268	0.88	0.77	0.028
Spleen	0.003	0.788	0.0201	0.0198	0.032	0.8027	0.98	0.85	0.002
Plasma	0.042	0.945	0.0035	0.0023	0.032	0.9467			
Plasma (D*vo:w)	0.042	0.945	0.0035	0.0023	0.000	0.9466			
Whole blood	0.077	0.820	0.0032	0.0020	0.032	0.8215			
Whole blood (D*vo/w)	0.077	0.820	0.0032	0.0020	0.000	0.8214			
Erythrocytes	0.035							Vdss	**0.525**

Table D15. Partition coefficient calculations for 3,4-dihydroxy naphthyl sulfate

	HUMAN		Neutral Lipid	Phospholipids				3.4 DiHydroxy naphthyl sulfate	
Tissue	Tissue (Vt)	Water (Vw)	(Vnl)	(Vpl)	Ko:w	-num-	$P_{t:b}$	$P_{t:p}$	$Vt*P_{t:p}$
Adipose (D*vo:w)	0.120	0.180	0.7900	0.0020	0.000	0.1814	0.221	0.19	0.023
Adipose (Ko:w)	0.120	0.180	0.7900	0.0020	0.000				
Bone	0.086	0.439	0.0740	0.0011	0.000	0.4398	0.54	0.46	0.040
Brain	0.020	0.770	0.0510	0.0565	0.000	0.8096	0.99	0.86	0.017
Gut	0.017	0.718	0.0487	0.0163	0.000	0.7294	0.89	0.77	0.013
Heart	0.005	0.758	0.0115	0.0166	0.000	0.7696	0.94	0.81	0.004
Kidney	0.004	0.783	0.0207	0.0162	0.000	0.7944	0.97	0.84	0.004
Liver	0.026	0.751	0.0348	0.0252	0.000	0.7687	0.94	0.81	0.021
Lung	0.008	0.811	0.0030	0.0090	0.000	0.8173	1.00	0.86	0.007
Muscle	0.400	0.760	0.0238	0.0072	0.000	0.7651	0.93	0.81	0.323
Skin	0.037	0.718	0.0284	0.0111	0.000	0.7258	0.88	0.77	0.028
Spleen	0.003	0.788	0.0201	0.0198	0.000	0.8019	0.98	0.85	0.002
Plasma	0.042	0.945	0.0035	0.0023	0.000	0.9466			
Plasma (D*vo:w)	0.042	0.945	0.0035	0.0023	0.000	0.9466			
Whole blood	0.077	0.820	0.0032	0.0020	0.000	0.8214			
Whole blood (D*vo/w)	0.077	0.820	0.0032	0.0020	0.000	0.8214			
Erythrocytes	0.035							Vdss	**0.525**

Table D16. Partition coefficient calculations for 4-OH carbaryl

Tissue	**HUMAN** Tissue (Vt)	Water (Vw)	Neutral Lipid (Vnl)	Phospholipids (Vpl)	Ko:w	-num-	4-OH Carbaryl $P_{t:b}$	$P_{t:p}$	$Vt*P_{t:p}$
Adipose (D*vo:w)	0.120	0.180	0.7900	0.0020	5.323	4.3895	5.216	4.53	0.542
Adipose (Ko:w)	0.120	0.180	0.7900	0.0020	72.778				
Bone	0.086	0.439	0.0740	0.0011	72.778	5.8494	5.33	4.68	0.401
Brain	0.020	0.770	0.0510	0.0565	72.778	5.7548	5.24	4.60	0.092
Gut	0.017	0.718	0.0487	0.0163	72.778	4.6296	4.22	3.70	0.063
Heart	0.005	0.758	0.0115	0.0166	72.778	1.9690	1.79	1.57	0.007
Kidney	0.004	0.783	0.0207	0.0162	72.778	2.6550	2.42	2.12	0.009
Liver	0.026	0.751	0.0348	0.0252	72.778	3.8515	3.51	3.08	0.080
Lung	0.008	0.811	0.0030	0.0090	72.778	1.2321	1.12	0.99	0.007
Muscle	0.400	0.760	0.0238	0.0072	72.778	2.6544	2.42	2.12	0.849
Skin	0.037	0.718	0.0284	0.0111	72.778	3.0350	2.76	2.43	0.090
Spleen	0.003	0.788	0.0201	0.0198	72.778	2.6970	2.46	2.16	0.006
Plasma	0.042	0.945	0.0035	0.0023	72.778	1.2504			
Plasma (D*vo:w)	0.042	0.945	0.0035	0.0023	5.323	0.9688			
Whole blood	0.077	0.820	0.0032	0.0020	72.778	1.0980			
Whole blood (D*vo/w)	0.077	0.820	0.0032	0.0020	5.323	0.8416			
Erythrocytes	0.035							Vdss	**2.189**

Table D17. Partition coefficient calculations for 4-OH carbaryl glucuronide

Tissue	**HUMAN** Tissue (Vt)	Water (Vw)	Neutral Lipid (Vnl)	Phospholipids (Vpl)	Ko:w	-num-	$P_{t:b}$	4-OH Carbaryl glucuronide $P_{t:p}$	$Vt*P_{t:p}$
Adipose (D*vo:w)	0.120	0.180	0.7900	0.0020	0.000	0.1814	0.221	0.19	0.023
Adipose (Ko:w)	0.120	0.180	0.7900	0.0020	1.051				
Bone	0.086	0.439	0.0740	0.0011	1.051	0.5179	0.63	0.54	0.047
Brain	0.020	0.770	0.0510	0.0565	1.051	0.8809	1.07	0.93	0.019
Gut	0.017	0.718	0.0487	0.0163	1.051	0.7857	0.95	0.83	0.014
Heart	0.005	0.758	0.0115	0.0166	1.051	0.7869	0.95	0.83	0.004
Kidney	0.004	0.783	0.0207	0.0162	1.051	0.8212	0.99	0.86	0.004
Liver	0.026	0.751	0.0348	0.0252	1.051	0.8131	0.99	0.86	0.022
Lung	0.008	0.811	0.0030	0.0090	1.051	0.8233	1.00	0.87	0.007
Muscle	0.400	0.760	0.0238	0.0072	1.051	0.7923	0.96	0.83	0.333
Skin	0.037	0.718	0.0284	0.0111	1.051	0.7591	0.92	0.80	0.030
Spleen	0.003	0.788	0.0201	0.0198	1.051	0.8292	1.00	0.87	0.002
Plasma	0.042	0.945	0.0035	0.0023	1.051	0.9510			
Plasma (D*vo:w)	0.042	0.945	0.0035	0.0023	0.000	0.9466			
Whole blood	0.077	0.820	0.0032	0.0020	1.051	0.8254			
Whole blood (D*vo/w)	0.077	0.820	0.0032	0.0020	0.000	0.8214			
Erythrocytes	0.035							Vdss	**0.546**

Table D18. Partition coefficient calculations for 4-OH carbaryl sulfate

	HUMAN		Neutral Lipid	Phospholipids				4-OH Carbaryl sulfate	
Tissue	Tissue (Vt)	Water (Vw)	(Vnl)	(Vpl)	Ko:w	-num-	$P_{t:b}$	$P_{t:p}$	$Vt*P_{t:p}$
Adipose (D*vo:w)	0.120	0.180	0.7900	0.0020	0.000	0.1814	0.221	0.19	0.023
Adipose (Ko:w)	0.120	0.180	0.7900	0.0020	0.053				
Bone	0.086	0.439	0.0740	0.0011	0.053	0.4437	0.54	0.47	0.040
Brain	0.020	0.770	0.0510	0.0565	0.053	0.8131	0.99	0.86	0.017
Gut	0.017	0.718	0.0487	0.0163	0.053	0.7322	0.89	0.77	0.013
Heart	0.005	0.758	0.0115	0.0166	0.053	0.7705	0.94	0.81	0.004
Kidney	0.004	0.783	0.0207	0.0162	0.053	0.7957	0.97	0.84	0.004
Liver	0.026	0.751	0.0348	0.0252	0.053	0.7709	0.94	0.81	0.021
Lung	0.008	0.811	0.0030	0.0090	0.053	0.8176	1.00	0.86	0.007
Muscle	0.400	0.760	0.0238	0.0072	0.053	0.7664	0.93	0.81	0.324
Skin	0.037	0.718	0.0284	0.0111	0.053	0.7275	0.89	0.77	0.029
Spleen	0.003	0.788	0.0201	0.0198	0.053	0.8032	0.98	0.85	0.002
Plasma	0.042	0.945	0.0035	0.0023	0.053	0.9468			
Plasma (D*vo:w)	0.042	0.945	0.0035	0.0023	0.000	0.9466			
Whole blood	0.077	0.820	0.0032	0.0020	0.053	0.8216			
Whole blood (D*vo/w)	0.077	0.820	0.0032	0.0020	0.000	0.8214			
Erythrocytes	0.035							Vdss	**0.526**

2.4 References

Haddad S, Poulin P, Krishnan K.(2000). Relative lipid content as the sole mechanistic determinant of the adipose tissue:blood partition coefficients of highly lipophilic organic chemicals. Chemosphere 839-843.

Laskowski, DA (2002) Physical and Chemical Properties of Pyrethroids. Rev Environ Contam Toxicol 174:49-170

Leo A, Hansh C, Elkins D.(1971). Partition coefficients and their uses. Chem Rev 71: 525-615. .

Meylen WM, Howard PH. (2001). Log n-octanol:water partition coefficients. KOWWIN database. Syracuse Research Corporation, Environmental Science Center, Syracuse, NY 13210

Poulin P, Theil FP. (2000). A priori prediction of tissue:plasma partition coefficients of drugs to facilitate the use of physiologically based pharmacokinetic models in drug discovery. J Pharm Sci 89:16-35

Poulin P, Theil FP.(2002). Prediction of pharmacokinetics prior to *in vivo* studies. 1. Mechanism-based prediction of volume of distribution. J Pharm Sci 91:129-156.

Poulin P, Krishnan K. (1996) A mechanistic algorithm for predicting blood:air partition coefficients of organic chemicals with the consideration of reversible binding in hemoglobin. Toxicol Appl Pharmacol 136:131-137.

Verschueren, K. Handbook of Environmental Data on Organic Chemicals. 2nd Ed. Van Nostrand Reinhold. New York. 1983. pp. 799-803.

Appendix E. Additional Model Simulation Results

The comparisons of the results from the PBPK model used in this assessment to the available data (Table 1) are shown here, organized by study. The parameter estimates focused on the low dose experiments, since the environmental exposure is expected to be below most levels simulated in the laboratory. The parameter values are intended to be representative across studies, not exact to only a single study, due to variations across data sets.

1.0 Bayer Metabolism Studies (Bayer 2004a)

These studies were conducted in Sprague-Dawley rats. The PBPK model predictions of naphthol concentrations in tissues only reflect the concentration of 1-naphthol, not its subsequent metabolites or conjugates.

1.1 Oral dose of approximately 1 mg/kg

The administered dose was 1.05 mg/kg in Sragues-Dawley rats. The data points are the average values for 4 animals at each sample time.

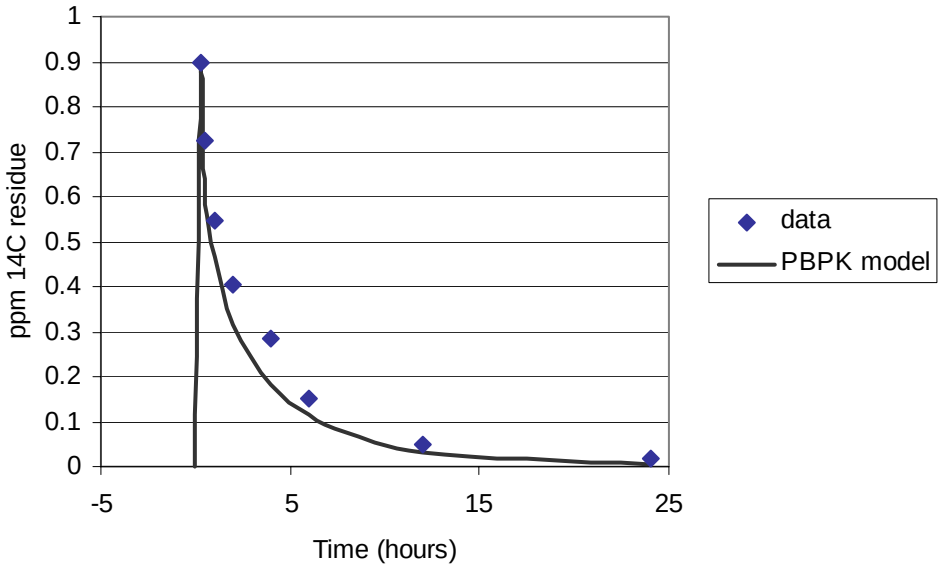

Figure E1. Blood concentration ^{14}C.

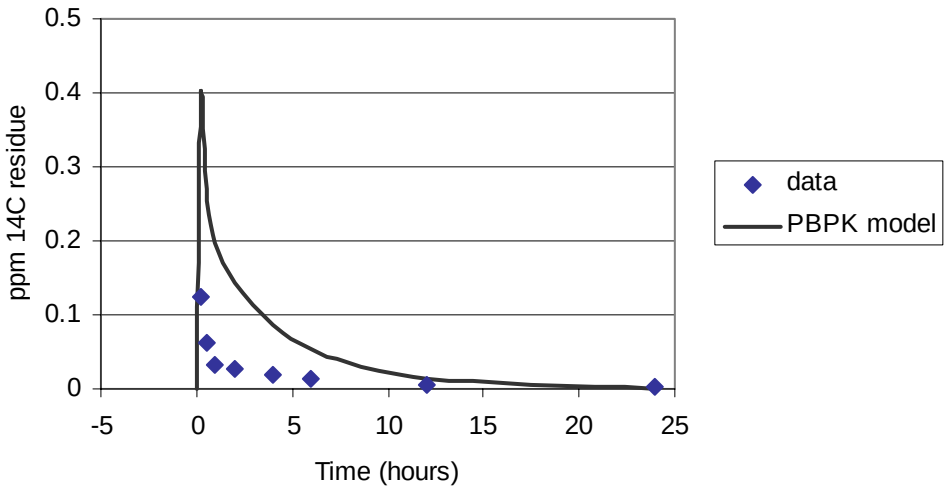

Figure E2. Brain concentration ^{14}C.

1.2 Oral dose of approximately 10 mg/kg

The actual administered dose was 8.45 mg/kg to Sprague-Dawley rats. The data points are the average values for 4 animals at each sample time.

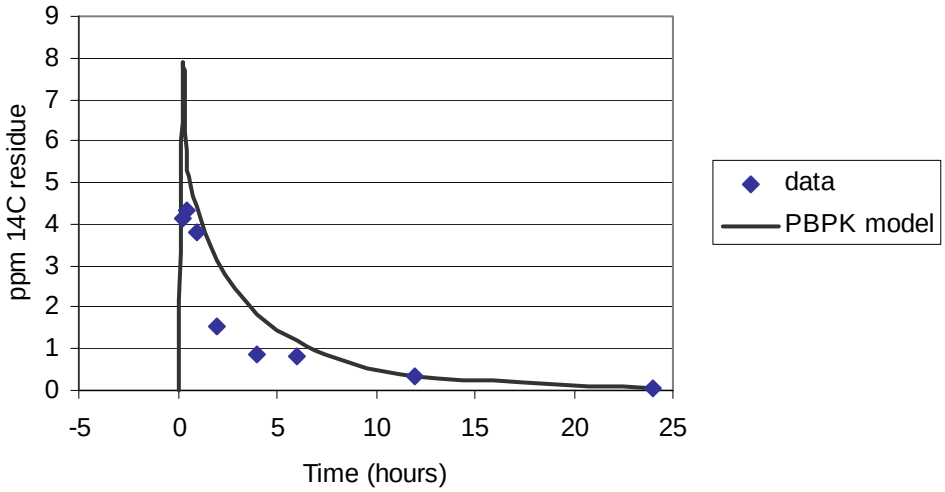

Figure E3. Blood concentration ^{14}C.

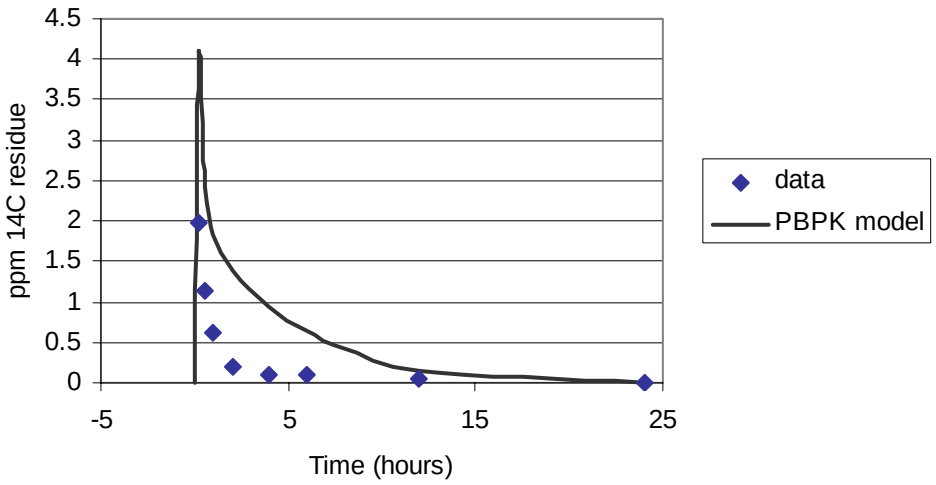

Figure E4. Brain concentration ^{14}C.

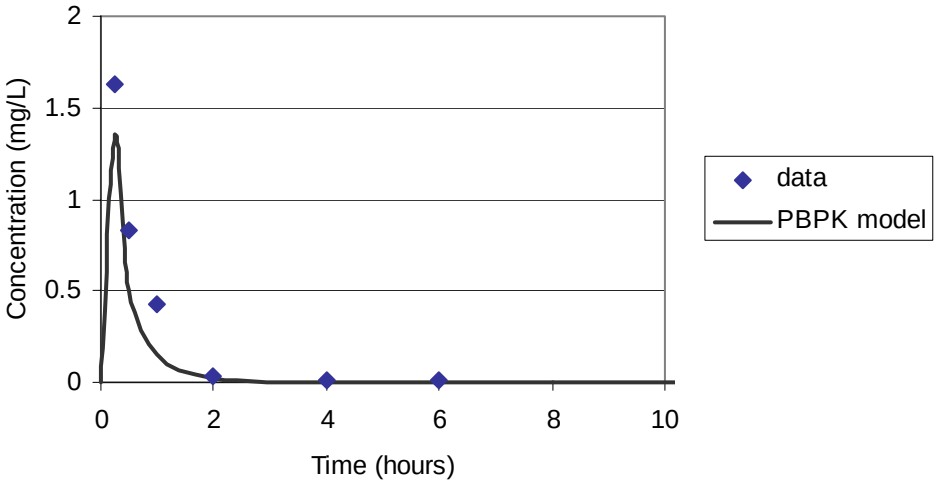

Figure E5. Brain carbaryl concentration.

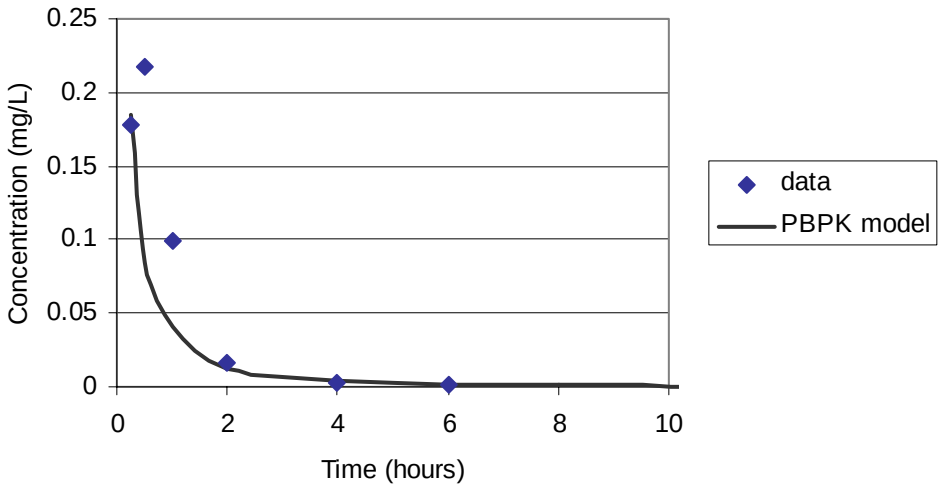

Figure E6. Brain naphthol concentration.

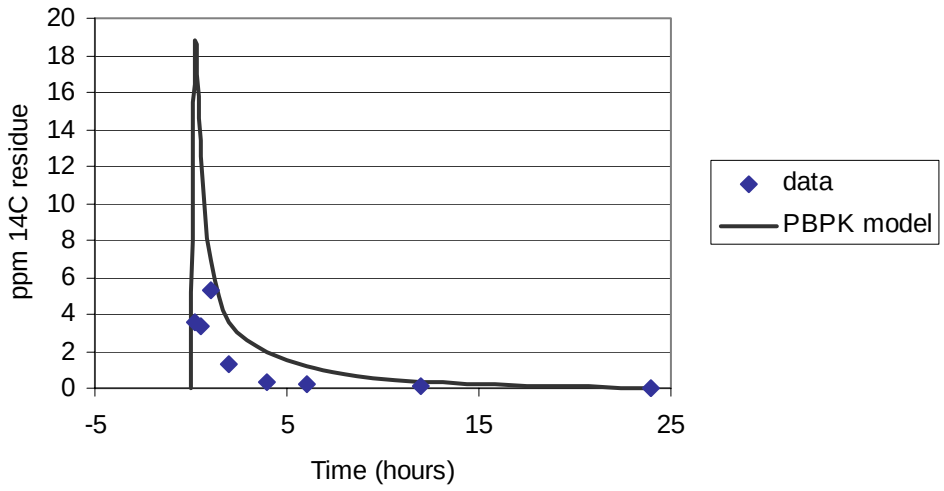

Figure E7. Fat concentration ^{14}C.

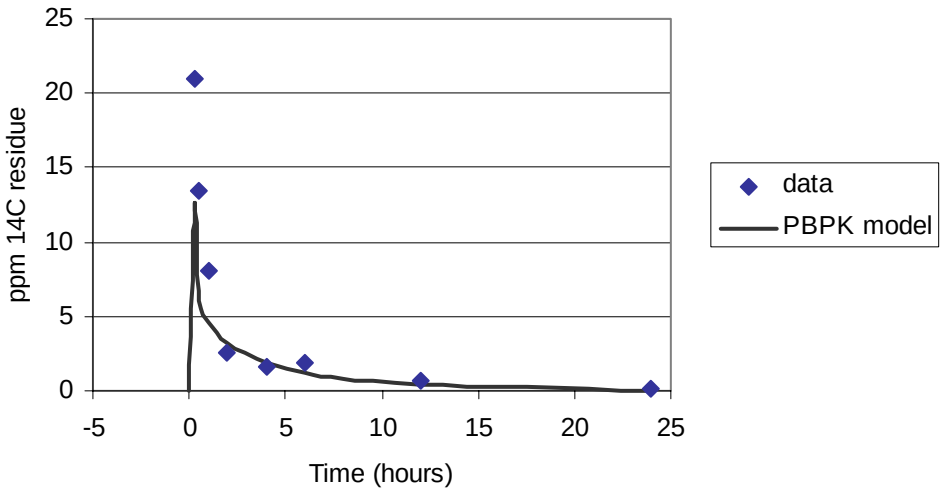

Figure E8. Liver concentration ^{14}C.

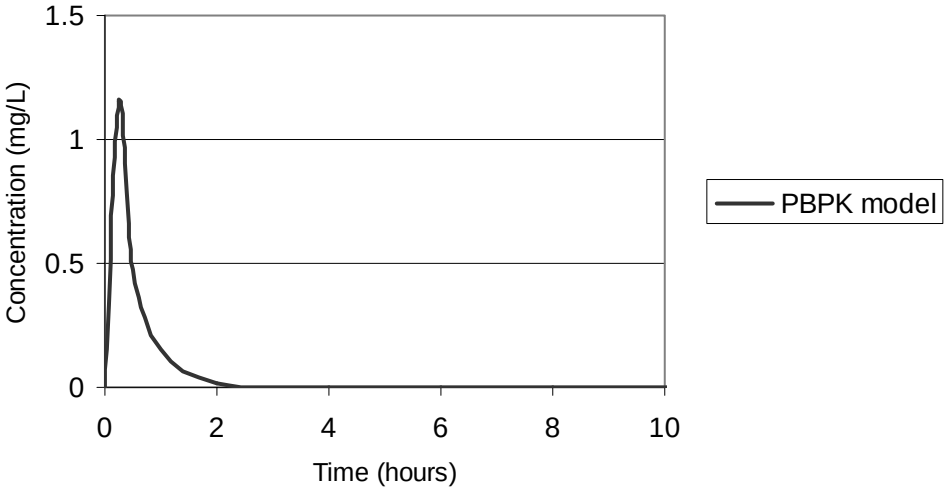

Figure E9. Blood carbaryl concentration. None was detected at 15 minutes.

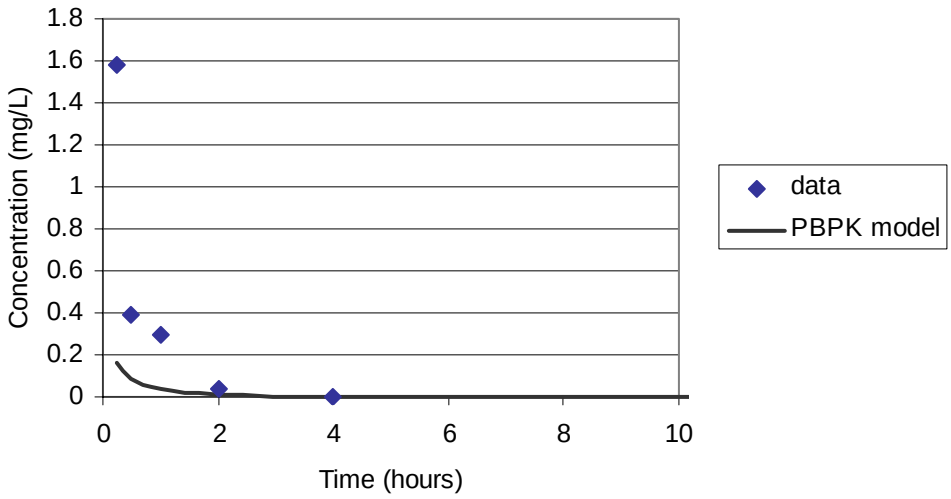

Figure E10. Blood naphthol concentration.

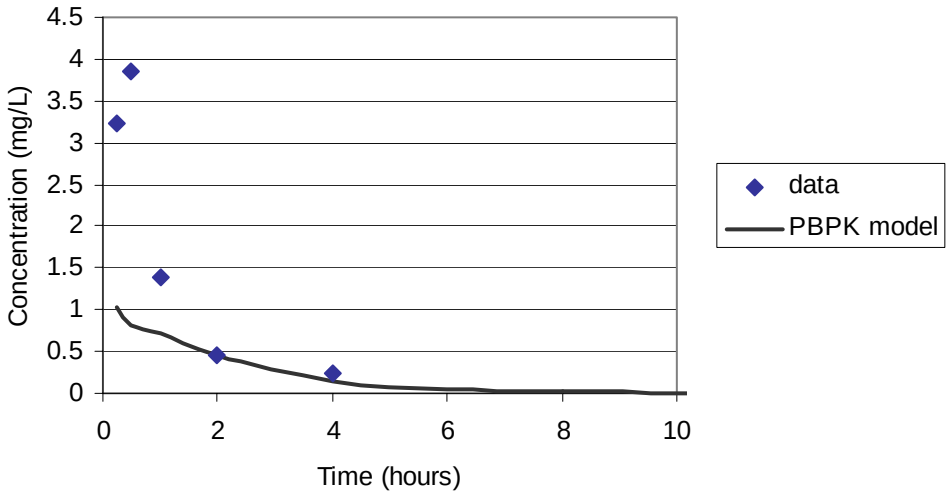

Figure E11. Blood naphthol sulfate concentration.

1.3IV dose of approximately 1 mg/kg

The administered dose was 0.8 mg/kg in Sprague-Dawley rats. The data points are the average values for 4 animals at each sample time.

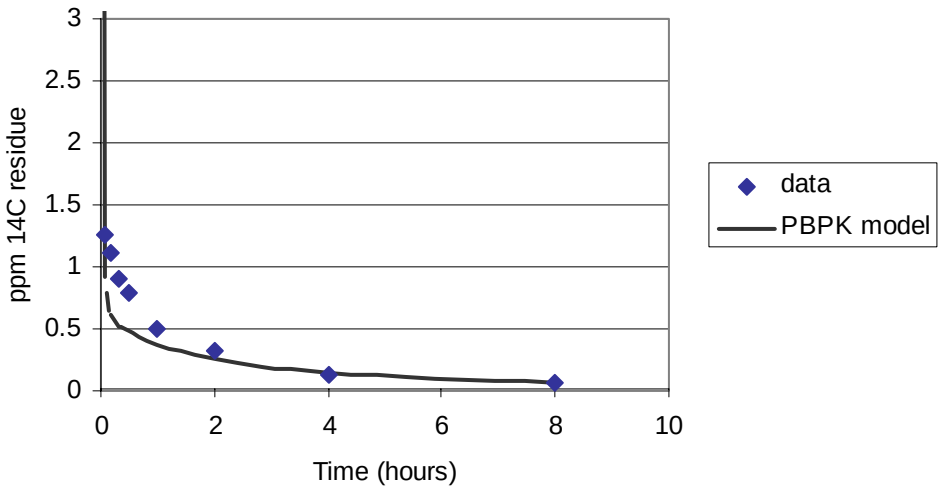

Figure E12. Blood concentration ^{14}C.

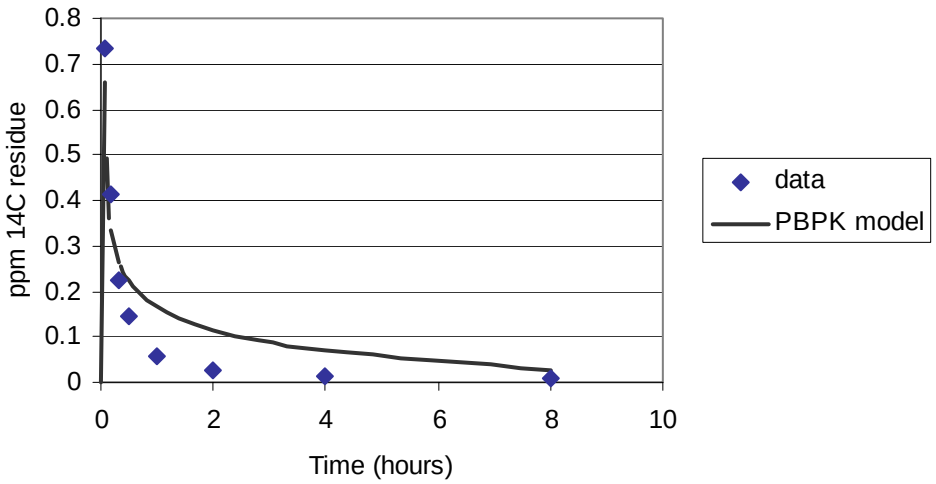

Figure E13. Brain concentration ^{14}C.

1.4 IV dose of approximately 10 mg/kg

The administered dose was 9.2 mg/kg in Sprague-Dawley rats. The data points are the average values for 4 animals at each sample time.

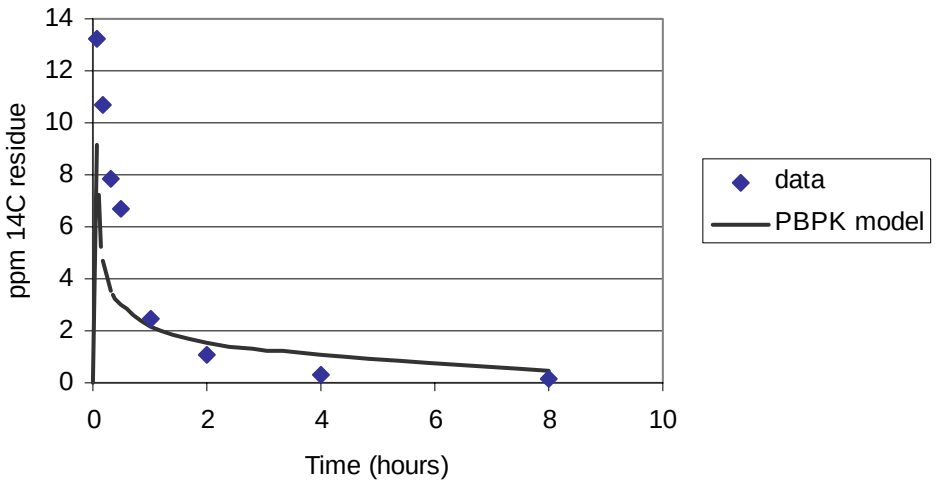

Figure E14. Brain concentration ^{14}C.

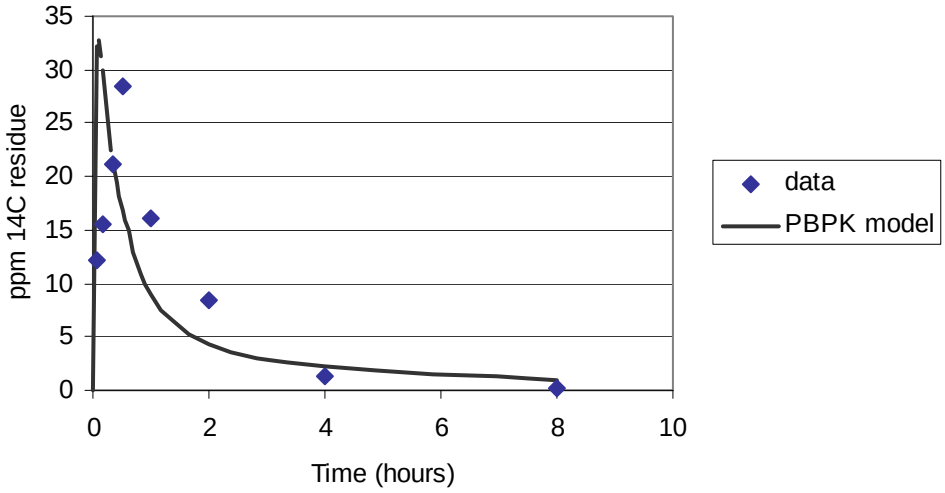

Figure E15. Fat concentration ^{14}C.

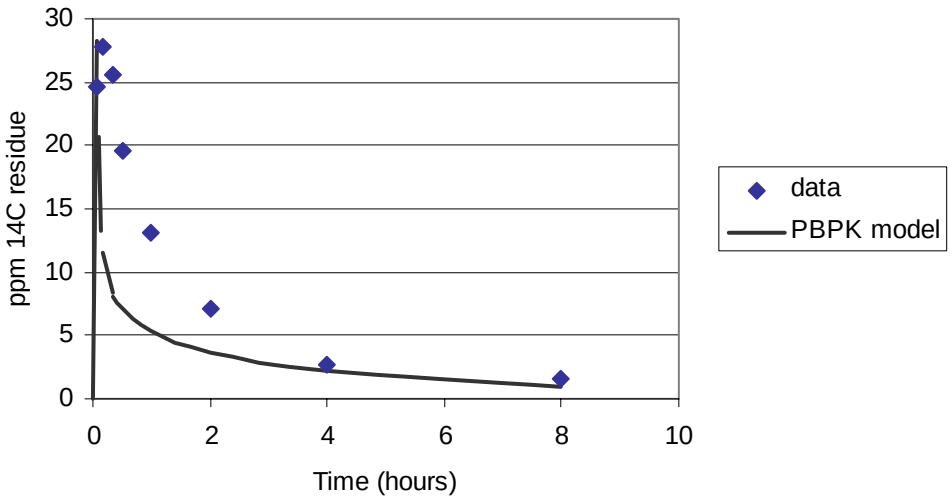

Figure E16. Liver concentration ^{14}C.

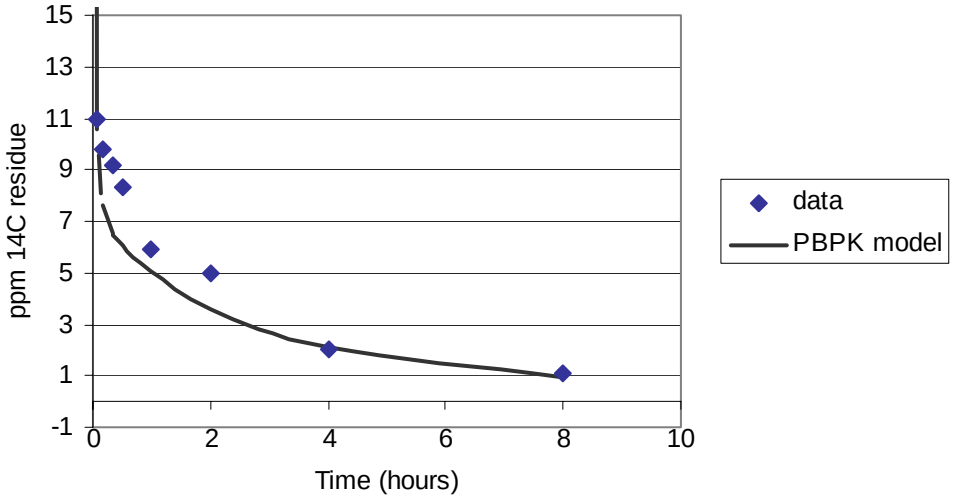

Figure E17. Blood concentration ^{14}C.

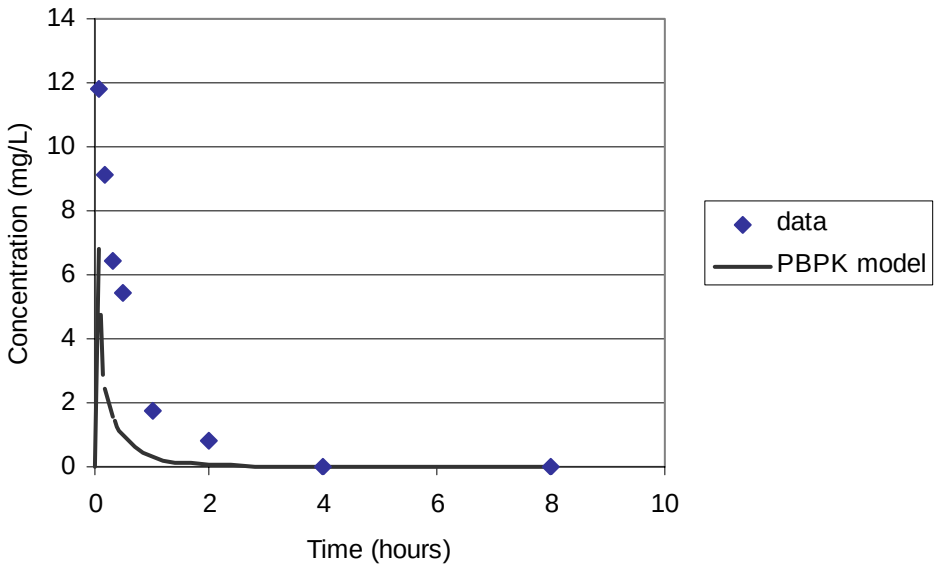

Figure E18. Brain carbaryl concentration.

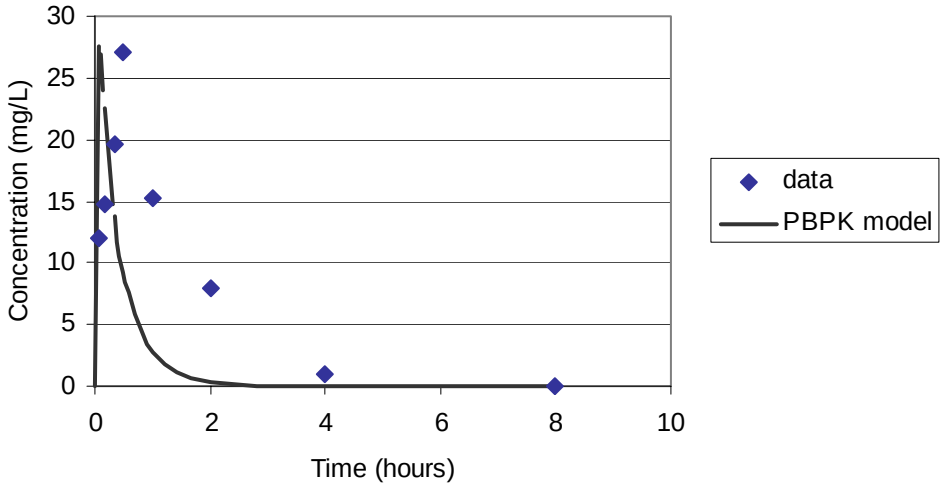

Figure E19. Fat carbaryl concentration.

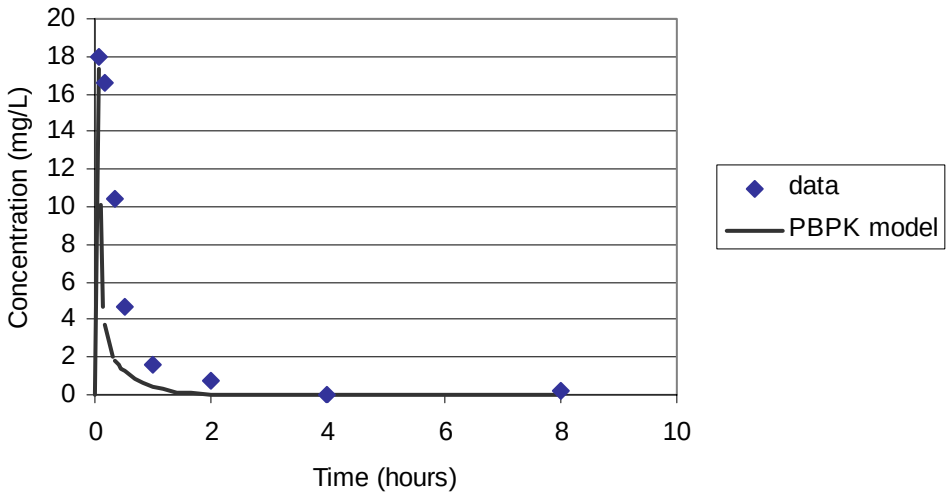

Figure E20. Liver carbaryl concentration.

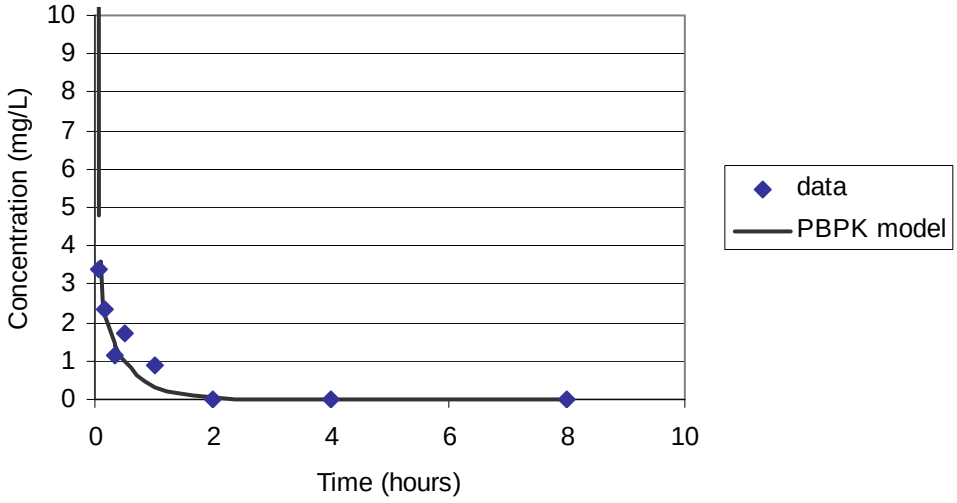

Figure E21. Blood carbaryl concentration.

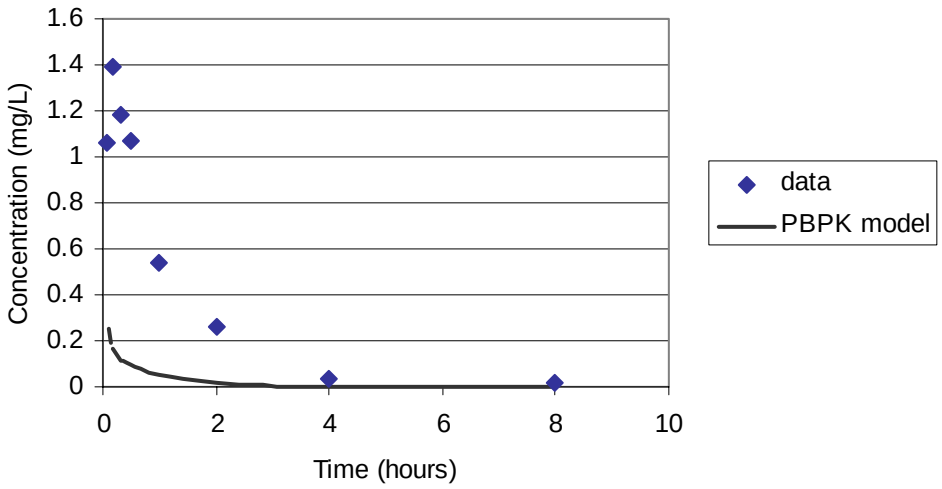

Figure E22. Brain naphthol concentration.

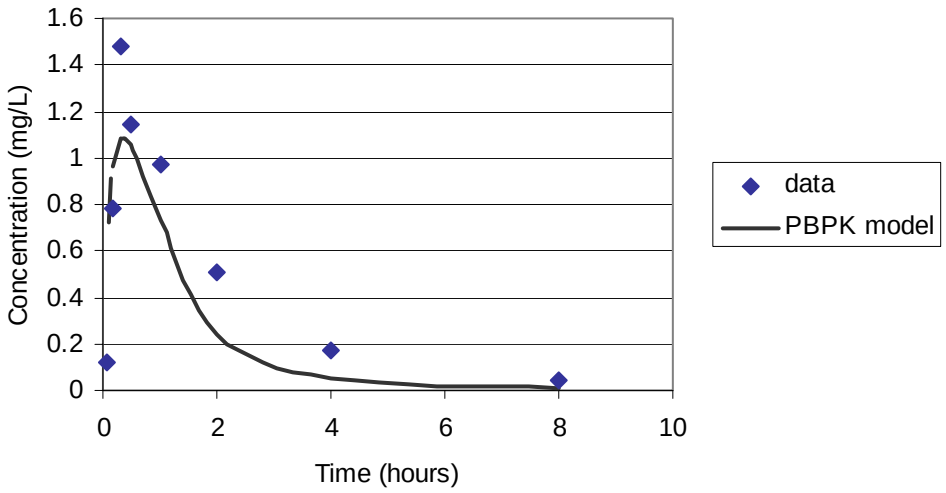

Figure E23. Fat naphthol concentration.

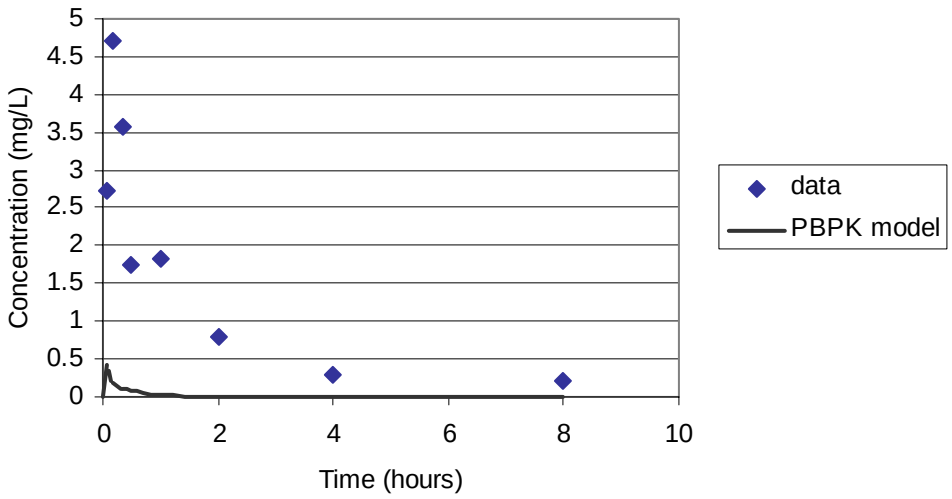

Figure E24. Liver naphthol concentration.

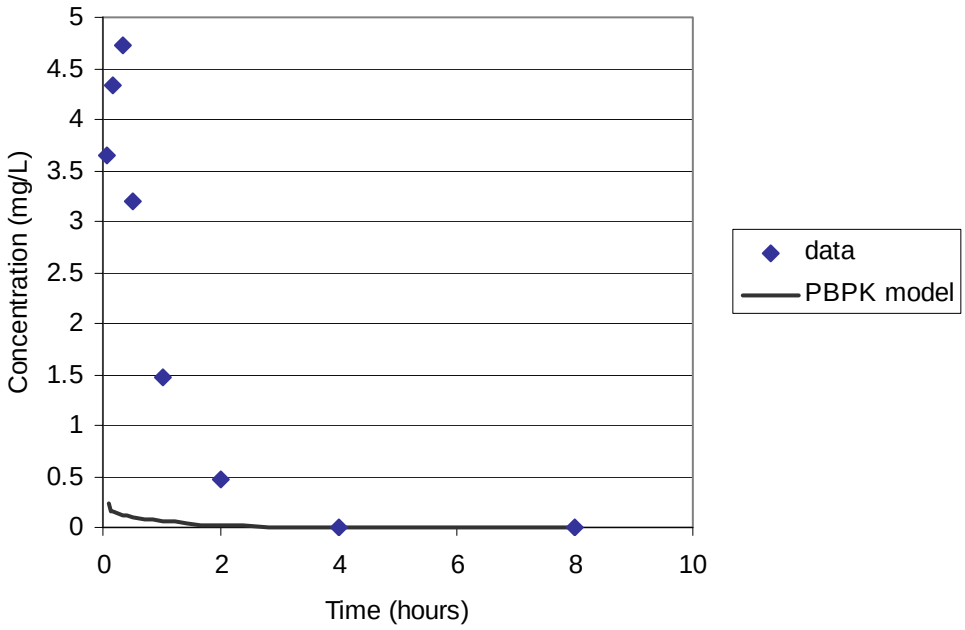

Figure E25. Blood naphthol concentration.

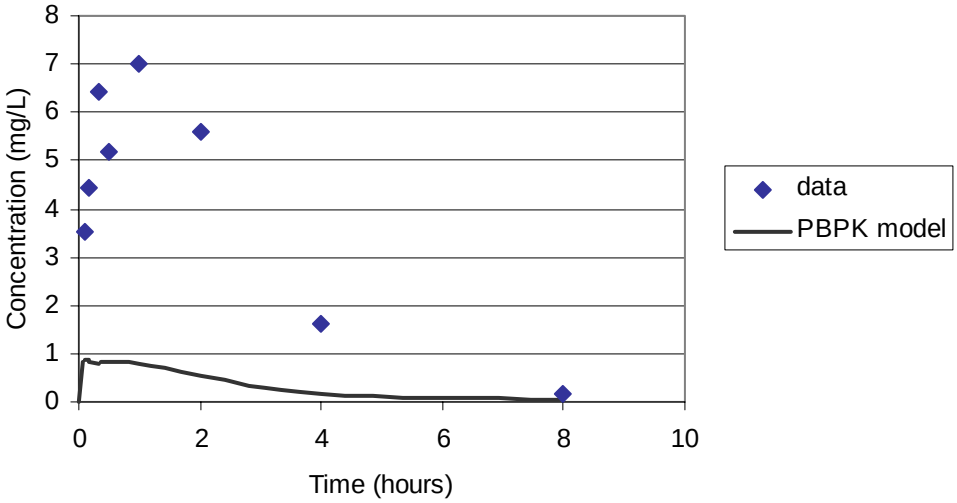

Figure E26. Blood naphthol sulfate concentration.

1.5 Mixed oral and dermal dose

Two oral doses of 0.075 mg/kg were administered to Sprague-Dawley rats at hour 0 and hour 1 respectively. A dermal dose of 0.75 mg/kg was also applied during this period, although the simulation results are nearly identical with or without the dermal contribution. The data points are the average values for 4 animals at each sample time.

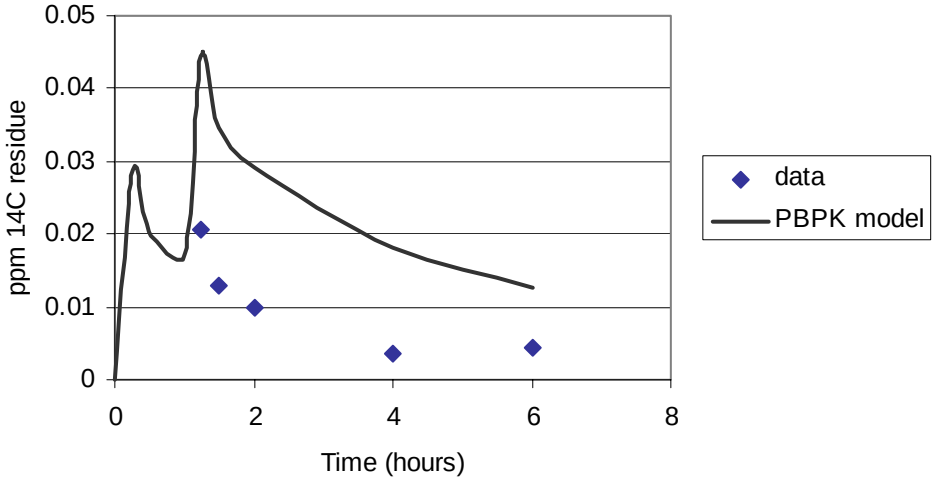

Figure E27. Brain concentration ^{14}C.

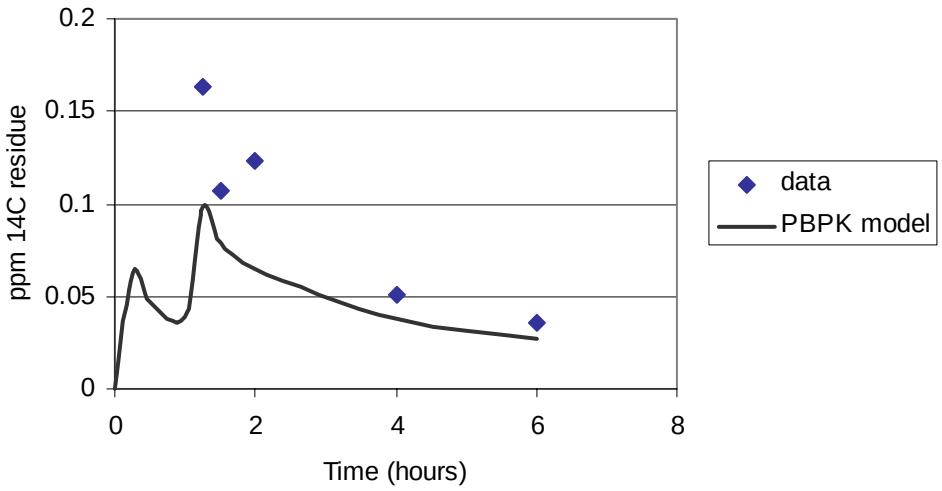

Figure E28. Blood concentration ^{14}C.

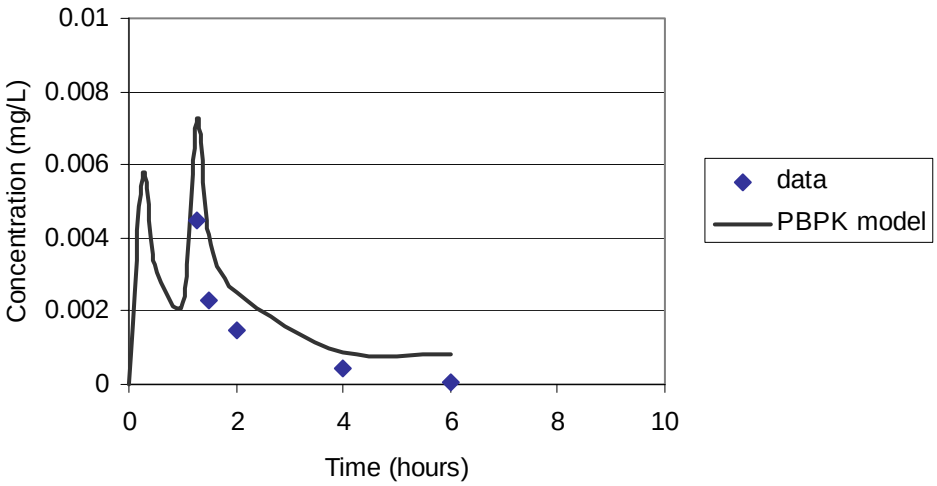

Figure E29. Brain carbaryl concentration.

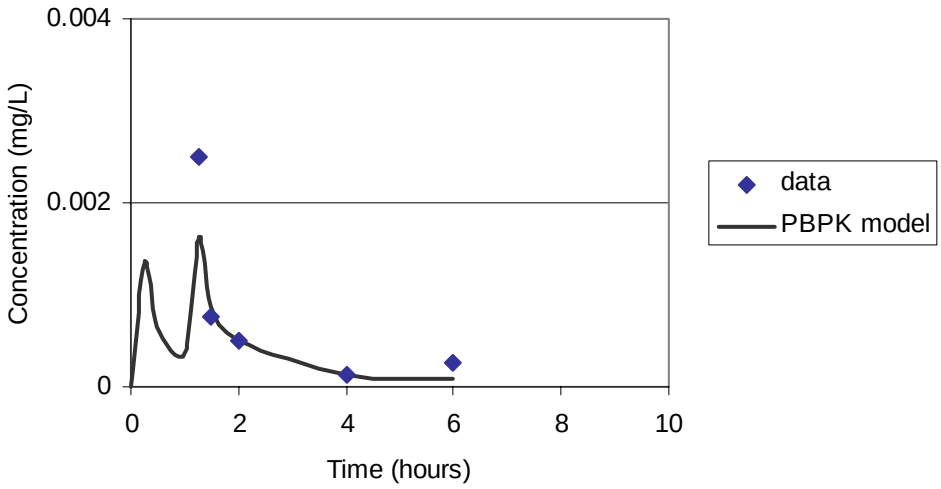

Figure E30. Brain naphthol concentration.

2.0 Cholinesterase inhibition studies

Carbaryl at 10 to 125 mg/kg was administered to Sprague-Dawley rats (Brooks and Broxup 1995a,b). Only the 10 mg/kg data were considered for parameter estimation. The data points are the average value for 12 animals at each time point (6 male, 6 female).

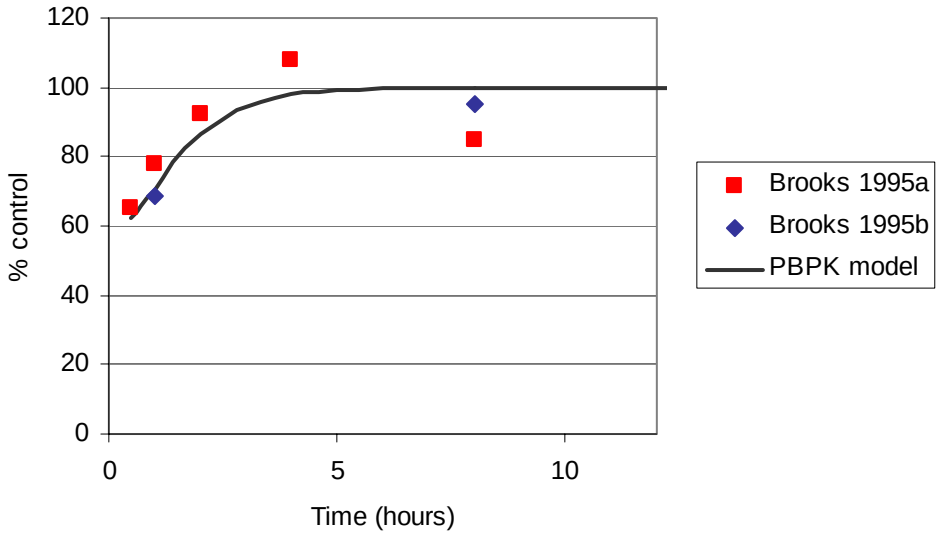

Figure E31. Blood acetylcholinesterase inhibition after administration of 10 mg/kg.

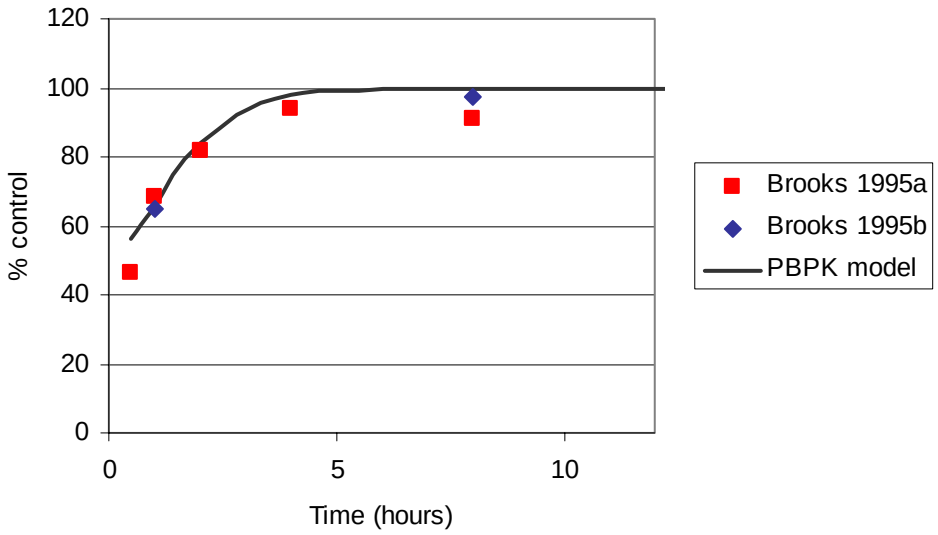

Figure E32. Brain acetylcholinesterase inhibition after administration of 10 mg/kg.

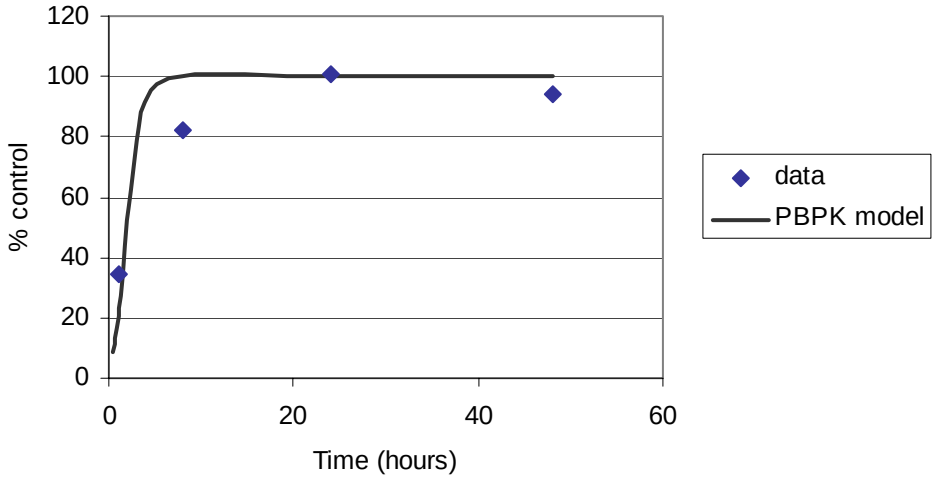

Figure E33. Brain acetylcholinesterase inhibition after administration of 30 mg/kg.

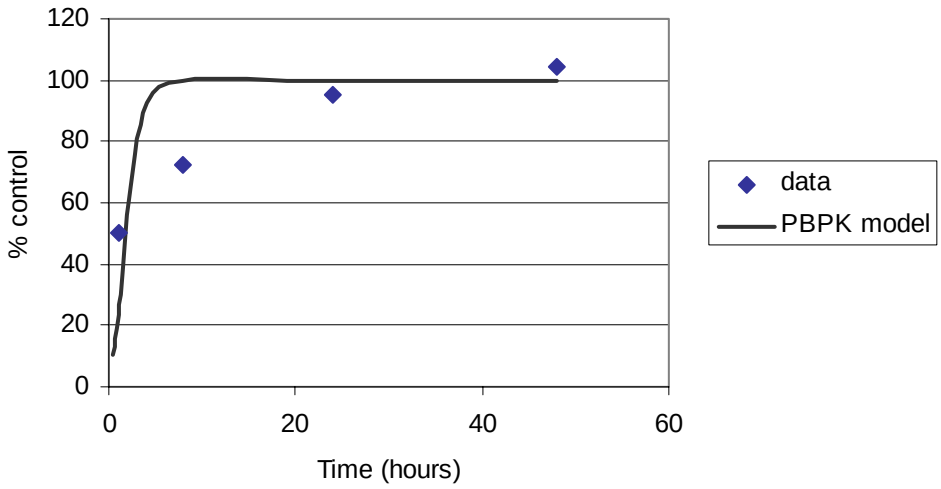

Figure E34. Blood acetylcholinesterase inhibition after administration of 30 mg/kg.

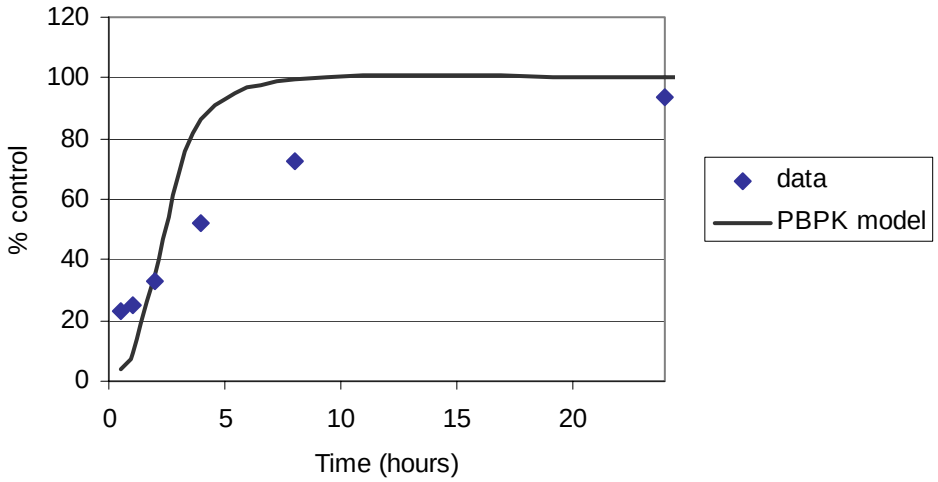

Figure E35. Brain acetylcholinesterase inhibition after administration of 50 mg/kg.

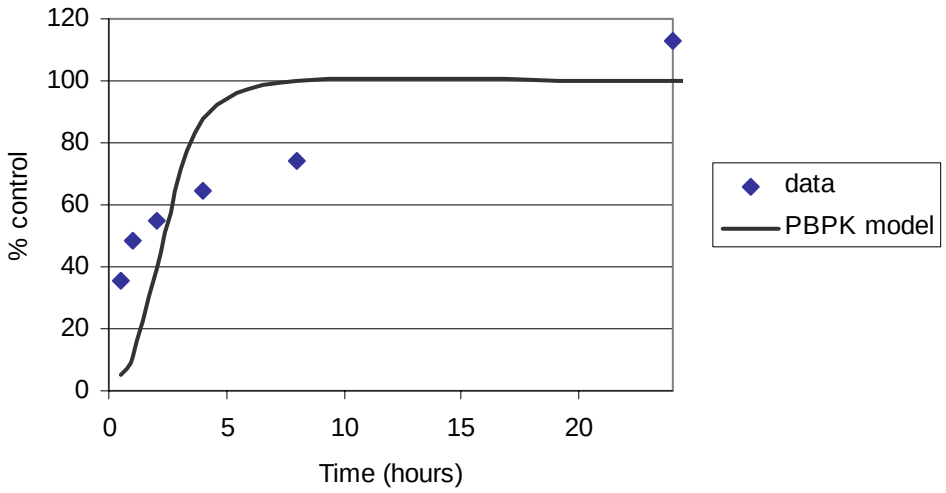

Figure E36. Blood acetylcholinesterase inhibition after administration of 50 mg/kg.

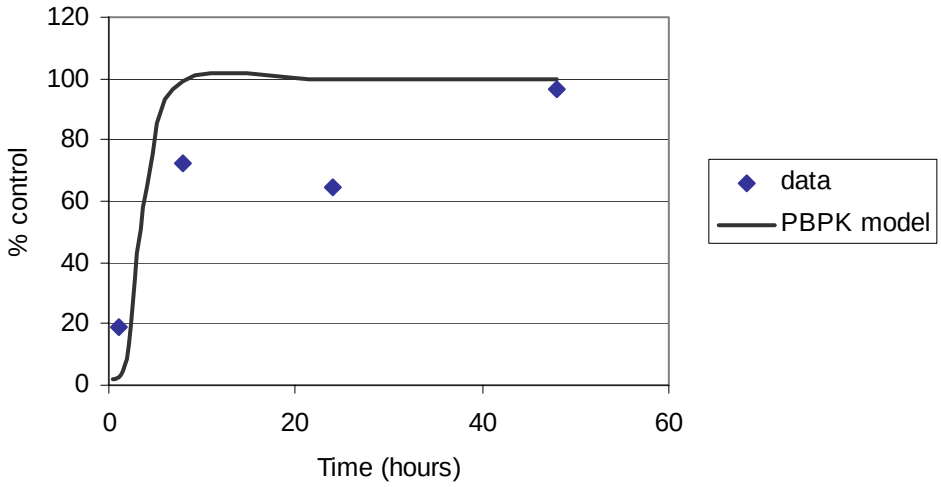

Figure E37. Brain acetylcholinesterase inhibition after administration of 90 mg/kg.

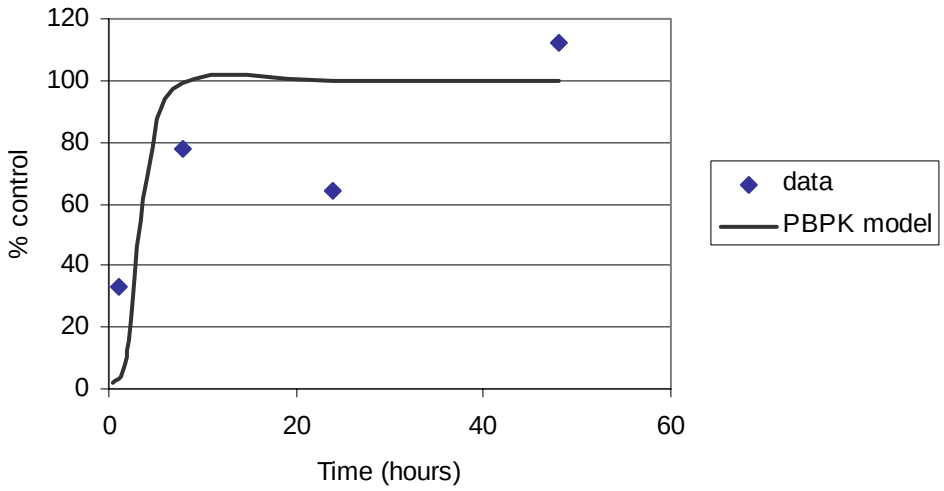

Figure E38. Blood acetylcholinesterase inhibition after administration of 90 mg/kg.

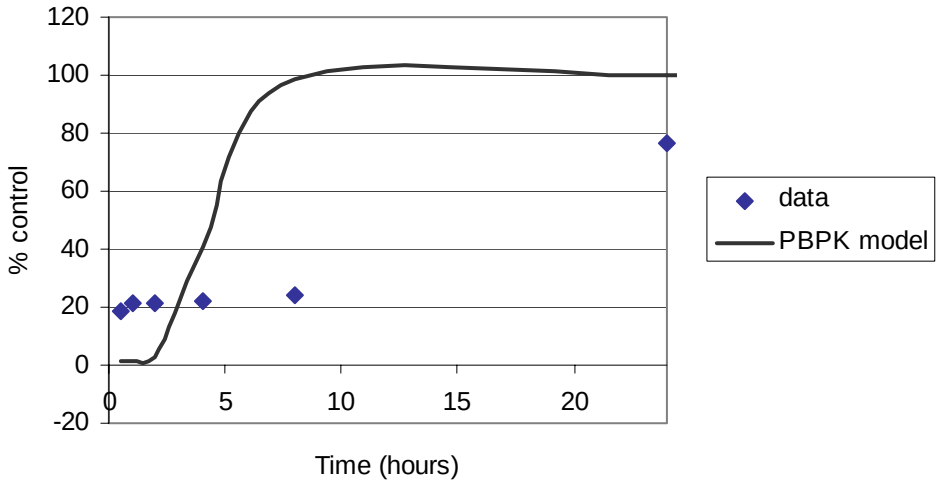

Figure E39. Brain acetylcholinesterase inhibition after administration of 125 mg/kg.

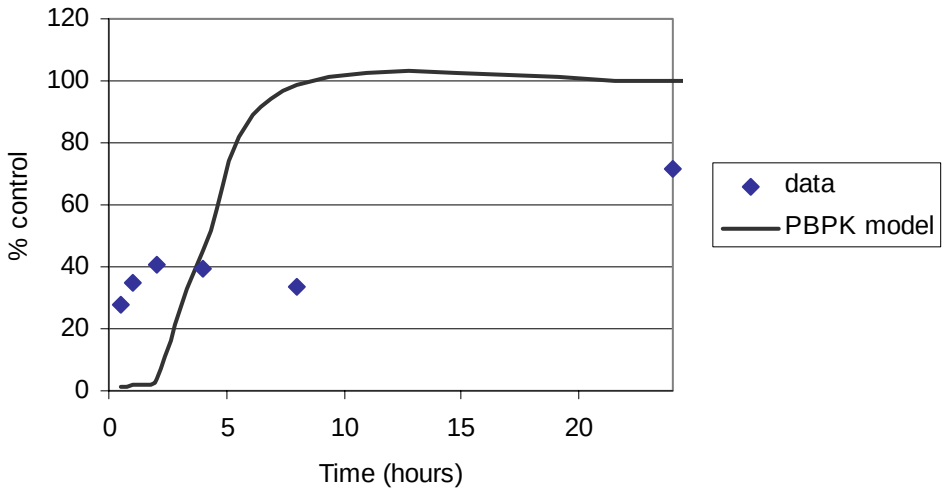

Figure E40. Blood acetylcholinesterase inhibition after administration of 125 mg/kg.

3.0 Dermal study at 0.793 mg/12.5 cm^2 (Cheng 1994)

Carbaryl was applied to the skin of Sprague-Dawley rats. The data points are the average values for 4 animals at each sample time.

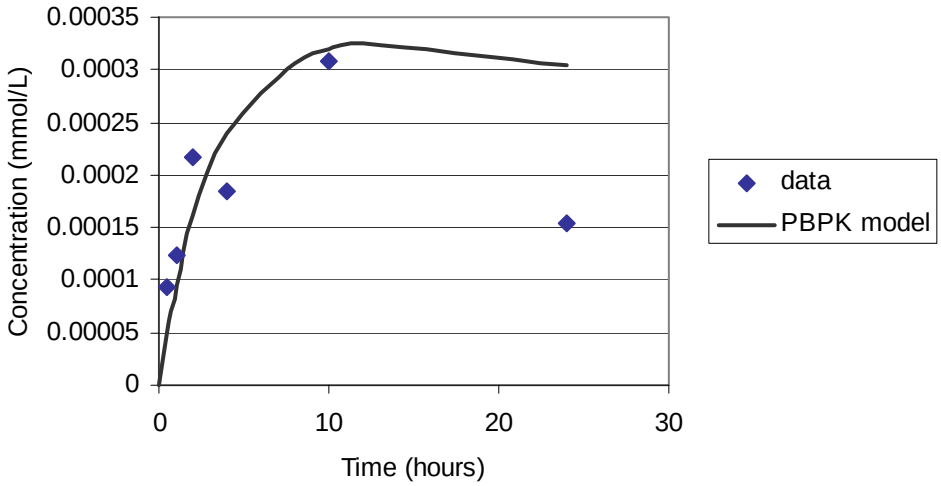

Figure E 41. Blood concentration ^{14}C.

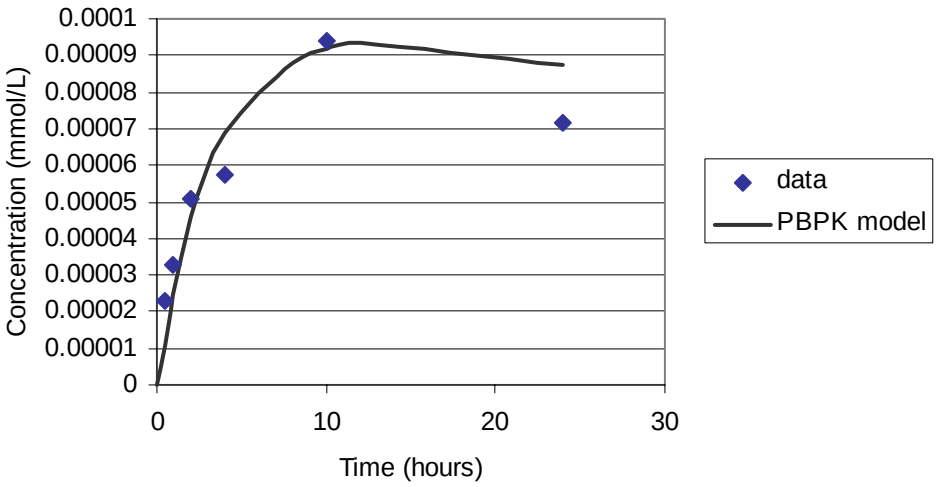

Figure E42. Carcass concentration ^{14}C.

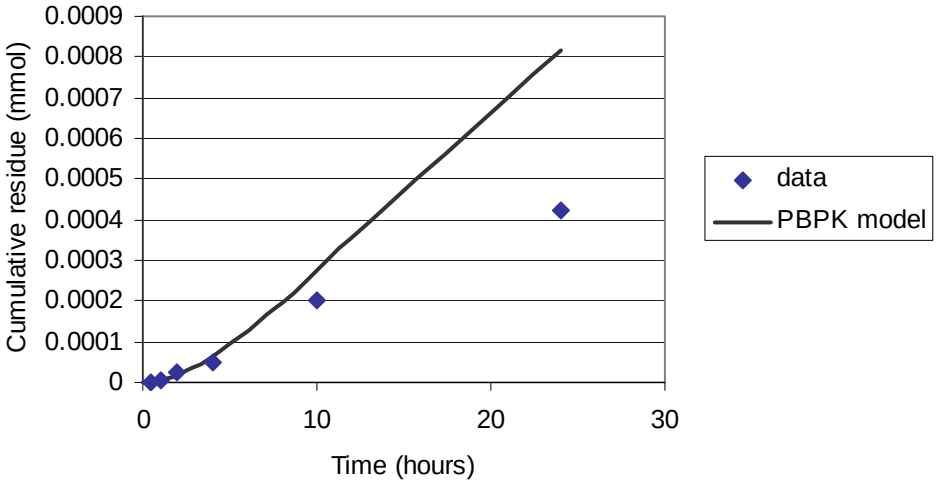

Figure E43. Cumulative ^{14}C residues in urine.

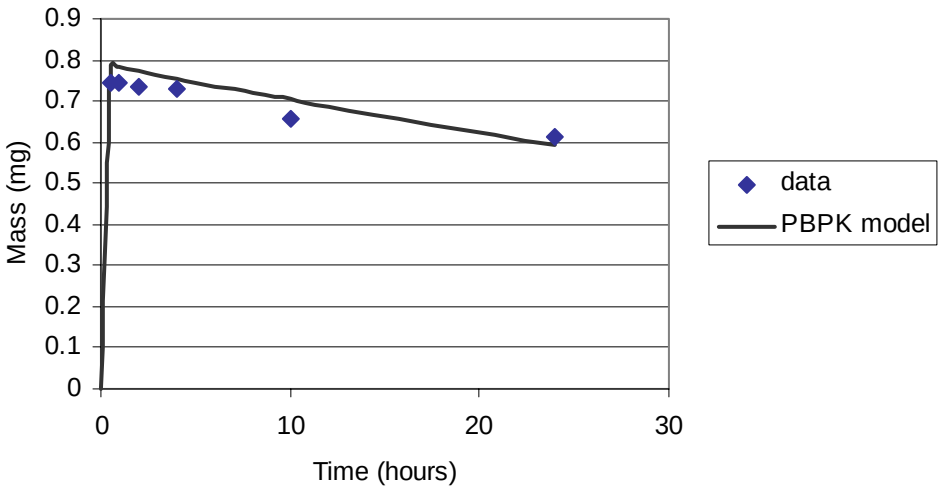

Figure E44. Carbaryl mass on skin.

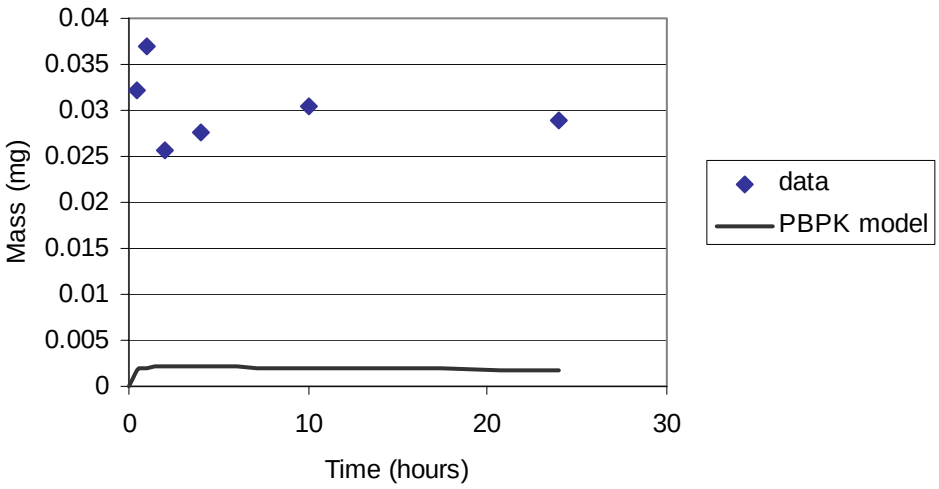

Figure E45. Carbaryl mass in skin.

4.0 Dermal study 1.74 mg/20cm^2 (Knaak *et al.* 1984)

Carbaryl was applied to the skin of Sprague-Dawley rats. The data points are the average values for 3 animals at each sample time.

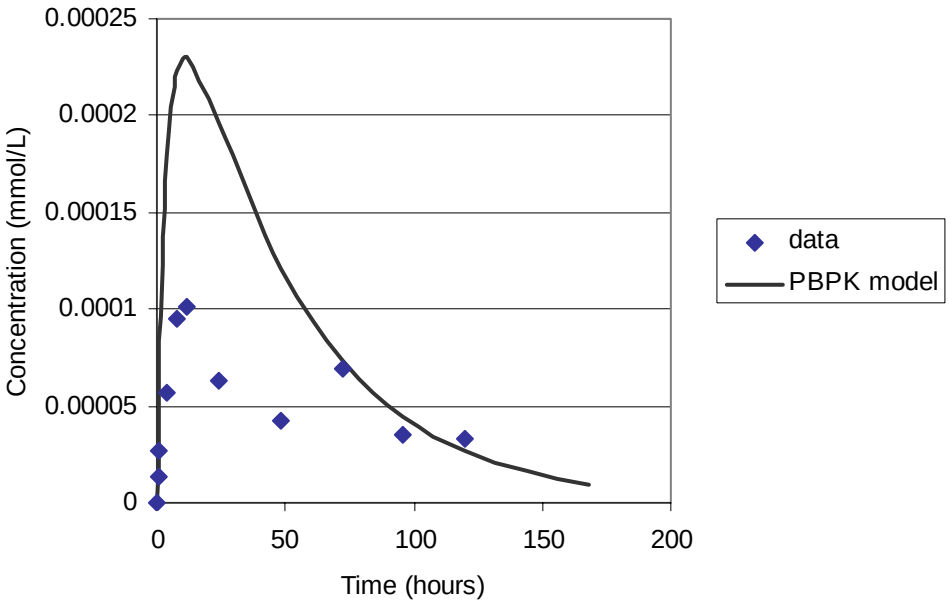

Figure E46. Blood concentration ^{14}C.

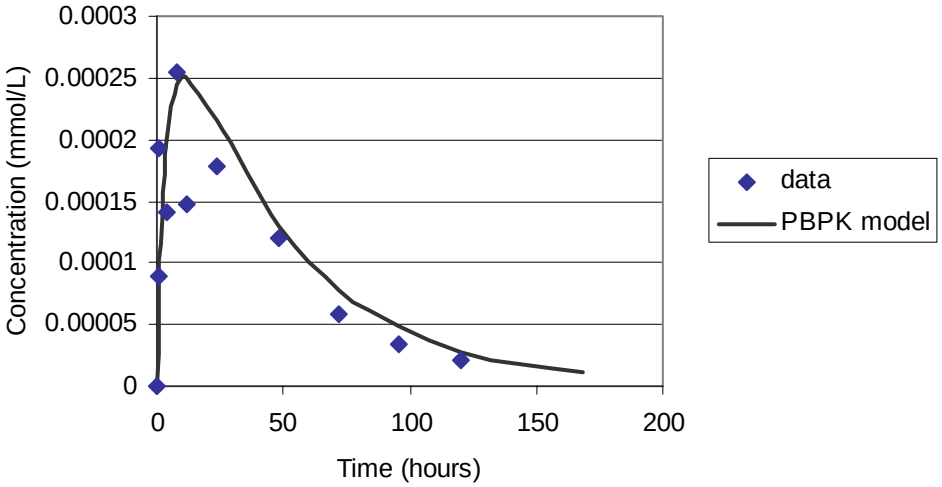

Figure E47. Liver concentration ^{14}C.

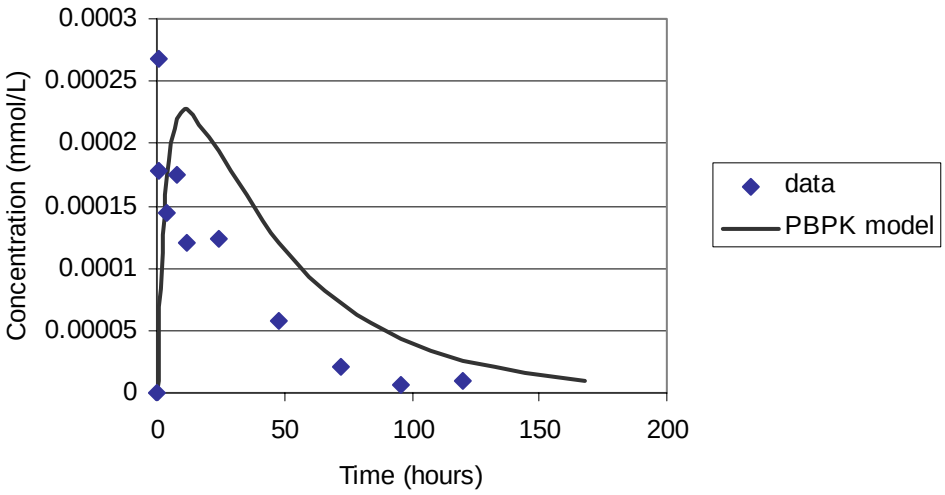

Figure E48. Slowly perfused concentration ^{14}C.

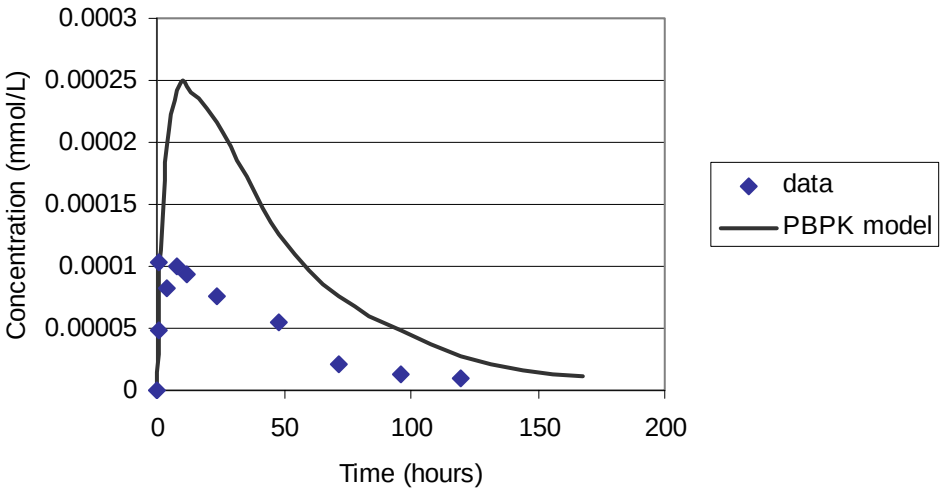

Figure E49. Rapidly perfused concentration ^{14}C.

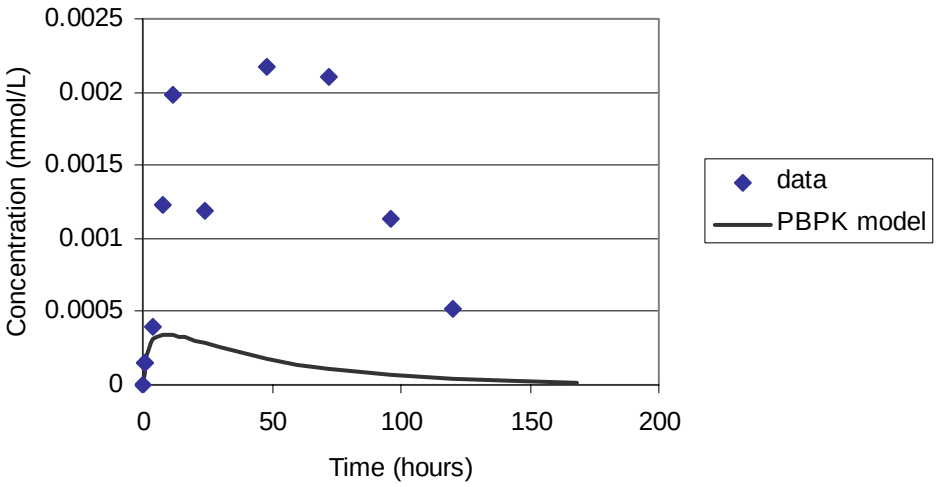

Figure E50. Fat concentration ^{14}C.

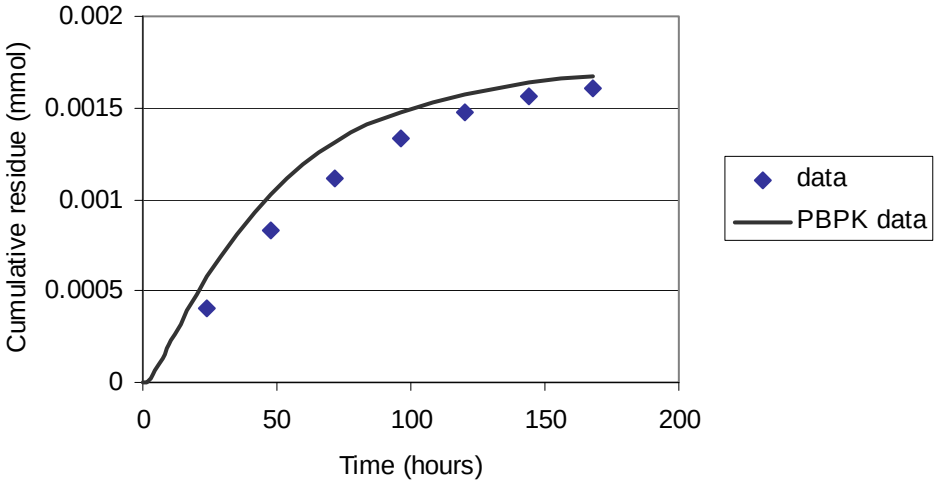

Figure E51. Cumulative ^{14}C residues in urine.

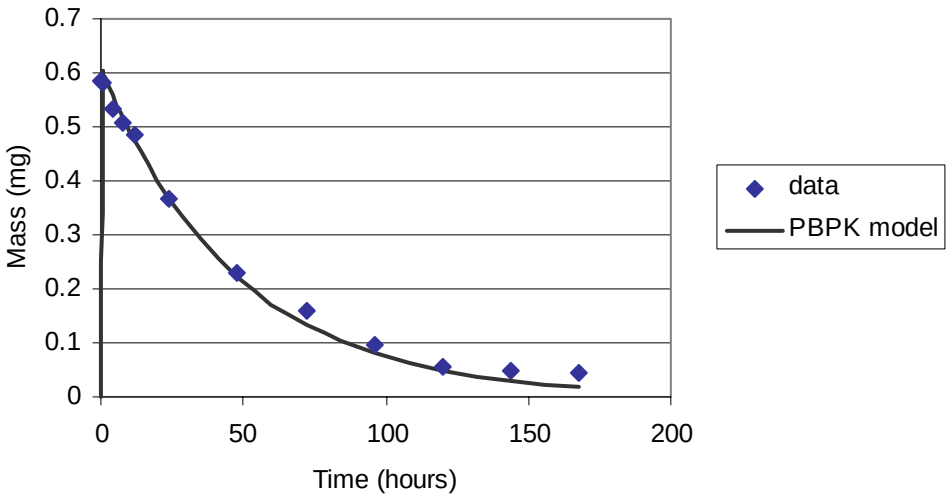

Figure E52. Carbaryl mass on skin.

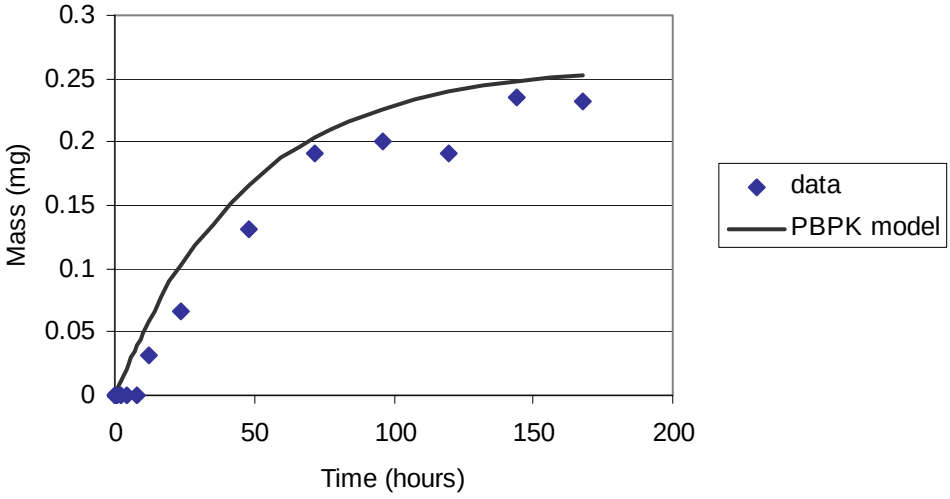

Figure E53. Evaporated carbaryl.

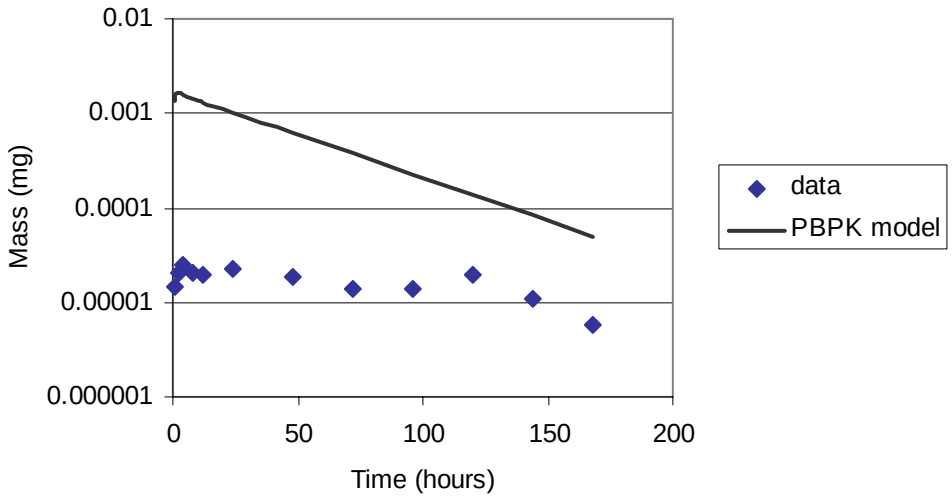

Figure E54. Carbaryl in skin.

5.0 IP dose of 20 mg/kg (Knaak *et al.* 1965)

Carbaryl was given IP to Sprague-Dawley rats for the purpose of studying the metabolism of carbaryl. The data points are for pooled urine samples from 3 animals.

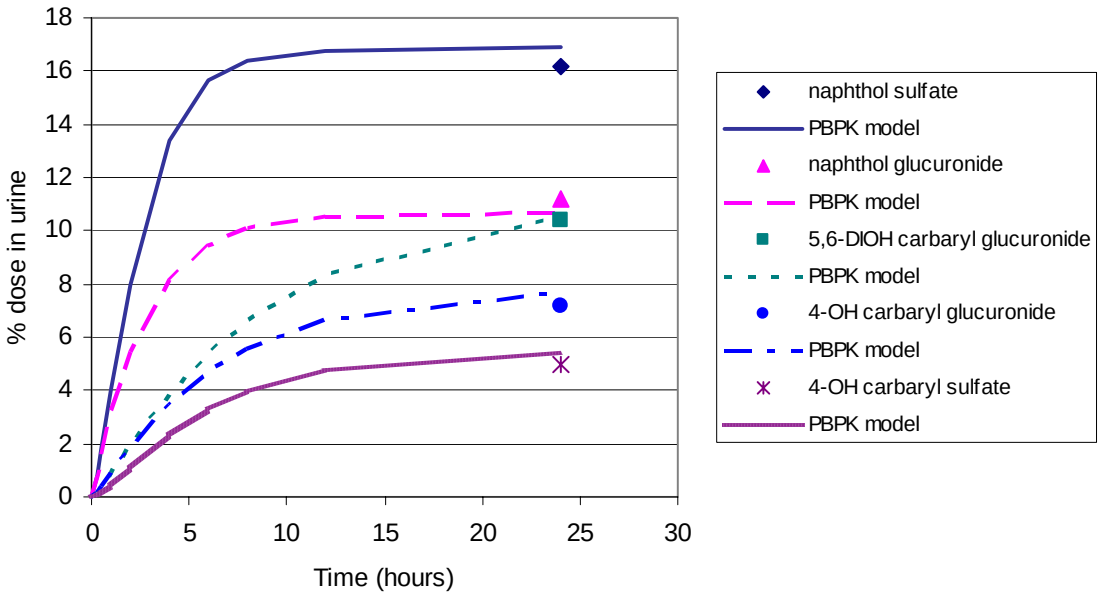

Figure E55. Carbaryl metabolites in urine.

6.0 Bile cannulation experiments

Oral doses of 0.01 mg/kg carbaryl were administered to Sprague-Dawley rats. The data points are the average values for 2 animals.

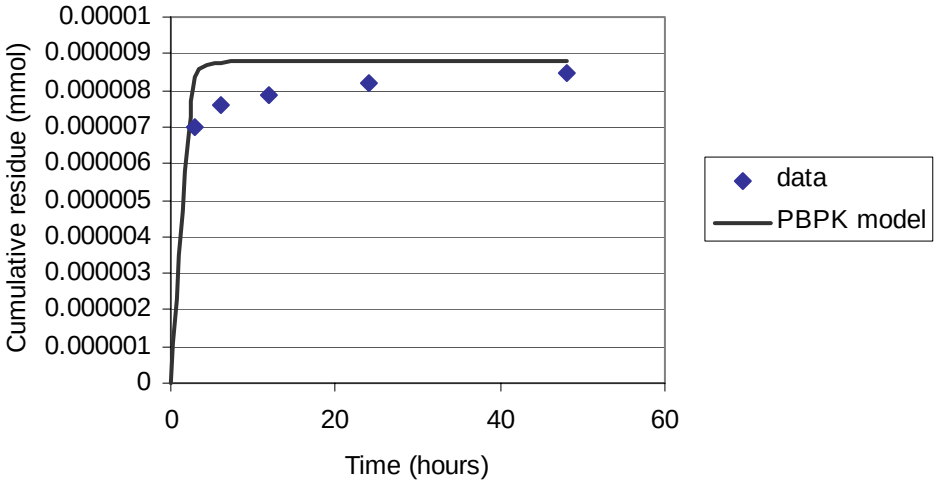

Figure E56. Cumulative ^{14}C residue in bile.

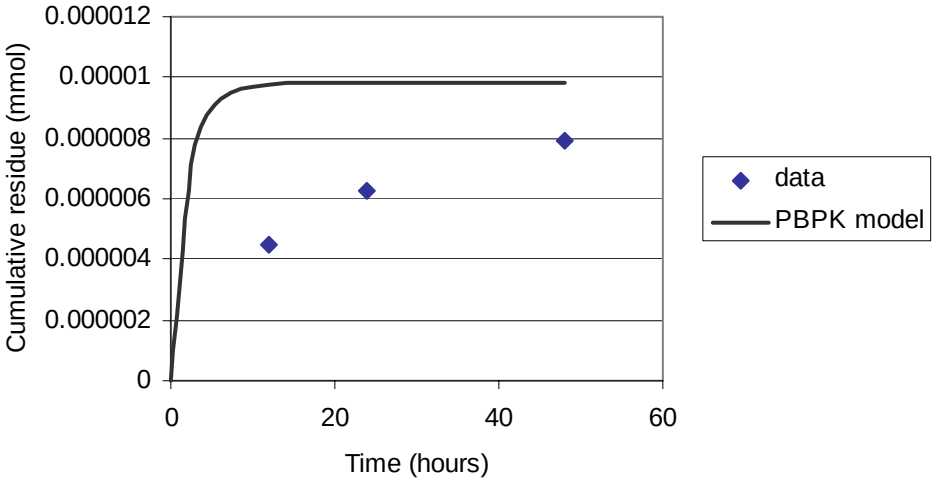

Figure E57. Cumulative ^{14}C residue in urine.